Book of abstracts of EUROMECH Colloquium 525 - Instabilities and transition in three-dimensional flows with rotation

Benoît Pier

EUROPEAN MECHANICS SOCIETY

LMFA

EUROMECH colloquium 525

Instabilities and transition in three-dimensional flows with rotation

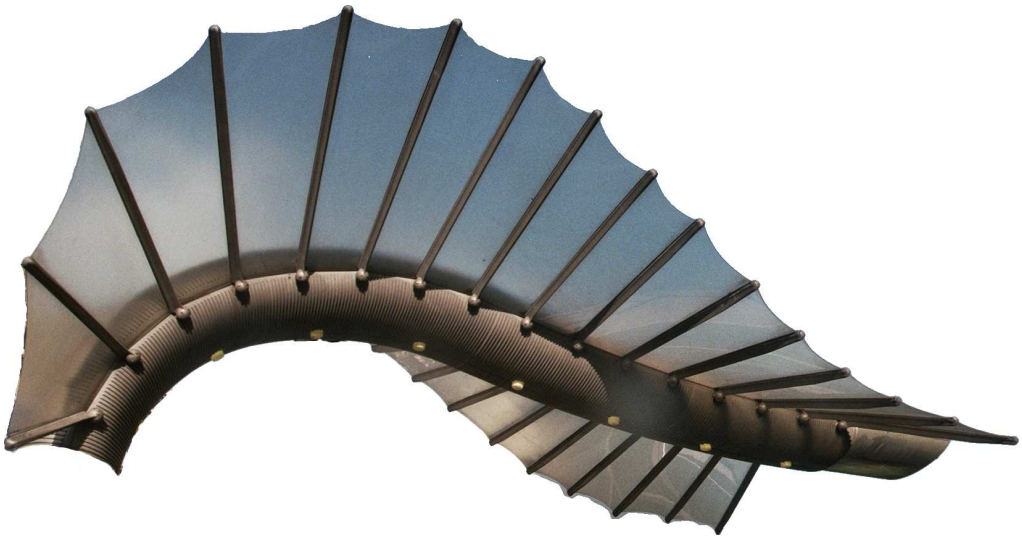

21–23 June 2011 — École centrale de Lyon — France

Laboratoire de mécanique des fluides et d'acoustique

http://lmfa.ec-lyon.fr/EC525/

Book of abstracts

1 EUROMECH Colloquium 525

Scientific scope and topics

Shear flows are known to display a variety of spatio-temporal instabilities and very complex transition scenarios. The route from laminar flow to the fully turbulent régime cannot be understood without taking into account three-dimensional effects. Particularly interesting phenomena are observed in the presence of rotation — either external, through rotating boundaries, or internal, through large-scale vorticity. Recently, our understanding of such flows has been improved by technical advances in analysis and experiments as well as a vast increase in computational capabilities. This allows consideration of increasingly complex mean flow distortions. The hydrodynamic stability community and the turbulence community tackle the additional complexity arising from three-dimensional coupling with different techniques. These techniques can however be compared and, whenever possible, linked.
By bringing together experts in experimental, analytical and numerical approaches, this colloquium attempts to clarify the global picture prevailing near transition and to narrow the gap between stability and turbulence analyses. It is expected that the development of modern analytical tools will suggest new experiments, and that novel experimental observations will in turn inspire more theoretical work.
Contributions have been received from the following topics:

- Three-dimensional boundary layers
- Flows around or inside rotating bodies
- Vortex breakdown
- Spatio-temporal development of perturbations
- Transition scenarios
- Flow control
- Transient phenomena
- Inhomogenous and anisotropic turbulence

Organizing committee

Chairman:
Benoît PIER, LMFA, CNRS—Université de Lyon

Co-chairmen:
Fabien GODEFERD, LMFA, CNRS—Université de Lyon
Nigel PEAKE, DAMTP, Cambridge University, UK

Scientific committee:
François GALLAIRE, École polytechnique fédérale de Lausanne, Switzerland
Matthew P. JUNIPER, Engineering, Cambridge University, UK
Robert RUBINSTEIN, NASA Langley, US

HAL — Hyper articles en ligne

All the abstracts contained in the present *Book of Abstracts* are made freely available in electronic form on the public open-access archive HAL under `http://hal.archives-ouvertes.fr/EC525/`.

Sponsors

ÉCOLE CENTRALE LYON École centrale de Lyon

Laboratoire de mécanique des fluides et d'acoustique

EUROMECH

Ercoftac

Association française de mécanique

2 Keynote lectures

Towards a direct route to turbulence in an open rotating cavity

Eric Serre[1], Bertrand Viaud[2] and Jean-Marc Chomaz[3]

[1] M2P2, UMR CNRS Aix Marseille Universites, Marseille
[2]Centre de Recherche de l'Armee de l'Air, CReA BA701, Salon de Provence
[3]LadHyX, UMR CNRS-Ecole Polytechnique, Palaiseau

The transition to turbulence is analyzed in an annular cavity made of two parallel co-rotating disks of finite radial extent, fed by a forced inflow at the hub. This configuration provides a simple model of technological devices such as turbo-machinery and it is also relevant to geophysical flows (Launder *et al.* 2010). In the limit of large rotation, centrifugal and Coriolis forces produce a secondary flow in the meridian plane composed of two thin boundary-layers along the disks separated by a non-viscous geostrophic core where the axial gradient of pressure nearly equilibrates the Coriolis force. The flow stability is primarily governed by the disk boundary-layers and the waves they support that can be locally analysed by reference to theoretical results from infinite disks. Early results of local linear stability analysis are the object of a general agreement (Launder *et al.* 2010) and have revealed that such boundary layer is subject to two generic types of instability referred as type I (crossflow) and type II (viscous).

New interest has been stimulated by the experimental and theoretical studies of Lingwood (1996, 1997) which showed that the onset of absolute instability in both the von Kármán and Ekman layers adjacent to a single disk occurred at a value of Reynolds number which closely corresponded to that obtained experimentally for laminar-turbulent transition. This major contribution to the turbulent breakdown process opened the possibility of a direct route towards turbulence through a global instability. But to this day, if further studies have confirmed these local linear stability results, no general agreement exists concerning their outcome in terms of global behaviour due to the competition between nonlinear and nonparallel effects. Numerical investigations of the linearized Navier Stokes equations by Davies & Carpenter (2003) showed that non-parallel effects can stabilize the flow whereas Pier (2003) assuming the existence of a non-linear global mode and computing the non-linear homogenous wave that should immediately follows the front, showed this primary nonlinear global mode should therefore be unstable toward a secondary instability with the possibility of a rapid transition to turbulence shortly behind the primary front. In such context, study of transition to turbulence must incorporate both nonlinear (destabilizing) and nonparallel effects (stabilizing).

The impulse response of the boundary layer in sectorial cavities of azimuthal extent $2\pi/68$ and $2\pi/4$ has been investigated by pseudo-spectral DNS. Numerical results establish the existence of a primary subcritical bifurcation to nonlinear global mode with angular phase velocity and radial envelop coherent with the so-called elephant mode theory (Pier & Huerre 2001). Numerical observations of an elephant

mode agrees with Pier's conjecture (Pier 2003) on the existence of a nonlinear global mode due to the presence of an absolutely unstable region, even when the flow is linearly globally stable (Davies & Carpenter, 2003). Moreover, this self-sustained saturated wave is itself globally unstable. A second front appears in the lee of the primary where small-scale instability develops with characteristics indicating a Floquet mode of zero azimuthal wavenumber. This secondary instability leads to a much disorganized state, defining transition to turbulence. This transition, linked to the secondary instability of a global mode, confirms for the first time on a real flow the possibility of a direct transition to turbulence through an elephant cascade, a scenario up to now only observed on the Ginzburg-Landau model.

Further work investigates alternative routes, when the initial perturbation is very low or when the azimuthal wavenumber is limited to smaller values.

References

Davies, C. & Carpenter, P. W. 2003. J. Fluid Mech. 486, 287–329.
Launder, B.E., Poncet, S. & Serre E., 2010, Ann. Rev. Fluid. Mech. **42**, 229–248.
Lingwood, R. J. 1995. J. Fluid Mech. 299, 17–33.
Lingwood, R. J. 1996. J. Fluid Mech. 314, 373 405.
Pier, B. & Huerre, P. 2001a J. Fluid Mech. 435, 145{174.
Viaud, B., Serre, E. & Chomaz, J.M. 2008 J. Fluid Mech. 598, 451–464.

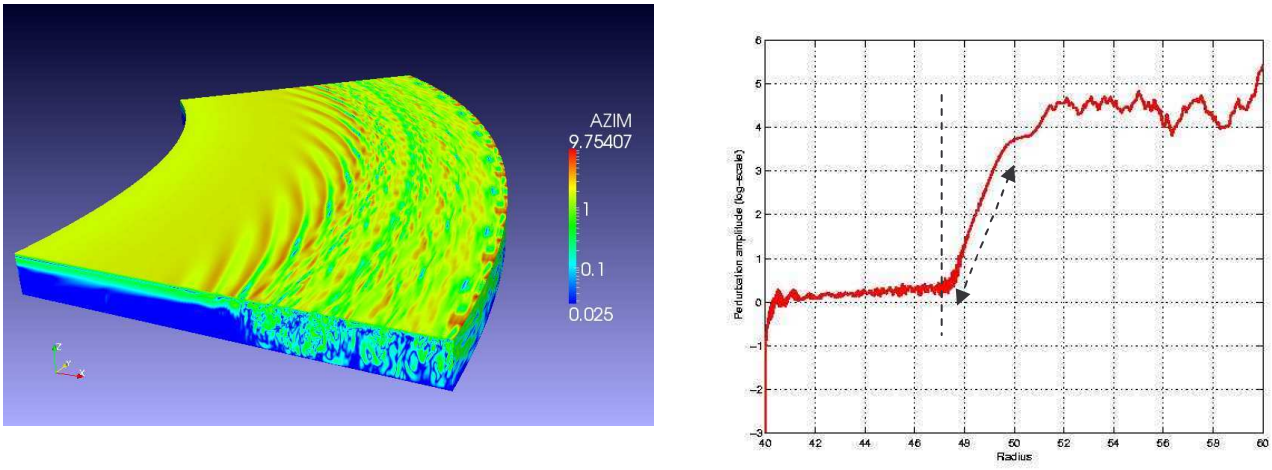

Flow pictures for Cw = 1995, Reh = 780 (Re_ 2 [330; 491], Ro 2 [−0.9;−0.45]). On the left, iso-lines of vorticity showing the saturated primary spiral front (m=68) followed by turbulence. On the right, profile of the linear-log amplitude of the perturbation-energy of m = 68 as a function of the radial coordinate. The radial position of the primary front is located at the transition from convective to absolute instability at r_c=43 and its slope matches the expected slope according to elephant-mode theory.

RESONANCES OF A ROTOR/STATOR CAVITY IN THE VICINITY OF THE CRITICAL POINT OF SF_6

Patrice LE GAL, Gautier VERHILLE
Institut de Recherche sur les Phénomènes Hors Equilibre, UMR 6594, CNRS & Universités d'Aix-Marseille, 49 rue F. Joliot-Curie, BP146, 13384 Marseille, France.

The extreme hydrodynamic regimes of spatial turbo-pumps are sources of complex phenomena which can be critical to their operation: appearance of instabilities, excitation of vibrational modes, new sources of dissipation and heat transfer. Thus, understanding and accurately predict the hydrodynamics in industrial rotating systems play a key role in the estimation of the reliability and the performances of these machines. To achieve the very high Reynolds numbers (10^7 to 10^8) of these flows and also to highlight the resonances of cavity modes induced by the compressibility of the fluid, we performed an experimental study of a rotor/stator flow using sulfur hexafluoride (SF_6) near its critical point as a working fluid. SF_6 is an inert gas whose critical temperature and pressure are 45.5 C and 37.6 bar. These thermodynamics conditions are sufficiently accessible to allow a laboratory experimental study. Near critical points, the behavior of fluids density with pressure is singular and a substantial reduction in the speed of sound is usually observed. For SF_6, values as low as 73 m/s are possible if pressure and temperature are sufficiently close to their critical values. This high compressibility should thus permit to explore typical compressible phenomena such as cavity resonances. Moreover, the kinematic viscosity of SF_6 in its liquid phase allows us to gain at least a factor 20 on the value of the Reynolds number relatively to water. This gain has allowed us to reduce the size of the facility. Consequently, the rate of rotation of the rotor could be significantly increased compared to conventional systems in water in order to reach Reynolds numbers above 10^7 that is close to the industrial case but also to reach the range of the cavity mode frequencies where resonances are expected. The aim of our experimental study is thus to investigate and if possible, simulate the vibrations present in spatial turbo-pumps rotor/stator cavities. In particular, we expect to determine the different characteristics of the cavity modes for a fluid layer between a rotor and a stator. A Helmholtz type theoretical model is first derived and shows that the characteristic frequencies of these modes change with the square root of the pressure in the fluid. From an experimental point of view, a rotor/stator cavity with its motor (maximum speed 12,000 rpm) is inserted into a pressure vessel. This vessel is thermalized by circulating water from a thermostatic bath. The stator is mounted on an elastic membrane that allows its motions in the axial direction and an accelerometer can record its vibrations. The first experiment is devoted to the detection of the different vibration modes of the cavity using an electromagnet and a spring that initially pushed up the stator before releasing it suddenly. The stator then oscillates freely and we can record its damped vibrations by the use of the accelerometer. This experiment is conducted for various pressures of SF_6 and for a fixed temperature of 45 C. The fundamental mode of vibration can be easily detected by comparison with the theoretical model. However, we show that we should take into account in the model a fluid added mass (by 40 times the mass of fluid in the cavity). This added mass is our only free parameter and our measurements confirm the existence of the cavity mode as described by the Helmholtz type resonator model. The second step in the experimental study is to excite directly the cavity mode by the motions of the fluid through the rotation of the rotor. As expected, during the passage of the rotation frequency through the mode frequency band, a resonance peak is perfectly observed. As projected in this study, it appears that the rotation of the stator can indeed excite pressure fluctuations in the cavity which in turn can cause the resonance of the compressible fluid layer between the stator ad the rotor. Thus, although it seems not necessary to take into account the fast and highly turbulent rotating flow (the Mach number of the flow is a few tenths) we prove that the compressibility of the fluid plays however a key role in the mechanical behavior of the rotor/stator cavity.

GLOBAL INSTABILITY OF FLOWS ACROSS A JUNCTION

Jonathan J. HEALEY
Department of Mathematics, Keele University, UK.

1 Global instability in infinite domains

Hydrodynamic stability theory originally developed through the study of flows where the streamwise development of the flow could be neglected. Under this parallel-flow approximation linearized disturbance equations can be reduced to ordinary differential equations, like the Rayleigh or Orr-Sommerfeld equations, by representing an arbitrary disturbance by a superposition of waves. The results of these 'local' stability theories are assumed to be applicable close to the chosen point in the flow where the velocity profile has been extracted from the streamwise-developing flow, and made parallel by ignoring its streamwise-dependence. The issue of how these local stability results can be interpreted to predict the stability of the whole flow is referred to as the 'global' stability problem.

When the basic flow varies strongly in the streamwise direction nonparallel effects cannot be ignored, local results are meaningless, and the global stability problem must usually be approached by solving partial differential disturbance equations numerically. But when the basic flow only varies slowly in the streamwise direction, the local theory is the correct leading order approximation in a WKB theory that allows weak nonparallel effects to be included. In this case global stability properties can be inferred from local stability properties.

Global instability is related to local absolute instability, which describes the growth or decay of disturbances in the rest frame. Consideration of the upstream and downstream responses to periodic forcing at a point in a weakly inhomogeneous flow leads to the conclusion that the global mode is given at leading order by the absolute instability at a saddle point where $\partial\omega_0/\partial x = 0$, where ω_0 is the local absolute frequency and x the streamwise coordinate (this saddle is a turning point in the WKB theory), see [1], [2] and the review by [3]. If $\mathrm{Re}(\omega_0)$ does not depend on x, i.e. if there is no detuning, then the saddle $\partial\omega_0/\partial x = 0$ lies on the real x-axis, and the intuitively reasonable expectation that the x station with greatest absolute growth rate should act as the wave-maker for the flow holds. Less obvious is the fact that when there is detuning the saddle will lie at a complex value of x and then the global instability given by ω_0 at the saddle will have smaller growth rate than that of the most unstable absolute instability on the real x-axis.

2 Global instability in semi-infinite domains

[4] considered global instability in a semi-infinite domain in which the absolute growth rate decreases with downstream distance, as a model for wake flow, and they found that the global mode was given by ω_0 at the upstream boundary. [5] considered global instability in a domain in which the absolute growth rate increases with downstream distance, but the detuning effect is strong enough to maintain global stability. [6] argued that this global stabilization by detuning explained the global stability observed in the numerical solutions of the linearized Navier-Stokes equations for disturbances to the rotating-disc boundary-layer obtained in [7], and observed in experiments on the same flow by [8]. However, [5] showed that imposing a downstream boundary condition in this type of flow in a region of local absolute instability can create a global instability driven by the absolute instability at the downstream boundary. In rotating-disc flow the radial coordinate is the relevant streamwise coordinate, suggesting that the edge of the disc could be crucial in creating global instability.

3 Global instability in semi-infinite domains joined by a junction

The present work is motivated by these findings. They encourage us to explore the local stability properies near the edge of the disc in more detail. In particular, we seek to form a global mode in which the disturbance solution in the flow *over* the disc is matched to the disturbance solution in the flow *beyond* the edge of the disc.

Existing experiments on the stability of the rotating disc have not included measurements of velocity profiles for the flow beyond the edge of the disc. [9] used interactive boundary-layer theory to calculate the flow separating from the edge of a thin disc when there is von Kármán flow [10] over both the upper and lower surfaces of the disc. However, most stability experiments use a thick disc to reduce the effects of vibration, and the substantial mountings and motor arrangements below the disc are likely to prevent von Kármán flow from being established on the lower surface. Although a detailed study of the flow beyond the edge of a rotating disc used in a stability experiment would be desirable, in the present work we take a similar approach to that taken

in [5], and explore instead the qualitative phenomena that arise when one considers the global instability of flow across a junction using the Ginzburg-Landau equation. Nonetheless, the stability and propagation properties of the flows on either side of the junction are taken from stability calculations for a simplified model of von Kármán flow over the disc, and for two simplified, but plausible, flows that could exist beyond the edge of the disc.

4 Results

Our most important finding is that in some circumstances the global mode can be more unstable than the local absolute instability on either side of the junction. For example, a stable flow upstream of a junction connecting to a downstream flow that is only convectively unstable can nonetheless be globally unstable, despite the absence of any local absolute instability. This arrangement can arise in a wide variety of practical applications, not just at the edge of a rotating disc, e.g. when stable flow in a nozzle becomes a convectively unstable jet flow after leaving the nozzle. The nozzle then acts as a junction between a channel (or pipe) flow and the jet. Another example is when a boundary layer separates from a surface: the separation point then acts as a junction between (possibly) stable attached flow, and convectively unstable separated flow. This applies both to the case of separation from a sharp edge and separation from a smooth surface. The origins of this unexpected behaviour will be explained.

References

[1] A. M. Soward & C. A. Jones, The linear stability of the flow in the narrow gap between two concentric rotating spheres. *Quart. J. Mech. Appl. Math.* **36**, 19–42 (1983).

[2] J. M. Chomaz, P. Huerre & L. G. Redekopp, A frequency selection criterion in spatially developing flows. *Stud. Appl. Math.* **84**, 119–144 (1991).

[3] P. Huerre, Open shear flow instabilities. In *Perspectives in Fluid Dynamics*. Eds. G. K. Batchelor, H. K. Moffatt & M. G. Worster, CUP, 159–229 (2000).

[4] J. M. Chomaz, P. Huerre & L. G. Redekopp, Models of hydrodynamic resonances in separated shear flows. In *Proc. 6th Symp. on Turbulent Shear Flows* Toulouse, 119–144 (1987).

[5] J. J. Healey, Model for unstable global modes in the rotating-disk boundary layer. *J. Fluid Mech.* **663**, 148–159 (2010).

[6] C. Davies, C. Thomas & P. W. Carpenter, Global stability of the rotating-disc boundary layer. *J. Eng. Math.* **57**, 219–236 (2007).

[7] C. Davies & P. W. Carpenter, Global behaviour corresponding to the absolute instability of the rotating-disk boundary layer. *J. Fluid Mech.* **486**, 287–329 (2003).

[8] H. Othman & T. C. Corke, Experimental investigation of absolute instability of a rotating-disk boundary layer. *J. Fluid Mech.* **565**, 63–94 (2006).

[9] F. T. Smith, A note on a wall jet negotiating a trailing edge. *Q. J. Mech. Appl. Math.* **31**(4), (1978).

[10] Th. von Kármán, Über laminare und turbulente Reibung. *Z. Angew. Math. Mech.* **1**, 233–252 (1921).

DYNAMO ACTION IN FINITE CYLINDERS

C. Nore[1], J.-L. Guermond[1,2], J. Léorat[3] & F. Luddens[1,2]
[1]*LIMSI, CNRS, UPR3251, BP 133, 91403 Orsay cedex, France, Université Paris-Sud 11 and Institut Universitaire de France.*
[2]*Department of Mathematics, Texas A&M University, College Station, TX 77843-3368, USA.*
[3]*Luth, Observatoire de Paris-Meudon, place Janssen, 92195-Meudon, France.*

Motivation

Using numerical simulations, we investigate two magnetohydrodynamics (MHD) problems in a cylindrical cavity, namely the von Kármán Sodium (VKS) experiment and a precessing cylinder filled with a conducting fluid. We use a parallel code denoted SFEMaNS [1], which is able to integrate nonlinear MHD equations for incompressible fluids in heterogenous domains (with jump distributions of electrical conductivity or magnetic permeability) with axisymmetric interfaces embedded in a vacuum. We numerically demonstrate that using high permeability disks in VKS decreases the dynamo threshold and that precession is able to drive a cylindrical dynamo.

1 Impact of soft iron impellers in the VKS dynamo experiment

The VKS experiment [2] leads to dynamo action, at the available power, using soft iron impellers but not using steel impellers. This demonstrates the crucial role played by ferromagnetic material that numerical studies can handle on simplified configurations. Therefore kinematic simulations of the induction equation (with imposed velocity field) are carried out for different setups suitable for this experiment. The impellers are modeled by flat disks of high conductivity or high permeability and drive the flow in a cylinder filled with a conducting fluid. Ohmic decay and kinematic dynamo problems using various configurations and physical parameters are investigated. The material properties of the disks change drastically the field geometry and growth rates while external boundary conditions have nearly no influence. Using a VKS like mean fluid flow and high permeability disks decreases the critical magnetic Reynolds number Rm^c for the onset of dynamo action of the simplest non-axisymmetric field mode and confines the magnetic field lines in between the two ferromagnetic disks (see figure 1). In contrast, using high conducting disks increases Rm^c. From the experimental point of view the utilization of disks with a conductivity that is 100 times larger than the conductivity of liquid sodium remains purely academic. Nevertheless, the simulations show a crucial difference between heterogeneous permeabilities and conductivities: even if these two quantities may appear in the definition of an effective Reynolds number $Rm^{\text{eff}} = \mu_0 \mu_{\text{r}}^{\text{eff}} \sigma^{\text{eff}} UL$, they do not play the same role [3]. Increasing the permeability of the disks increases

(a) $\mu = 1$, $Rm = 50$ (b) $\mu = 100$, $Rm = 50$

Figure 1: Magnetic lines and iso-value of the magnetic energy density corresponding to 25% of the maximum magnetic energy for two disks with different magnetic permeability μ.

the decay time of the axisymmetric mode, especially the toroidal mode when permeability is high enough. It may thus appear as the dominant mode of the dynamo when the flow axisymmetry is broken, as it seems to be observed in the VKS experiment.

2 Dynamo action in a precessing cylinder

The possible contribution of precession to dynamo action is a long-standing debate (see for example [4]). Modern astrophysical observations of some planetary dynamos can contribute to resolving this issue, although definite

evidence is still lacking. Because of the large computing resources required, it was only recently that numerical computations could demonstrate that dynamo action occurs in two different precessing containers: spherical [5] and spheroidal [6] ones. Since neither shape is convenient for large-scale experiments, it is instructive to investigate whether similar results can be obtained in cylindrical containers. Five parameters govern the flow: the aspect ratio of the container, the precession angle and precession rate (forcing parameters), and the kinetic and magnetic Reynolds numbers (fluid parameters, Re and Rm). Choosing the container length equal to its diameter, a precession axis orthogonal to the rotation axis and a precession rate of 0.15, the non-magnetic flow breaks its central symmetry when the kinetic Reynolds number becomes large enough ($Re \geq 10^3$). The nonlinear MHD problem starts after a small magnetic seed field is added. When the magnetic dissipation is small enough, i.e. for magnetic Reynolds numbers Rm above a critical value $Rm^c(Re)$, dynamo action appears after symmetry breaking of the flow, as was also observed in the spherical and spheroidal dynamos. A snapshot of a dynamo run shows the complex fluid flow in the container and the spatial distribution of the magnetic field lines in the cylinder and the vacuum. An experimental approach could be relevant to natural dynamos and seems within reach using a cylindrical container (cf. DRESDYN proposal in Germany, F. Stefani, personal communication).

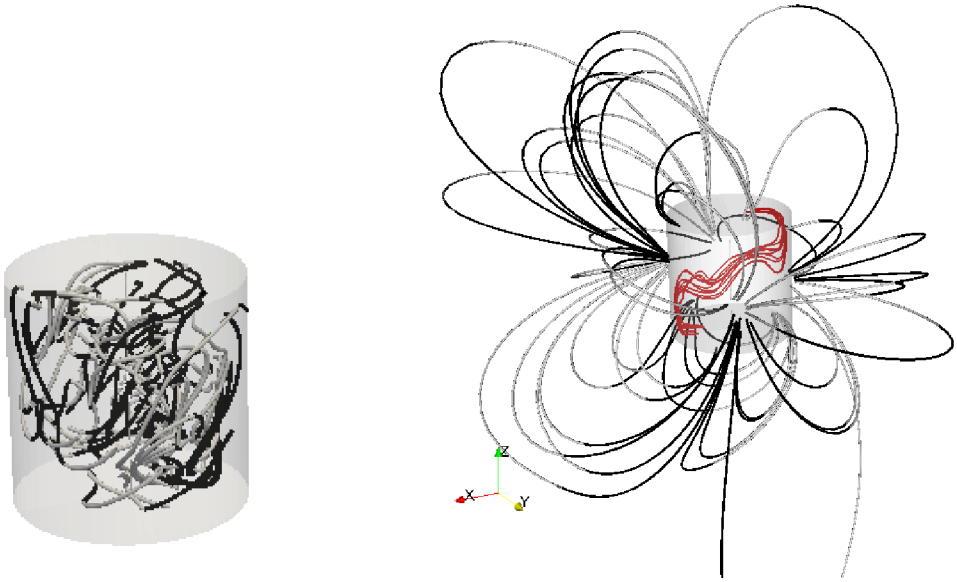

(a) (b)

Figure 2: Snapshot of a dynamo run at $Re = 1200$, $Rm = 2400$ showing (a) internal magnetic field lines in the cylinder cavity, colored by the axial component vorticity (grey/black for positive/negative axial component) and (b) vorticity field lines (red) in the container and external magnetic field lines colored by the axial component. The cylinder is seen from the side, the Oz (respectively Ox) axis is the rotation (respectively precession) axis.

References

[1] J.-L. Guermond, R. Laguerre, J. Léorat and C. Nore, Nonlinear magnetohydrodynamics in axisymmetric heterogeneous domains using a Fourier/finite element technique and an interior penalty method, *J. Comput. Phys.*, 228:2739–2757, 2009.

[2] R. Monchaux, M. Berhanu, M. Bourgoin, M. Moulin, Ph. Odier, J.-F. Pinton, R. Volk, S. Fauve, N. Mordant, F. Pétrélis, A. Chiffaudel, F. Daviaud, B. Dubrulle, C. Gasquet, L. Mari and F. Ravelet, Generation of a magnetic field by dynamo action in a turbulent flow of liquid sodium *Phys. Rev. Lett.*, 98, 044702 (2007).

[3] A. Giesecke , C. Nore, F. Luddens, F. Stefani, G. Gerbeth, J. Léorat and J.-L. Guermond, Electromagnetic induction in non-uniform domains, *Geophys. Astrophys. Fluid Dyn.*, 1029-0419, 104:505–529, 2010.

[4] W. V. R. Malkus, Precession of the Earth as the cause of geomagnetism: Experiments lend support to the proposal that precessional torques drive the Earth's dynamo, *Science*, 160(3825):259–264, 1968.

[5] A. Tilgner, Precession driven dynamos, *Phys. Fluids*, 17(3):034104, 2005.

[6] C.-C. Wu and P. Roberts, On a dynamo driven by topographic precession, *Geophys. Astrophys. Fluid Dyn.*, 103(6):467–501, 2009.

ANISOTROPIC ENERGY TRANSFERS IN DECAYING ROTATING TURBULENCE

Frédéric MOISY, Cyril LAMRIBEN & Pierre-Philippe CORTET
Laboratoire FAST, CNRS, Univ Paris-Sud, UPMC Univ Paris 06, Bât. 502, Campus universitaire, 91405 Orsay, France.

1 Introduction

In the presence of a background rotation, a situation which is relevant for most geophysical and astrophysical flows, the energy cascade from large to small scales is modified by the Coriolis force, resulting in a gradual columnar structuring of the turbulence along the rotation axis. In the limit of large rotation rates, turbulence tends to become two-dimensional —but still three-component (2D-3C)—, in agreement with the Taylor-Proudman theorem.

The anisotropic energy transfers responsible for this non-trivial flow organization have been characterized mainly in the spectral space [1, 2, 3]. On the other hand, direct evidence of the anisotropy of the energy transfers in the physical space is still lacking.

If homogeneity (but not necessarily isotropy) holds, the energy transfers in the physical space are governed by the Kármán-Howarth-Monin (KHM) equation [4, 5]

$$\frac{1}{2}\frac{\partial}{\partial t}R = \frac{1}{4}\nabla\cdot\mathbf{F} + \nu\nabla^2 R, \tag{1}$$

where $R(\mathbf{r},t) = \langle \mathbf{u}(\mathbf{x},t)\cdot\mathbf{u}(\mathbf{x}+\mathbf{r},t)\rangle$ is the two-point velocity correlation, $\mathbf{F}(\mathbf{r},t) = \langle \delta\mathbf{u}\,(\delta\mathbf{u})^2\rangle$ is the energy flux density, and $\delta\mathbf{u} = \mathbf{u}(\mathbf{x}+\mathbf{r},t) - \mathbf{u}(\mathbf{x},t)$ is the velocity vector increment over separation $\mathbf{r}$. Eq. (1) reduces to the Kolmogorov's 4/5th law in the inertial range if isotropy is assumed. Importantly, this equation is still valid for homogeneous anisotropic turbulence, and in particular for axisymmetric turbulence in a rotating frame [6].

2 Experiment

Experiments of decaying grid turbulence mounted on the "Gyroflow" rotating platform have been performed [7, 8]. Turbulence is generated by rapidly towing a square grid at a velocity $V_g = 1.0$ m s^{-1} from the bottom to the top of a tank filled with 240 liters of water. The grid consists in 8 mm thick bars with a mesh size $M = 40$ mm. Runs for three rotation rates, $\Omega = 4$, 8 and 16 rpm, as well as a reference run without rotation, have been carried out. The Reynolds number based on the grid mesh is $Re_g = V_g M/\nu = 40\,000$, and the Rossby number $Ro_g = V_g/2\Omega M$ ranges from 7.4 to 30, indicating that the flow in the wake of the grid is fully turbulent and weakly affected by rotation.

Velocity measurements are performed in the rotating frame using a corotating PIV system. Two velocity components (u_x, u_z) are measured, in a vertical 16×16 cm^2 field of view, where z is the rotation axis. From these 2D PIV fields, surrogates of the energy distribution and flux density are computed,

$$E(\mathbf{r}) = \langle \delta u_x^2 + \delta u_z^2\rangle_{x,z}, \quad \mathbf{F}(\mathbf{r}) = \langle \delta\mathbf{u}(\delta u_x^2 + \delta u_z^2)\rangle_{x,z}. \tag{2}$$

Statistics are averaged over 600 independent realizations of the turbulence decay, ensuring a convergence of order of 20% for $\mathbf{F}(\mathbf{r})$, and better than 1% for $E(\mathbf{r})$.

3 Results

Our main findings are summarized in figure 1. In the absence of rotation (Fig. 1a), the raw vector map of the energy flux density $\mathbf{F}(\mathbf{r})$ is found nearly radial, pointing towards the origin, giving direct evidence of the isotropic energy cascade in the physical space, from the large to the small scales. The map of the energy flux $\nabla\cdot\mathbf{F}$ is remarkably circular, showing a broad negative minimum in an annular region spanning over $r \simeq 5-20$ mm, providing an indication of the extent of the inertial range.

Surprisingly, the flux density $\mathbf{F}(\mathbf{r})$ in the rotating case (Fig. 1b) is also nearly radial, except at the smallest scales, for $r < 10$ mm, where a marked deflection towards the rotation axis is observed. Such horizontally tilted $\mathbf{F}$ is indeed consistent with an asymptotic 2D-3C flow, for which $\mathbf{F}$ must be a strictly horizontal vector, function of the horizontal component of the separation only. The inertial range, where the energy flux $\nabla\cdot\mathbf{F}$ is

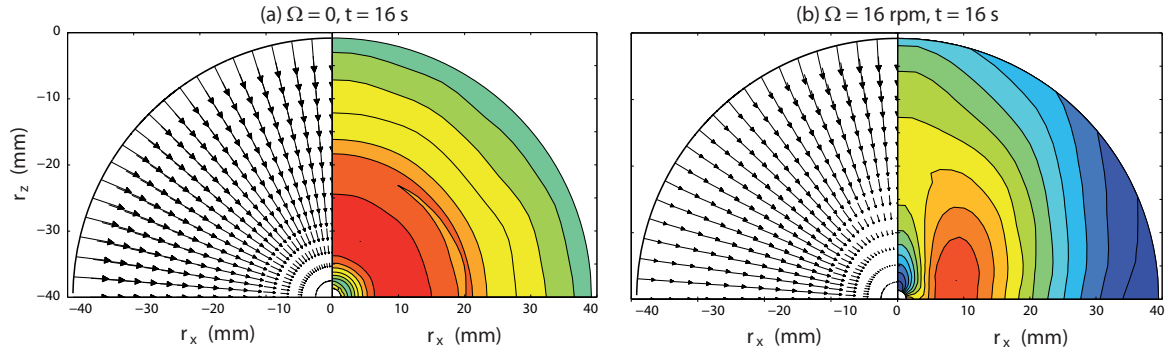

Figure 1: Maps of the energy flux density, in the separation space $\mathbf{r}$. (a) without rotation; (b) with rotation, at a time corresponding to 4.3 frame rotations. The vertical axis z corresponds to the rotation axis. Left: raw vector field $\mathbf{F}(\mathbf{r})$, showing the direct energy cascade from large to small scales. Right: Energy flux $-\nabla \cdot \mathbf{F}(\mathbf{r})$. The annular or vertically elongated region where the flux is approximately constant (red area) corresponds to the inertial range. Adapted from Ref. [8].

negative and approximately constant (red area in figure 1), becomes vertically elongated in the rotating case as time proceeds. This spatial structure is consistent with a growing anisotropy of the turbulence. Indeed, neglecting the viscous term in the KHM equation (1), the vertically elongated region where $\nabla \cdot \mathbf{F} < 0$ induces a stronger reduction of the velocity correlation R along x than along z, resulting in a relative growth of the vertical correlation along z. The striking result here is that the strongly anisotropic energy flux $\nabla \cdot \mathbf{F}$ originates from an almost purely radial, but angle-dependent, density flux $\mathbf{F}$. In particular, setting the polar component of $\mathbf{F}$ to zero yields an almost unchanged flux map $\nabla \cdot \mathbf{F}$.

These first results of the energy transfers in the physical space are a useful alternative to the more classical description in the spectral space [3], and shed new light on the anisotropy growth of decaying rotating turbulence.

References

[1] C. Cambon and L. Jacquin, J. Fluid Mech. **202**, 295 (1989).

[2] F. Waleffe, Phys. Fluids A **5**, 677 (1993).

[3] P. Sagaut and C. Cambon, *Homogeneous Turbulence Dynamics* (Cambridge University Press, Cambridge, 2008).

[4] A. S. Monin and A. M. Yaglom, *Statistical Fluid Mechanics*, vol. 2 (MIT Press, Cambridge, 1975).

[5] U. Frisch, *Turbulence - The Legacy of A. N. Kolmogorov* (Cambridge University Press, Cambridge, 1995).

[6] S. Galtier, Phys. Rev. E **80**, 046301 (2009).

[7] C. Lamriben, P.-P. Cortet, F. Moisy, and L.R.M. Maas, Phys. Fluids **23**, 015102 (2011).

[8] C. Lamriben, P.-P. Cortet, and F. Moisy, subm. to Phys. Rev. Lett. (2011).

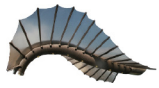

SPANWISE ROTATION EFFECTS ON SHEAR FLOWS

P. Henrik ALFREDSSON[1], Nils TILLMARK[1] & Takahiro TSUKAHARA[2]
[1] *Linne FLOW Centre, KTH Mechanics, Royal Institute of Technology, Stockholm, Sweden.*
[2] *Department of Mechanical Engineering, Tokyo University of Science, Japan.*

1 Introduction

Spanwise rotation on shear flows may give rise to strong instabilities due to the influence of the Coriolis force ($\mathbf{f}_{\text{Coriolis}} = 2\mathbf{U} \times \mathbf{\Omega}$). Here we define spanwise rotation as rotation along the z-axis, whereas the undisturbed flow U is in the x-direction and the shear is in the y-direction. In plane Poiseuille flow one half of the channel is destabilized whereas the other is stabilized. In plane Couette flow on the other hand the full flow field is either stabilized or destabilized depending on the direction of rotation (see figure 1). Another interesting complication arises if the flow in addition is affected by a centrifugal force which would occur if a curved channel flow is subjected to spanwise rotation. In certain limits these flows can also be described by the Taylor-Couette system. Both rotation and centrifugal effects may have strong influence in many technical applications such as rotating machinery (e.g. compressors, turbines, pumps and fans) but also in the natural sciences such as planetary flows and astrophysical situations.

In this presentation we will illustrate the strong influence on rotation in several laboratory shear flows, both stabilizing and destabilizing effects as well as in combination with centrifugal forces. The presentation is based on results obtained in our laboratory (see e.g. [1]) but also results from other experiments, theory and DNS.

2 Results from linear stability analysis

Rotating shear flows can be described by two parameters, one is the Reynolds number

$$Re = \frac{Uh}{\nu}$$

and the other describes the rotation effect as for instance

$$Ro = \frac{2\Omega_z h}{U} \quad \text{or} \quad \Omega = \frac{2\Omega_z h^2}{\nu}$$

The introduction of two different non-dimensional numbers characterizing the effects of rotation is due to the fact that the linear stability problem is preferably solved using Ro since the problem then has certain symmetry properties, whereas for an experimental study Ω is preferable since then Re can be changed by changing U without affecting the rotation parameter, i.e. Ω.

Assuming that the primary instability occurs in the form of counterrotating vortices we can write a neutral disturbance in the form

$$v = \hat{v}(y) \exp\left(i\beta z/2h\right)$$

and the stability equation reduces to

$$\nabla^6 \hat{v} - Re^2 Ro(U' - Ro)\beta^2 \hat{v} = 0$$

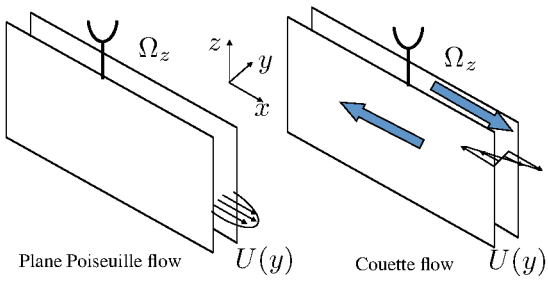

Figure 1: Schematics of spanwise rotating plane Poiseuille and Couette flows.

where $\nabla^2 = d^2/dy^2 - \beta^2$. For plane Couette flow where $U' = 1$ it is possible to show that the neutral stability curve can be given as (see ref. [2])

$$Re^2_{\text{critical}} = \frac{107}{Ro(1 - Ro)}$$

and this gives the lowest critical Re as 20.7 at $Ro = 0.5$. As can be seen instability only exists in the range $0 < Ro < 1$, otherwise the flow is stable.

3 Experimental results

The experimental apparatus used for the rotating Couette flow studies are shown in figure 2. The $Re - \Omega$ space has been mapped in great detail and up to 17 different flow regimes have been observed. One example is shown in figure 3. The details of this mapping and specific flow cases will be given in the presentation.

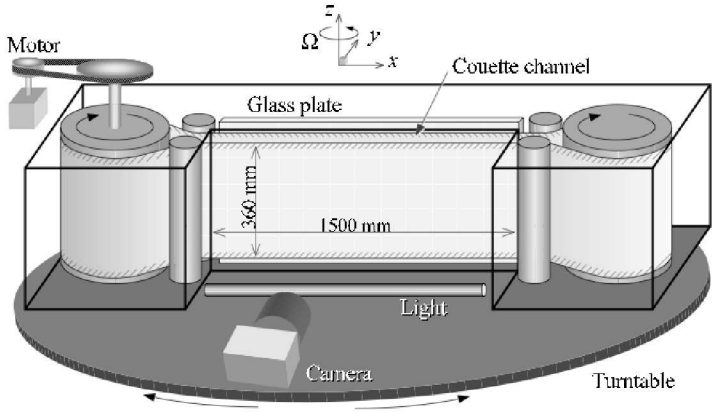

Figure 2: Schematic of the rotating Couette flow channel.

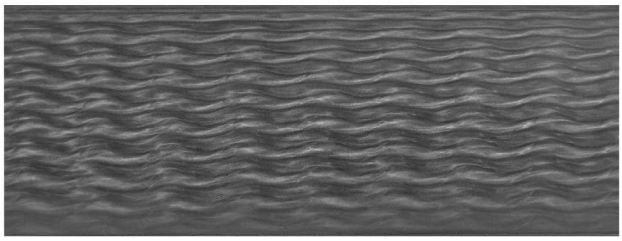

Figure 3: Flow visualization of rotating Couette flow at $Re = 250$ and $\Omega = 21$ from ref. [1].

References

[1] T. Tsukahara, T., N. Tillmark & P.H. Alfredsson 2010 Flow regimes in a plane Couette flow with system rotation. *J.* Fluid Mech. **648**, 5–33.

[2] Lezius, D. K. & Johnston, J. P. 1976 Roll-cell instabilities in rotating laminar and turbulent channel flows. *J. Fluid Mech.* **77**, 153–175.

3 Oral presentations

LOCAL AND GLOBAL STABILITY OF ROTATING DISK BOUNDARY LAYERS

Christopher DAVIES[1], Christian THOMAS[2]
[1]*School of Mathematics, Cardiff University, Cardiff, Wales, United Kingdom.*
[2]*School of Mathematics and Statistics, University of Western Australia, Perth, Australia.*

The von Kármán boundary-layer flow above a rotating disk can be shown to be absolutely unstable, by deploying a local linear analysis where the base flow is artificially simplified by taking it to be homogeneous along the radial direction [5]. Making use of the same approximation to represent the base flow, absolute instability has also been identified for the whole family of rotating disk boundary layers that, through the variation of the Rossby number, continuously connect the Kármán flow to the Bödewadt flow [6]. Moreover, absolute instability still persists if suction is introduced at the disk surface [7] or there is an applied axial magnetic field [4], though its onset is postponed to higher Reynolds numbers. Thus absolute instability is pervasive for rotating disk boundary layers. However, we will illustrate how the results obtained using a localized analysis for the homogenized version of the base flow cannot just be taken, in an immediate manner, to predict the correct global behavior for the genuine radially inhomogeneous base flow. The relationship between the local and global stability properties turns out be rather more complex and interesting than many researchers might have anticipated.

For the case of the von Kármán boundary-layer flow, direct numerical simulations of linearized disturbance development in the genuine flow showed that the predicted absolute instability does not in fact give rise to any unstable linear global modes [1]. This is despite the fact that the temporal growth rates for the absolute instability display a marked increase with the radial distance from the rotation axis [2]. The apparent disparity between the radially increasing strength of the absolute instability and the absence of any global instability can be understood by considering analogous behaviour in impulse solutions of the linearized complex Ginzburg-Landau equation [3]. These solutions show that *detuning*, arising from the radial variation of the temporal frequency of the absolute instability, may be enough to globally stabilize disturbances. Depending on the precise balance between the radial increase in the growth rates and the corresponding shifts in the frequencies, it is possible for an absolutely unstable flow to remain globally stable.

Globally stable behaviour was found to persist in numerical simulations where mass injection was introduced at the rotating disk surface, modifying the base flow. More interestingly, it was discovered that globally unstable behaviour is promoted when suction is applied [8]. This contrasts with the locally stabilizing influence of suction that had previously been identified, using the approximation of a radially homogenized base flow. For the inhomogeneous flow, impulsively excited disturbances display an increasingly rapid temporal growth at the radial position of the impulse, albeit without any selection of a dominant frequency, as would be more usual for an unstable global mode. A similar form of global destabilization, overcoming locally stabilizing effects, was reproduced when an axial magnetic field was applied.

We will discuss numerical simulation results to illustrate the new type of instability, and show how it can be successfully described using impulse solutions of the linearized Ginzburg-Landau equation. More generally, we will review the subtle connections that can persist between the local and global linear behavior, for a range of the rotating disk boundary layer flows that have been mentioned above. For example, the figure depicts the space-time development of a disturbance that was generated in a rotating disk boundary layer with Rossby number $Ro = 0.4$. Results for both the artificially homogenized version of the flow and the genuine flow are shown. The flow parameters were chosen so that, for the homogenized version of the base flow, the disturbance is at the margin of absolutely instability. In marked contrast to what might have been predicted by a naive use of local stability results, it may be very clearly seen that there is a strong form of global stability in the genuine flow. The disturbance is not even convectively unstable, although it does display transient growth.

The previously unsuspected complexity of the relationships between the local and global stability properties of linearized disturbances in rotating disk boundary layers can be expected to have important consequences for any nonlinear developments. It is conceivable that, in some instances, the character of the linearly unstable disturbance may be such as to discount the possibility of any analytical approach to describing the emergence of nonlinearity that, in the interests of tractability, tries to postpone the incorporation of the effects of the inhomogeneity of the base flow. For the case of the rotating disk boundary layer with suction, for example, destabilization due to the radial inhomogeneity may need to be accounted for right from the very outset of the analysis, irrespective of the smallness of the initial disturbance amplitude.

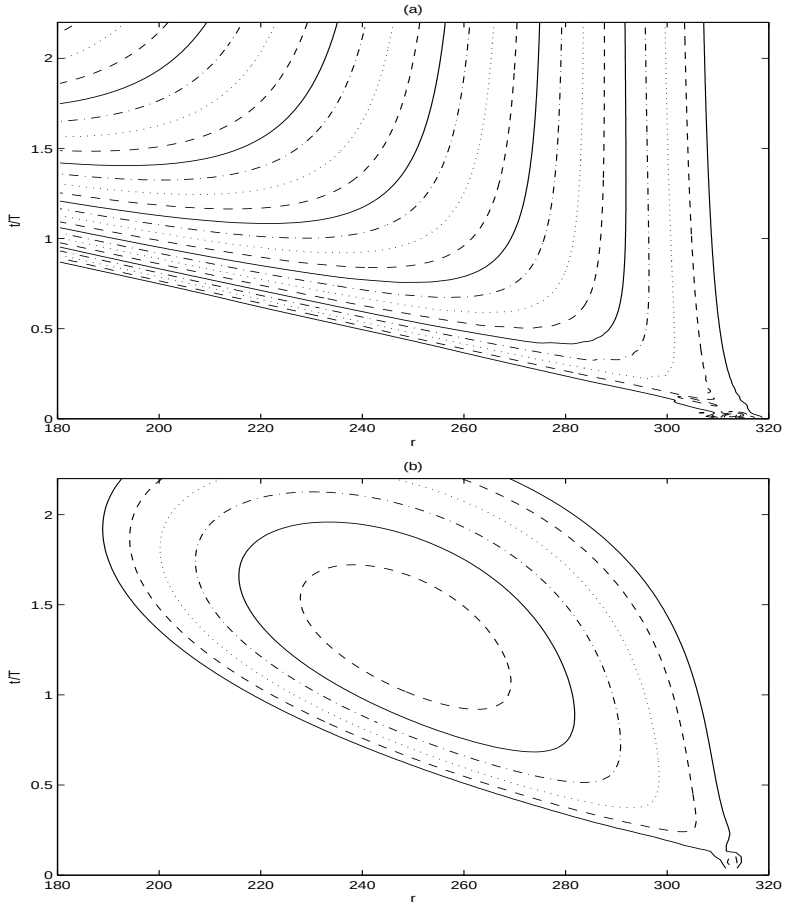

Figure 1: Spatio-temporal development of the azimuthal vorticity at the disk surface for an impulsively excited disturbance with $Ro = 0.4$ and azimuthal mode number $n = 20$. The disturbance was excited at $r_e = Re/Ro = 313$. (a) Homogenized flow with $Re = 125$ (b) Radially inhomogeneous flow.

References

[1] Davies, C. and Carpenter, P. W., Global behaviour corresponding to the absolute instability of the rotating-disc boundary layer, *J. Fluid Mech.*, **486**, 287-329, (2003).

[2] Davies, C. , Thomas, C and Carpenter, P. W, Global stability of the rotating disc boundary layer, *J. Eng. Math.*, **57**, 219-236, (2007).

[3] Hunt, R. E. and Crighton, D. G., Instability of flows in spatially developing media, *Proc. R. Soc. London, Ser A*, **435**, 109-128, (1991).

[4] Jasmine, H. A. and Gajjar, J. S. B., Convective and absolute instability in the incompressible boundary layer on a rotating disk in the presence of a uniform magnetic field, *J. Eng. Math.*, **52**, 337-353, (2005).

[5] Lingwood, R. J., Absolute Instability of the Boundary-Layer on a Rotating-Disk, *J. Fluid Mech.*, **299**,17-33, (1995).

[6] Lingwood, R. J., Absolute instability of the Ekman layer and related rotating flows, *J. Fluid Mech.*, **331**, 405-428, (1997a).

[7] Lingwood, R. J., On the effects of suction and injection on the absolute instability of the rotating-disk boundary layers, *Phys. Fluids*, **9**, 1317-1328, (1997b).

[8] Thomas, C. and Davies C., The effects of mass transfer on the global stability of the rotating-disk boundary layer, *J. Fluid Mech.*, **663**, 401-433, (2010).

AN EXPERIMENTAL STUDY OF LAMINAR-TURBULENT TRANSITION OF A ROTATING-DISK FLOW

Shintaro Imayama, P. Henrik Alfredsson & R. J. Lingwood
Linné Flow Centre, KTH Mechanics, SE-100 44 Stockholm, Sweden.

1 INTRODUCTION

The main objective of this experimental study is to measure the laminar-turbulent transitional region of the rotating-disk boundary layer. In 1921, von Kármán (1921) derived the exact similarity solution of the Navier-Stokes equations for the basic laminar flow on an infinite rotating disk. Typically 28 to 32 stationary vortices are observed within the convectively unstable region in unforced experiments (e.g. Gregory et al. 1955), which are excited by unavoidable roughnesses fixed at the disk surface, but the flow is unstable to travelling modes as well. Lingwood (1995a) suggested that instability on the rotating disk is not only of convective nature but also that the flow becomes absolute unstable at R=510 ($R = r^*(\Omega^*/\nu^*)^{1/2}$, where r^* is the radius of the disk at the measurement position, Ω^* is the rotational speed of the disk, ν^* is the kinematic viscosity of the flow and * means dimensional value). In the present work we map the flow regimes from the stable laminar flow region, through the unstable and transitional regions, into the fully turbulent region.

2 EXPERIMENTAL CONDITIONS

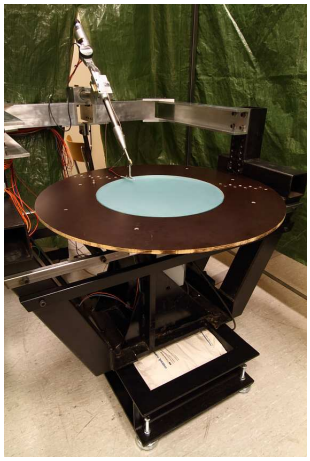

Figure 1: The experimental setup of the rotating disk.

The measurements were performed on a rotating disk shown in Figure 1. The apparatus is in principle the same as used by Lingwood (1996) and has been lent by Cambridge University to KTH, where it has undergone certain modifications. The disk is now made of glass and has a diameter of 474 mm and a thickness of 24 mm and is mounted on the original aluminium-alloy disk. The aluminium-alloy disk is connected to DC-servo motor through an iron disk and a vertical shaft. The air bearing mounted around the shaft is operated with high pressure air to achieve low noise and vibration levels. The surface of the glass disk is polished and the roughness is within 1 μm and the imbalance within 10 μm at the edge of the glass disk. To attenuate the effect of the disk edge, a stationary wood plate is fixed around the glass disk. A single hot-wire probe, operated by a constant temperature anemometer (CTA) with overheat ratio 0.8, is used for the velocity measurement. The sensitive area is made of platinum, with a diameter of 5 μm and a length of 1 mm. The signal from the CTA is digitized using a computer with a 16 bit A/D converter and is sampled at a rate of 720 data points per revolution. The hot-wire is mounted on a two-axis traverse system. One of the traverses moves in the horizontal (radial) direction, and the other traverse is mounted on the horizontal traverse at a 45° inclination to not disturb the axial flow which approaches the rotating disk from above.

The hot-wire orientation makes it mainly sensitive to the circumferential velocity component (i.e. the axis of the sensing wire is aligned with the radial direction) and although the flow is three-dimensional this component is much larger compared to the radial and axial components. The calibration of the hot-wire is carried out on the rotating disk using the theoretical laminar mean profile. The hot-wire was calibrated using a modified King's law to extend the low velocity range (Johansson & Alfredsson,1982). The measurements were carried out at a fixed radius position of 198 mm, varying the Reynolds number with the rotational speed.

3 RESULTS AND DISCUSSIONS

Measured circumferential mean velocity profiles spanning the range $R = 430 - 630$ are shown in Figure 2 . The abscissa axis is the non-dimensional circumferential velocity ($V = V^*/(r^*\Omega^*)$, where V^* is the circumferential velocity). The vertical axis is the non-dimensional height from the wall ($z = z^*(\Omega^*/\nu^*)^{1/2}$, where z^* is the wall normal position of hot wire). At Reynolds number R from 430 to 510, the experimental data correspond to theoretical laminar profile shown as a solid line, except in the very low velocity region where effects of heat convection on the hot-wire are observed. At $R = 550$, deviations of the experimental data from the theoretical

laminar profile can be observed. Lingwood (1995a) suggested that the absolute instability appears at $R = 510$ triggering nonlinear effects that one would expect to generate Reynolds stresses thereby distorting the laminar velocity profile. As the Reynolds number increases, the velocity profile changes completely. At $R = 630$ the boundary-layer thickness has become much larger and the velocity gradient has increased close to the wall.

Figure 3 shows the non-dimensional intensity of the circumferential velocity fluctuation ($v_{rms} = v^*_{rms}/r^*\Omega^*$, where v^*_{rms} is the root mean square of the circumferential velocity) against the wall normal position. At $R = 510$, the peak appears at $z = 1.3$. At $R = 550$, the rms has a higher value not only at $z = 1.3$ but also $z = 4$. At $R = 630$, fluctuations develop over the entire boundary-layer height. Figure 4 shows the spectra at each Reynolds number measured at $z = 1.3$. At around $\omega^*/\Omega^* = 30$, peaks start to appear and the intensity increases with Reynolds number. This result corresponds to the previous study that between 28 and 32 stationary vortices are observed once the individual patterns (generated by individual fixed roughnesses) have merged and filled the whole circumference of the disk. Above $R = 510$ harmonics of the basic frequency starts to appear, but at $R = 630$ the spectrum becomes flat without any distinct peaks characteristic of fully-developed turbulence.

The talk will include a further investigation of the transition region including intermittency and higher moments, as well as details of the turbulent flow itself.

This project is supported by the Swedish Research Council. The first author acknowledges support from the Scandinavia-Japan Sasakawa Foundation. We would also like to acknowledge the help of the late Dr Tim Nickels who was instrumental in arranging the loan of the rotating disk equipment from Cambridge University to KTH.

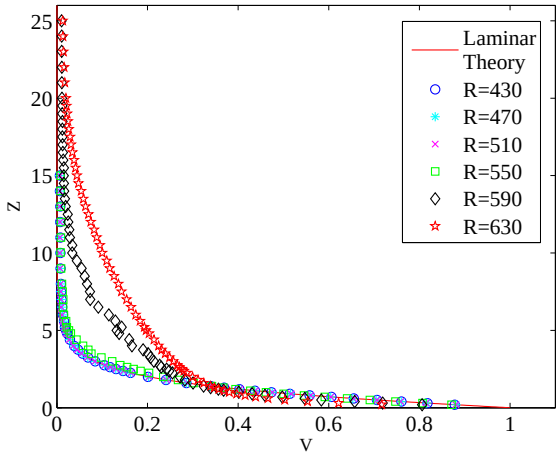

Figure 2: Mean velocity profiles in the range $R = 430 - 630$, spanning the stable laminar region, the unstable, transitional and turbulent regions.

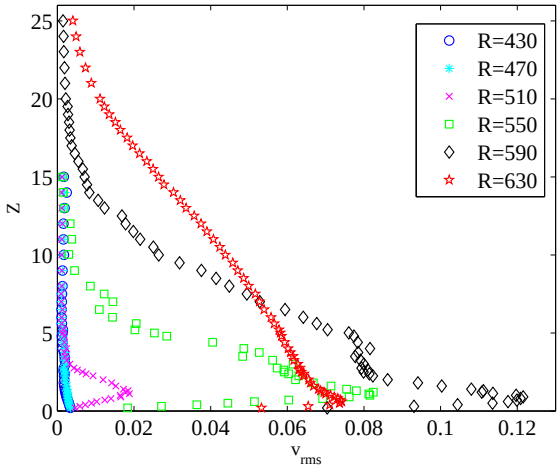

Figure 3: The rms-profiles for the same cases as in Figure 2.

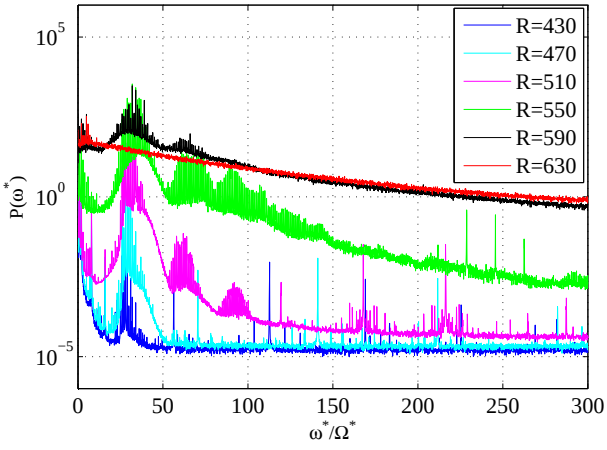

Figure 4: Fourier power spectra for ensemble averaged time series, for $z = 1.3$.

References

[1] V. T. Kármán, Über laminare und turbulente Reibung. *Z. Angew. Math. Mech.* **1**, 233–252 (1921).

[2] N. Gregory, J. T. Stuart, & W. S. Walker, On the stability of three-dimensional boundary layers with application to the flow due to a rotating disk. *Phil. Trans. R. Soc. Lond.* **A 248**, 155–199 (1955).

[3] R. J. Lingwood, Absolute instability of the boundary layer on a rotating disk. *J. Fluid Mech.* **299**, 17–33 (1995a).

[4] A. V. Johansson, & P. H. Alfredsson, On the structure of turbulent channel flow. *J. Fluid Mech.* **122**, 295–314 (1982).

[5] R. J. Lingwood, An experimental study of absolute instability of the rotating-disk boundary-layer flow. *J. Fluid Mech.* **314**, 373–405 (1996).

RESPONSE TO LOCALIZED FORCING OF THE BOUNDARY LAYER ON A ROTATING DISK

Mukund VASUDEVAN, M. Ehtisham SIDDIQUI, Benoît PIER, Julian SCOTT,
Alexandre AZOUZI, Roger MICHELET & Christian NICOT
Laboratoire de mécanique des fluides et d'acoustique (CNRS—Université de Lyon)
École centrale de Lyon, 36 avenue Guy-de-Collongue, 69134 Écully, France.

1 Introduction

The boundary layer that develops over a disk rotating in an otherwise still fluid undergoes an abrupt transition to turbulence at a non-dimensional radius of $R \simeq 500$, and has long served as a canonical configuration for the study of three-dimensional boundary layers [1]. Based on a fully nonlinear analysis and a secondary stability analysis [2], Pier [3] showed that it was possible to delay the onset of secondary perturbations, and hence the transition, by replacing the natural flow state with the response to an appropriate harmonic forcing.

As a first step towards implementing this control strategy, the experiments reported here study the response to a localized forcing applied with a prescribed frequency relative to the disk.

2 Experiments

2.1 Experimental setup

The experimental setup consists of a 50 cm diameter glass disk that is rotated at a constant angular speed Ω_d. The boundary layer on a rotating disk is of constant thickness, with the boundary layer unit given by $\delta = \sqrt{\nu/\Omega_d}$ (a typical value here is $\delta \simeq 550\,\mu$m), where ν is the kinematic viscosity. In the entire study, coordinates are nondimensionalized based on δ and Ω_d.

The forcing assembly consists of a hollow circular cylinder placed above, and concentric with, the disk. The cylinder, whose angular speed may be varied independently of the disk, has provisions for holding pins or forcing elements that extend down into the disk boundary layer and force the flow. In this study, we consider the response to forcing by an isolated forcing element, corresponding to a radially localized perturbation. Two different forcing elements (spherical and cylindrical) were used to see the influence on the flow dynamics.

The azimuthal velocities are measured by a hot-wire anemometer, which is positioned by a high-precision two-axes traversing mechanism.

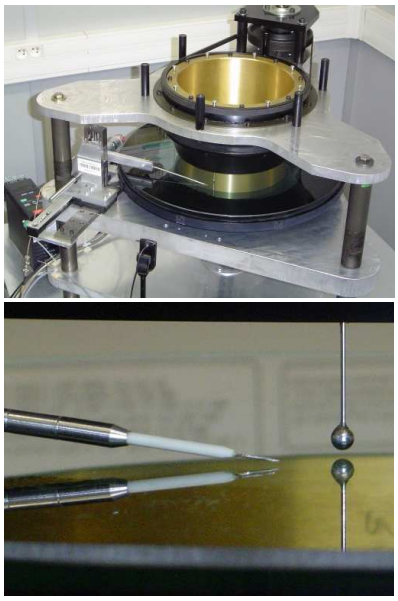

Figure 1: Experimental apparatus and close up of the hot-wire probe and spherical forcing element.

2.2 Response to forcing

The rotation rate of the disk was chosen such that the non-dimensional forcing radius was just below the theoretical onset of convective instability. The forcing elements were rotated at various frequencies ω_f in the range $0 \leq \omega_f \leq 1.0$, with $\omega_f = 1$ corresponding to forcing that is stationary with respect to the disk surface.

Time-series of azimuthal velocity are recorded at different radial and axial locations for a large number of forcing revolutions. To extract those components that are periodic with respect to the forcing, phase-locked averages are computed, which can be interpreted as the mean perturbed flow in the frame of reference of the forcing device.

Figure 2 shows how a forcing at $R_f = 250$ produces perturbation 'humps' that propagate radially outwards, along a trajectory with a nearly constant slope in the (R, θ)-plane. These slopes κ are found to increase with ω_f and to agree extremely well with predictions based on linear theory, as described in the next section.

3 Theoretical analysis

At the radial values of interest, the assumption of weak radial development is legitimate, and small-amplitude perturbations are then written in normal-mode form as $\mathbf{u}(z)\exp \mathrm{i}(\alpha r + \beta\theta - \omega t)$, where the radial wavenumber α, the azimuthal mode number β and the frequency ω are governed by the local dispersion relation

$$\omega = \Omega(\alpha, \beta; R),$$

obtained at each radial location R by solving the associated eigenvalue problem.

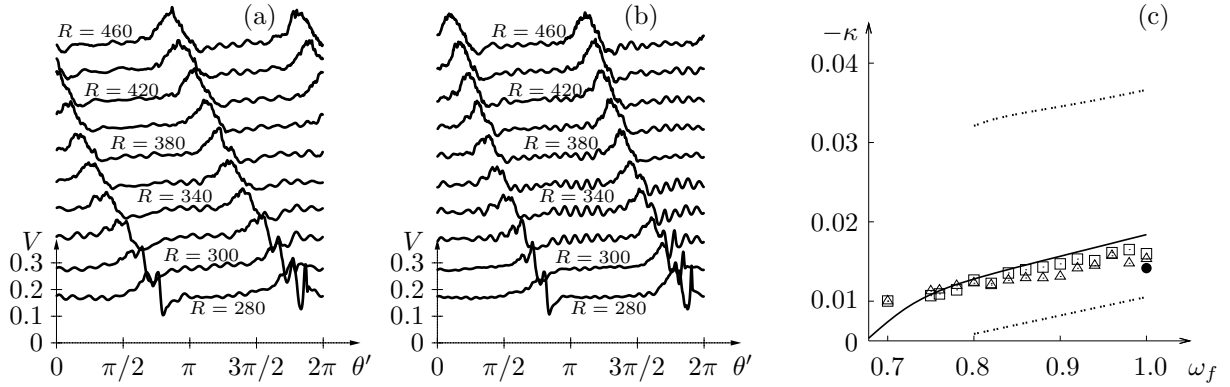

Figure 2: Response to rotating forcing applied at $R_f = 250$ using two forcing elements located at $\theta' = 0$ and π. (a,b) Phase-locked average of azimuthal velocity time series for $\omega_f = 1.0$ (a) and 0.8 (b). Measurements at $R = 280, 300, \ldots, 460$ are each shifted vertically by $\Delta V = 0.1$. (c) Experimentally determined slopes $\kappa = \Delta\theta'/\Delta R$ of the trajectories of perturbation maximum (open symbols) plotted together with the theoretical predictions of the maximum (solid line) and leading and trailing edges (dotted lines). Also shown is the result from experiments [4] with a roughness element fixed to the disk surface (filled circle).

Solving the dispersion relation for complex α with given real values of β and ω yields two spatial branches $\alpha^{\pm}(\beta, \omega; R)$, with the α^{+} branch corresponding to a response developing radially outwards from the forcing.

Now, consider a localized forcing element at radial position r_f rotating at a constant angular frequency ω_f, For simplicity, we consider a local linear theory at $R = r_f$, and assume that the perturbation due to the forcing is steady in the frame of reference of the forcing element. Then, for $r > r_f$, the full spatial response is given by

$$\mathbf{u}(r, \theta, z, t) \simeq \int_{\beta} \mathrm{d}\beta\, \mathbf{u}(z; \beta) \exp \mathrm{i}[\alpha(\beta)(r - r_f) + \beta_f \theta'],$$

where $\alpha(\beta) \equiv \alpha^{+}(\beta, \omega = \beta\omega_f; R = r_f)$ and $\theta' = \theta - \omega_f t$ is the azimuthal coordinate in the forcing frame; $\mathbf{u}$ represents the associated spatial eigenmode. For $r \gg r_f$, the integral may be evaluated by the classical method of stationary phase, and the maximum of the forced response is then expected to follow the ray $\theta'/r = \kappa_{max}$ where the slope κ_{max} is given by

$$\kappa_{max} = -\frac{\mathrm{d}\alpha}{\mathrm{d}\beta}(\beta_{max}) \quad \text{with} \quad \frac{\mathrm{d}\alpha_i}{\mathrm{d}\beta}(\beta_{max}) = 0.$$

The leading and trailing edges of the localized perturbation may be similarly computed.

4 Discussion

Figure 2(c) shows the experimentally measured and theoretically calculated trajectories as a function of the forcing frequency. Despite significant nonlinear effects in the experiment, the trajectory of the maximum of the forced perturbation is found to be in good agreement with the predictions of the local linear theory, over the range of ω_f for which theory predicts an amplified response. The perturbation trajectory for $\omega_f = 1$ also compares well with the results of experiments with a single roughness elements fixed to the disk surface [4]. Measurements using smaller forcing elements, expected to produce a linear response, will also be presented.

References

[1] W. S. Saric, H. L. Reed, and E. B. White, Stability and transition of three-dimensional boundary layers. *Ann. Rev. Fluid Mech.* **35**, 413–440 (2003).

[2] B. Pier, Finite amplitude crossflow vortices, secondary instability and transition in the rotating disk boundary layer. *J. Fluid Mech.* **487**, 315–343 (2003).

[3] B. Pier, Primary crossflow vortices, secondary absolute instabilities and their control in the rotating-disk boundary layer. *J. Eng. Math.* **57**, 237–251 (2007).

[4] S. Jarre, P. Le Gal & M. P. Chauve, Experimental study of rotating disk flow instability. II. Forced flow. *Phys. Fluids* **8**, 2985–2994 (1996).

INSTABILITY OF STATIONARY STREAMWISE VORTICES EMBEDDED IN A SWEPT-WING BOUNDARY LAYER

Viktor KOZLOV[1], Valery CHERNORAY,[2] Alexander DOVGAL[1] & Lennart LÖFDAHL [2]
[1]*Khristianovich Institute of Theoretical and Applied Mechanics SB RAS, Novosibirsk, Russia.*
[2]*Chalmers University of Technology, Göteborg, Sweden.*

1 Motivation

Research results on transition to turbulence in boundary layers testify to a pronounced contribution of streamwise vortices and streaky structures to the laminar flow breakdown. Modulating the base flow, they generate local velocity gradients with high-frequency instabilities starting to grow. The same applies to a swept-wing flow which is unstable to stationary crossflow vortices, the latter being subject to amplifying secondary oscillations. A number of experimental, theoretical and numerical studies has been performed on this topic indicating that the instability phenomenon under the consideration is of much importance during the boundary-layer transition, e.g., [1, 2, 3, 4, 5]; for an overview of the problem see [6].

In the present work we deal with the secondary disturbances of a swept-wing flow perturbed by the stationary vortices at their different transverse spacing. Most of all we are interested in the effect of the spatial arrangement of the vortices on the high-frequency boundary-layer oscillations. To make it clear, wind-tunnel experiments were performed focusing on the laminar flow disturbances excited in a controlled manner.

2 Experimental set-up

The experimental runs were carried out at the Department of Thermo and Fluid Dynamics, Chalmers University of Technology. A wing model with a C-16 profile was tested at a 45 degree sweep angle. The stationary vortices were generated in the laminar boundary layer by an elongated and a circular roughness elements placed one by one on the wing surface. The first of them produced at its tips a pair of isolated vortices of opposite rotation while the second element generated the vortices interacting with each other as is sketched in figure 1. The high-frequency harmonic perturbations evolving along the vortices were excited through a tiny hole on the wing surface behind the roughness elements. In each case, the secondary oscillations were excited underneath the primary vortices.

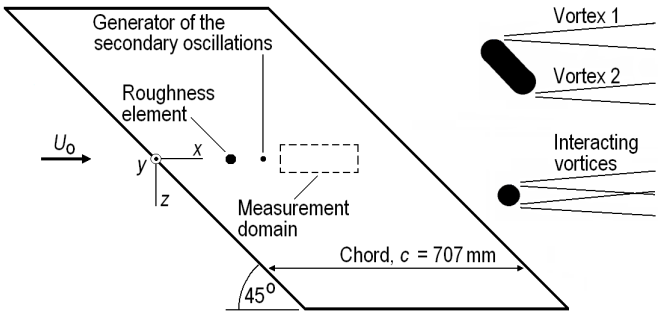

Figure 1: Experimental model and roughness elements generating the stationary vortices.

The flow pattern was examined through hot-wire measurements with single and V-wire probes which were positioned by a computer controlled traversing mechanism. To observe the secondary perturbations, velocity measurements at each point in the spatial domain were phase-locked with the disturbances generator so that volumetric flow patterns were created. Some of the obtained results are illustrated here as iso-surface plots of the nonstationary velocity component taken at a fixed time moment.

3 Wind-tunnel data

In the flow disturbed by the elongated roughness element two vortices (Vortex 1 and Vortex 2) are generated originating at the left-hand and the right-hand sides of the element, respectively. Spaced in the transverse direction, they seem to develop without significant interaction with each other. When changing the elongated

roughness element to the circular one, the counter-rotating vortices interfere at diminution of their spacing, thus, it is expected that mean-velocity gradients generated by the vortices become smaller and the boundary layer is stabilized to the high-frequency disturbances.

Indeed, such an effect was observed comparing the secondary oscillations evolving along the isolated and interacting vortices, an example is given in figure 2. In both cases, the disturbances were excited at low levels of the periodic forcing so that linear oscillations were induced at the position of their generator. As is seen, they appear as oblique waves which are transported in narrow regions of the basic-flow stationary modulation. Riding on the isolated vortex the perturbations are well periodic in the major part of the measurement domain, while propagating away from the generator they amplify and finally result in chaotic motion. One observe that the periodicity of the oscillations is contaminated by small-scale irregularities in the aft part of the box shown at the left of figure 2 testifying to a broad spectrum of velocity fluctuations. Otherwise, at the vortex interaction, the high-frequency disturbances do not evolve into 3D irregular structures so that their coherence is found in the entire measurement domain.

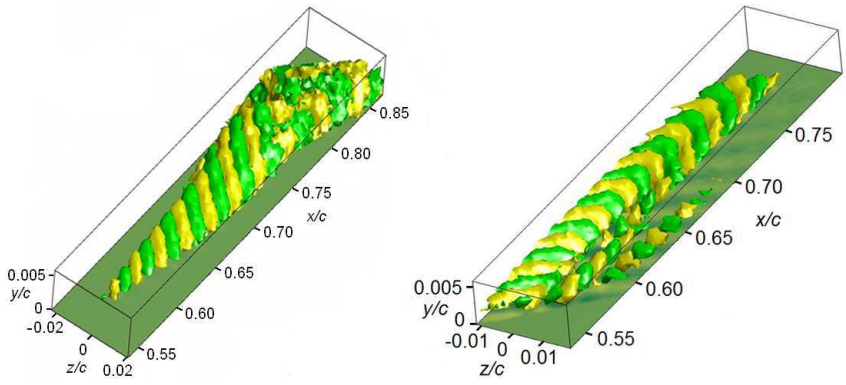

Figure 2: Controlled perturbations of Vortex 1 (*left*) and of the interacting vortices (*right*). Chord Reynolds number is 390,000, excitation frequency is 210 Hz, amplitude levels shown in *yellow* and *green* are ±0.5% of U_0 (*left*) and ±0.1% of U_0 (*right*).

Our conclusion is that the behavior of secondary perturbations involved in the swept-wing transition is quite different depending on the transverse spacing of the primary basic-flow disturbances. That is, amplification of the secondary oscillations is obviously reduced when the isolated counter-rotating vortices start to interact, approaching each other. In this way, the transitional flow can be controlled by roughness elements of a proper configuration, modulating the primary boundary layer perturbations and their secondary instabilities.

The present contribution to EC525 was supported by the Russian Foundation for Basic Research (08-01-00027), the Ministry of Education and Science of the Russian Federation (RNP.2.1.2.541), and the government contract (14.740.11.0354).

References

[1] P. Nitschke-Kowsky, H. Bippes, Instability and transition of a three-dimensional boundary layer on a swept flat plate. *Phys Fluids.* **31**, 786–795 (1988).

[2] E. White, W. Saric, Secondary instability of crossflow vortices. *J Fluid Mech.* **525**, 275–308 (2005).

[3] T. M. Fischer, U. Dallmann, Primary and secondary stability analysis of a three-dimensional boundary-layer flow. *Phys Fluids A.* **3**, 2378–2391 (1991).

[4] M. Malik, F. Li, M. Choudhari, C.-L. Chang, Secondary instability of crossflow vortices and swept-wing boundary-layer transition. *J Fluid Mech.* **399**, 85–115 (1999).

[5] M. Högberg, D. Henningson, Secondary instability of crossflow vortices in Falkner-Skan-Cooke boundary layers. *J Fluid Mech.* **368**, 339–357 (1998).

[6] W. Saric, H. Reed, E. White, Stability and transition of three-dimensional boundary layers. *Annu Rev Fluid Mech.* **35**, 413–440 (2003).

LOCAL LINEAR STABILITY ANALYSIS OF A TURBULENT SWIRLING JET UNDERGOING VORTEX BREAKDOWN

Lothar Rukes, Kilian Oberleithner & Christian Oliver Paschereit
Technische Universität Berlin, Institut für Strömungsmechanik und Technische Akustik, HFI, Müller-Breslau-Straße 8, D-10623 Berlin, Germany

1 Introduction

Swirling jets are known to exhibit a variety of instability phenomena. A number of different stability theories are available today that can partly explain these phenomena. Of the many theories the linear theory applied to a laminar base flow has probably been studied the most. Although this theory is in a strict theoretical sense only valid for a base flow that is a steady solution of the Navier-Stokes-equations, it can be successfully applied to time-averaged turbulent flows [2]. The results of such studies are often in very good agreement with experiments. Oberleithner et al. [4] found the wave-number and frequency of a global mode derived from the local linear theory to be in good agreement with the experimental observations. The goal of this study is to extend the results of [4] by using the linear theory to examine the properties of a global mode in a swirling turbulent jet for different stages of the vortex breakdown. Properties of the global mode are obtained from the results of a local analysis, as shown in Gallaire et al. [1]. Therefore, it is necessary to locate regions of absolute and convective instability in the flow domain. The analysis will be based on the time-averaged turbulent flow derived from PIV-measurements.

2 Experimental setup and data processing

The experimental apparatus used to generate the swirling jet is shown in fig. 1. The three-dimensional velocity-

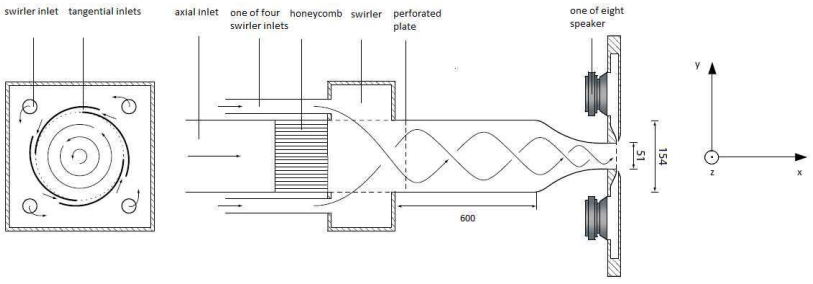

Figure 1: Experimental apparatus (all dimensions are in millimeters) [5]. The used coordinate system is indicated. The measurements presented here were obtained at a Reynolds number of around 21000.

field was measured using a Stereo-PIV system. The laser sheet was introduced perpendicular to the nozzle in the x-z-plane, extending up to seven nozzle diameters in the x- and 3.5 nozzle diameters in the z-direction (positive and negative). Measurements were taken for swirl numbers between 0 and 1.2, covering flow configurations from a non-swirling-jet to a fully developed breakdown state. Especially in the swirl number range between 0.7 and 0.9 measurements were concentrated, because in this range the vortex-breakdown was observed to develop.

3 Numerical method

The numerical discretization method employed is based on a Chebyshev collocation approach [3]. The stability of the flow is analyzed by solving the resulting matrix eigenvalue problem with MATLABs eig-, respectively eigs-routine. In order to find the saddle-points determining the type of the instability a method adapted from [6] is used. This method is based on a truncated Taylor-series expansion around the saddle point. Because the truncated series can only be expected to converge in the vicinity of the saddle-point, good starting values are needed. These are obtained by constructing a global picture and the corresponding cusp map at two axial positions and identifying the relevant saddle points by human eye. From these two known saddle points the wave-number and frequency of the relevant saddle point at the next axial location can be extrapolated and the

truncated Taylor series in conjunction with the eigs-routine is used to converge to the exact wave-number and frequency of the saddle-point.

4 Results

An exemplary result of the analysis is given in fig. 2. The streamline-plot illustrates the analyzed flow and the bottom right plot provides a magnified view of the absolutely unstable region. The computational code used to produce this graph was used in [4] as well, thus demonstrating that it produces correct predictions of the global modes frequency and wave-number. Furthermore, the existence of two regions of absolute instability seems plausible, since Gallaire et al. [1] found a similar behavior in their study. The results of the stability analysis are expected to provide a better understanding of the mode selection of the naturally occurring global mode and its properties. Additionally, the results are supposed to shed light on the global modes interaction with the dynamics of the vortex breakdown.

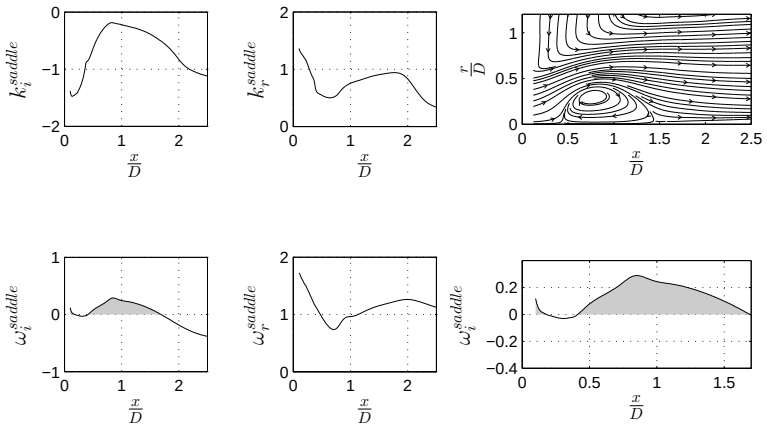

Figure 2: Wave-number k and frequency ω at the saddle point location for one measurement, plotted over the nondimensionalized axial coordinate (D denotes the nozzle diameter). The swirling jet exhibits vortex-breakdown in this case. The azimuthal wave-number was set to one, which is the azimuthal wave-number of the naturally occurring mode, as it is observed from experimental data. Two regions of absolute instability are present (indicated by gray shading in the graph). One immediately downstream of the nozzle exit and the other one in the region of the breakdown bubble.

References

[1] F. Gallaire, M. Ruith, E. Meiburg, J.-M. Chomaz, and P. Huerre. Spiral vortex breakdown as a global mode. *Journal of Fluid Mechanics*, 549:71–80, 2006.

[2] M. Gaster, E. Kit, and I. Wygnanski. Large-scale structures in a forced turbulent mixing layer. *Journal of Fluid Mechanics*, 150:23–39, 1985.

[3] M. R. Khorrami, M. R. Malik, and R. L. Ash. Application of spectral collocation techniques to the stability of swirling flow. *Journal of Computational Physics*, 81:206–229, 1989.

[4] K. Oberleithner, M. Sieber, C. N. Nayeri, C. O. Paschereit, C. Petz, H.-C. Hege, B. Noack, and I. Wygnanski. Self excited oscillations in swirling jets: Stability analysis and empirical mode construction. In *Bulletin of the American Physical Society, 63rd Annual Meeting of the APS Division of Fluid Dynamics*, volume 55. American Physical Society, 2010.

[5] K. Oberleithner, M. Sieber, C. N. Nayeri, C. O. Paschereit, C. Petz, H.-C. Hege, B. R. Noack, and I. Wygnanski. Three dimensional coherent structures of the swirling jet undergoing vortex breakdown: Stability analysis and empirical mode construction. submitted for publication in Journal of Fluid Mechanics 2010.

[6] S. J. Rees. *Hydrodynamic instability of confined jets & wakes & implications for gas turbine fuel injectors.* PhD thesis, Department of Engineering, University of Cambridge, 2009.

SENSITIVITY ANALYSIS OF SPIRAL VORTEX BREAKDOWN

Ubaid QADRI, Dhiren MISTRY & Matthew JUNIPER
Department of Engineering, Trumpington Street, Cambridge, CB2 1PZ, U.K.

1 Introduction

Vortex breakdown occurs in some swirling flows, such as those in gas turbine combustion chambers. Ruith *et al* [1] and Gallaire *et al* [2] established that the initial breakdown is steady and axisymmetric but that an unsteady spiralling breakdown mode develops on top of this, due to a region of absolute instability.

In this paper, we investigate the linear stability of the steady axisymmetric solutions obtained by Vyazmina *et al* [3] for vortex breakdown in incompressible flows at Re = 200. We compare local and global stability analyses and relate the global behaviour of the flow to its local stability properties. Using results from the global stability analysis, we map the regions of the flow that are most sensitive to external forcing and internal feedback.

2 Methodology

We use a Low Mach Number (LMN) formulation of the Navier–Stokes (N–S) equations to obtain steady axisymmetric solutions in a cylindrical domain with open lateral and convective outlet boundaries. The Grabowski velocity profile [1] is imposed at the inlet. We study the linear stability of these flows for a range of values of the swirl parameter.

In the global stability analysis, we superpose small perturbations of the form $\hat{\mathbf{u}}(x,r)\exp(\mathrm{i}m\theta+\sigma t)$, where m is the azimuthal wavenumber and σ is the complex eigenvalue. The direct and adjoint Linearized N–S (LN–S) equations are discretized with a compact finite difference scheme in space and a 4^{th} order Runge Kutta scheme in time. The resultant matrix eigenvalue problems are solved with the implicitly restarted Arnoldi algorithm. The regions that are most sensitive to external forcing and internal feedback are found from the direct and adjoint eigenmodes [4].

In the local stability analysis we apply the WKBJ approximation (*i.e.* we assume a locally parallel base flow) and superpose small perturbations of the form $\hat{\mathbf{u}}(r)\exp(\mathrm{i}(kx+m\theta-\omega t))$, where k is the local complex wavenumber and ω is the local complex angular frequency. The absolute frequency, ω_0, is calculated at each axial location. This distribution of ω_0 is interpolated with a Padé polynomial and then continued analytically into the complex x-plane. The linear global frequency, ω_g (which is equivalent to $\mathrm{i}\sigma$), and the wavemaker position are estimated from the position of the relevant saddle point of ω_0 in the complex x-plane. The response of each slice to the estimated global frequency, ω_g, is then calculated and the WKBJ approximation is inverted in order to obtain the mode shape $\tilde{\mathbf{u}}(x,r)$.

3 Results

Figure 1 shows the base flow at a swirl parameter of $Sw = 1.0$, together with the absolute growth rate, the most unstable direct and adjoint global modes and the structural sensitivity maps for $m = 1$ helical perturbations. There is an axisymmetric breakdown bubble around $x = 1$, which causes a wake downstream. The global stability analysis predicts one unstable eigenmode, which has $\mathrm{i}\sigma = 1.1655 + 0.0352\mathrm{i}$. This matches the results from nonlinear DNS [1], suggesting that linear wavefront theory is valid in this case. The direct global mode, which represents the flow structure that dominates in the long time limit, has maximum amplitude at $x = 9$, in the wake downstream of the bubble. The adjoint global mode, which represents the most unstable initial condition or the receptivity of the direct mode to external forcing, is localized between the inlet and the upstream edge of the bubble.

The direct and adjoint global modes are combined to give the structural sensitivity maps. These show where a modification in the linearized equations produces the greatest drift of the eigenvalue [4]. The first map shows the regions that have most influence on the growth rate of the direct global mode. The second map shows the regions where there is maximum coupling between the direct and adjoint velocity components, which indicates the core of the instability (Fig. 17 of [4]). We find that the instability core (as defined by [4]) is located in the upstream end of the breakdown bubble. By considering the global stability of the breakdown bubble and the wake separately, we find that the global frequency of the flow matches that of the bubble rather than that of the wake. We conclude that the wavemaker region is in the recirculation bubble, contrary to expectation.

The local stability analysis predicts two regions of absolute instability: a small region corresponding to the bubble and a large region corresponding to the wake. We find that the instability core obtained from the global analysis corresponds to the region of absolute instability in the bubble. This supports the conclusion that the linear global mode is being driven by a wavemaker situated in the breakdown bubble.

For a given azimuthal wavenumber, m, more eigenmodes become unstable as the swirl increases. Furthermore, eigenmodes at higher m also become unstable as the swirl increases. The local analysis indicates that there are one or two valid saddle points (*i.e.* k^+/k^- pinch points) at each streamwise location. Broadly, these group into one saddle point that dominates in the bubble and another saddle point that dominates in the wake. As the swirl increases, the saddle point in the wake becomes more absolutely unstable.

We find that the local analysis is valid only for slowly developing, weakly non-parallel flows. Furthermore, it cannot conclusively identify the location of the wavemaker region in flows which have more than one region of absolute instability.

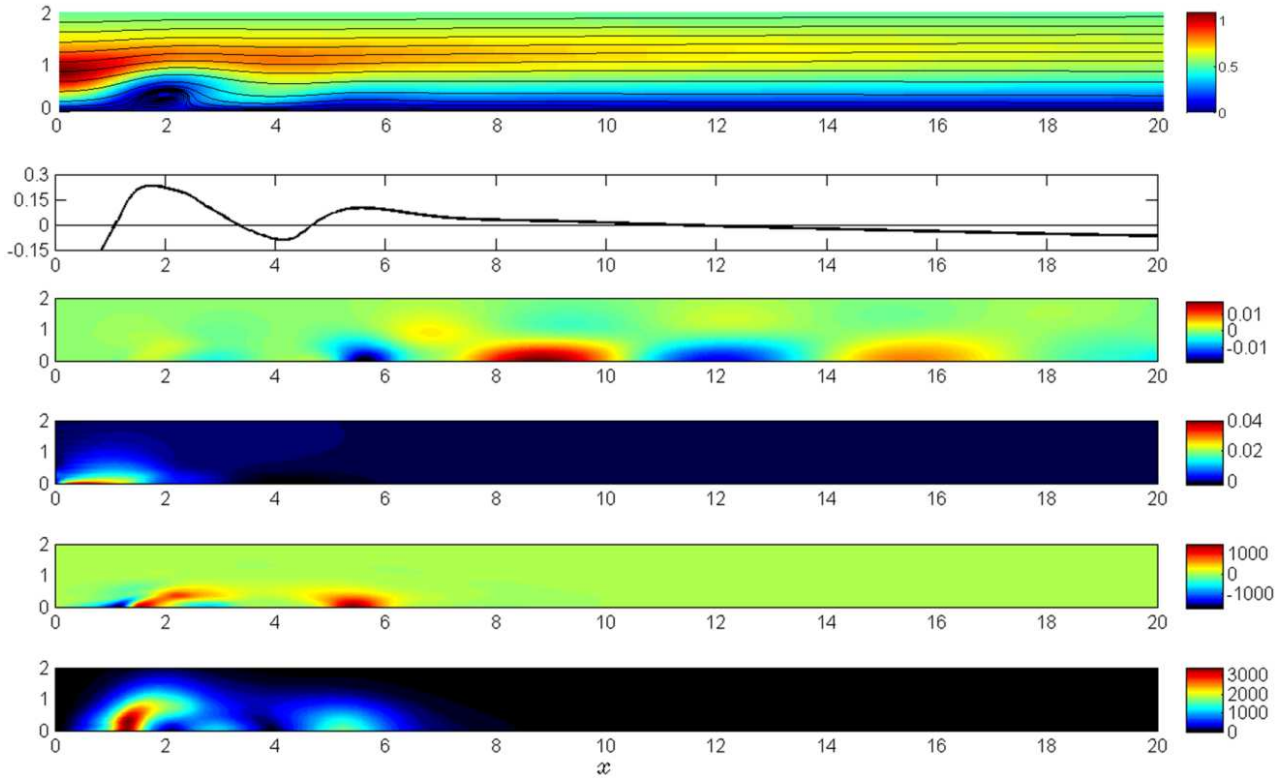

Figure 1: (a) streamlines and azimuthal velocity (colour) of the base flow for $Sw = 1.0$; (b) local absolute growth rate, $\omega_{0,i}$; (c) real component of the direct global mode for radial velocity; (d) real component of the adjoint global mode for radial velocity; (e) sensitivity of growth rate; (f) structural sensitivity as defined by [4]

References

[1] M. R. Ruith, P. Chen, E. Meiburg, T. Maxworthy. Three-dimensional vortex breakdown in swirling jets and wakes: direct numerical simulation. *J. Fluid Mechanics*, **486**, 331–378 (2003).

[2] F. Gallaire, M. R. Ruith, E. Meiburg, J-M. Chomaz, P. Huerre. Spiral vortex breakdown as a global mode. *J. Fluid Mechanics*, **549**, 71–80 (2006).

[3] E. Vyazmina, J. W. Nichols, J-M. Chomaz, and P. J. Schmid. The bifurcation structure of viscous steady axisymmetric vortex breakdown with open lateral boundaries. *Phys. Fluids*, **21**, 74107 (2009)

[4] F. Giannetti, P. Luchini. Structural sensitivity of the first instability of the cylinder wake. *J. Fluid Mechanics*, **581**, 167–197 (2007)

EUROMECH Colloquium 525, 21-23 June 2011, Ecully, France
Instabilities AND TRANSITIONS IN THREE-DIMENSIONAL FLOWS WITH ROTATION

Structural Transitions and Stability Issues in Swirling Compressible Flows

Alexander Ni
ALSTOM (Switzerland) Ltd.,Future Technologies Execution Zentralstrasse 40, CH-5242 Birr, Switzerland

A theory similar to that of Laval Nozzle is developed for swirling compressible flows in annular axisymmetric ducts. On the basis of this theory structural transitions in these flows and their stability are examined. The goal of the study is to provide a simple unified view of the topic, which gives insight into the key physical features, and the overall parametric dependence of the transitions behavior.

Vortex breakdown and shock waves are well-known flow structural transitions in many flows of technological interest. Being a useful flow element in gas turbine combustors as a flame holder, a vortex breakdown may stimulate a flow separation and corresponding undesirable losses in diffusers. Control of a vortex breakdown and shock wave is a serious technical challenge. Theory of shock waves is well advanced. In classical gas dynamics shock wave represents a surface where flow parameters change by jump, being connected by Hugoniot-Rankine conditions. In some cases this approximation does not work, and internal shock wave structure must be considered. The general theory of a vortex breakdown describing quantitatively all its aspects still does not exist despite the importance of the problem, and the efforts expended on it over a period of more than fifty years. This is due to extreme complexity of the flow.

Internal compressible swirling flows are of a growing interest for needs of modern technologies: supersonic compressors, supersonic separators in oil-processing industry etc. One of the main challenges of these technologies is a reduction of pressure losses. It makes an understanding of flow transitions from subsonic to supersonic regimes and vice versa to be the key issue for proper aerodynamic channel shape design. Currently a main theoretical instrument for complex flow prediction is computational fluid dynamics. However, analytical methods like the Laval Nozzle theory still preserve their importance for flow evaluations. Their advantage is in ability to capture main physical factors governing complex flows. In the paper a theory similar to that of Laval Nozzle is developed for swirling compressible flows. The presented analysis predicts existence of both structural transitions corresponding to vortex breakdown at low Mach numbers, and those analogous to shocks in supersonic velocities range. As distinct from non-swirled flows the “evolutionarity” (stability) of transitions is controlled by inertia waves. This fact was postulated for vortex breakdown in incompressible flows by Benjamin in [1] and is generalized in the article to the case of compressible flows. It is established that for each type of transition a wave mode responsible for its “evolutionarity” exists. Benjamin’s concept of flow transitions is linked closely with duct geometry. Benjamin treated a flow transition as a jump between flow states having same flow radial boundaries and flow integrals. These states can be connected virtually in a continuous way by introduction a duct of an appropriate shape. It is shown that the virtual duct must contain a critical cross-section (its geometrical interpretation is given in the text) where the speed of a corresponding to the transition wave mode turns to zero. The number of possible critical duct cross-sections coincides with the number of possible transitions and

depends on inlet flow parameters distribution. In all previous publications only first eigenmodes were considered to propagate in swirling flow. We show that higher orders eigenmodes are also possible. The proposed in the article approach allows easily investigate flows with arbitrary inlet density, entropy, velocity distributions. It is particularly important for analysis of flows in combustors where variations of these parameters are large. The approach provides guidelines for design of transitions-free channels.

Stability analysis of swirling flows relative 3D helical perturbations shows strong influence of losses to flow stability.

References

[1] Benjamin, T.B. 1962. Theory of the vortex breakdown phenomenon. J. Fluid Mech.14, 593-629.

CONTROL OF VORTEX BREAKDOWN BY DENSITY EFFECTS

Patrice MEUNIER[1], Mohd-Zulhilmi P. ISMADI[2,3], Andreas FOURAS[2] & Kerry HOURIGAN[2,3]
[1]*Institut de Recherche sur les Phénomènes Hors Equilibre,*
49 av. Joliot-Curie, 13384 Marseille Cedex 13, France.
[2]*Division of Biological Engineering and* [3]*Department of Mechanical and Aerospace Engineering,*
Monash University, Melbourne, VIC3800, Australia.

The flow inside a cylinder with a rotating end has been recently proposed as a suitable bioreactor for cells growth[1]. Indeed, it creates an efficient laminar mixing which is necessary for the homogeneization of oxygen and nutrients, and for the removal of carbon dioxide. Moreover, the shear created by this flow is much lower than in standard bioreactors which use a magnetic stirrer (rod, barrel or paddle). The properties and control of this flow are thus of critical importance for biological applications.

This flow is well known to lead to a vortex breakdown bubble[2]. Several attempts to control the transition to vortex breakdown have implied the use of a rotating rod[3] or disk[4], but these set-ups were either intrusive or needed a fast rotation speed. Recent numerical results[5] have shown that this flow is extremely sensitive to density differences. The goal of this study is thus to test experimentally this alternative method.

We present experimental results on the control of vortex breakdown inside a cylinder with a rotating top lid. The vortex breakdown is controlled by injecting at the bottom a fluid with a small density difference. The density difference is obtained by mixing a heavy dye or alcohol to water in order to create a jet heavier or lighter than water. The injection of a heavy fluid creates a buoyancy force toward the bottom, which counteracts the recirculation in the cylinder and thus enhances the formation of a vortex breakdown bubble. The stability diagram shows that even a very small density difference of 0.02% is able to decrease by a factor two the critical Reynolds number of appearance of the breakdown. On the other hand, the injection of a light fluid does not destroy the vortex breakdown. However, for large enough density differences (larger than 0.03%), the light fluid is able to pierce through the bubble and leads to a new structure of the vortex breakdown, as shown on figure 1.

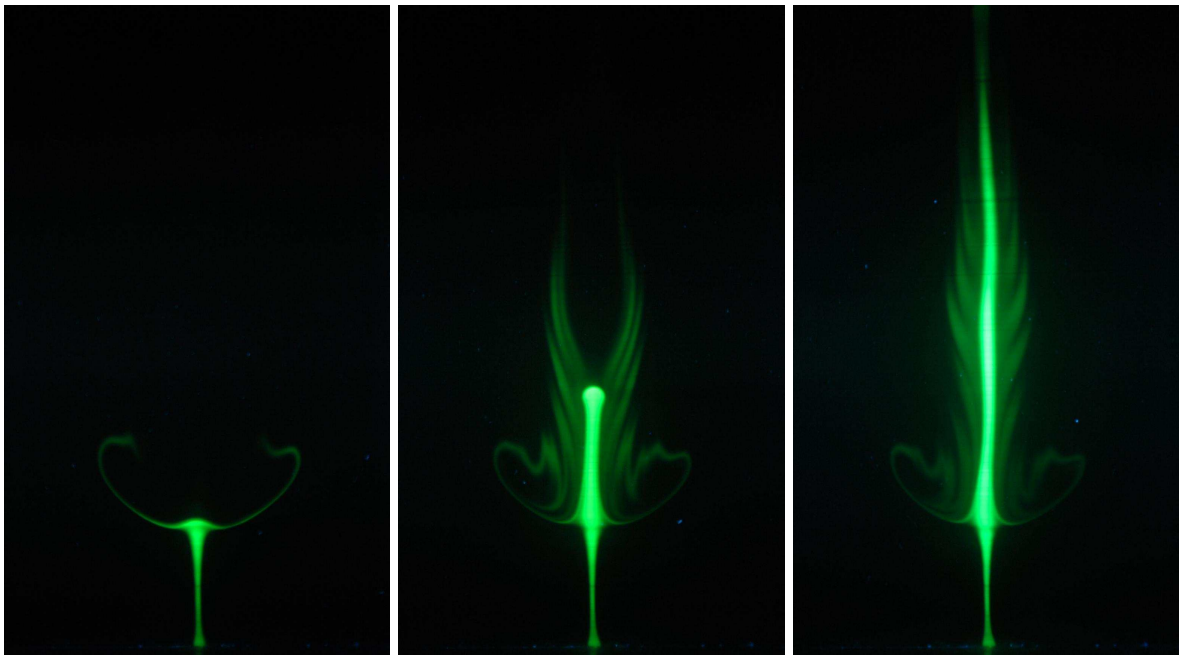

Figure 1: Temporal evolution of a light dye injected below the vortex breakdown and which pierces through the bubble without its destruction. Density difference: $\Delta\rho/\rho_0 = -2.3\ 10^{-4}$. $Re = 2423$.

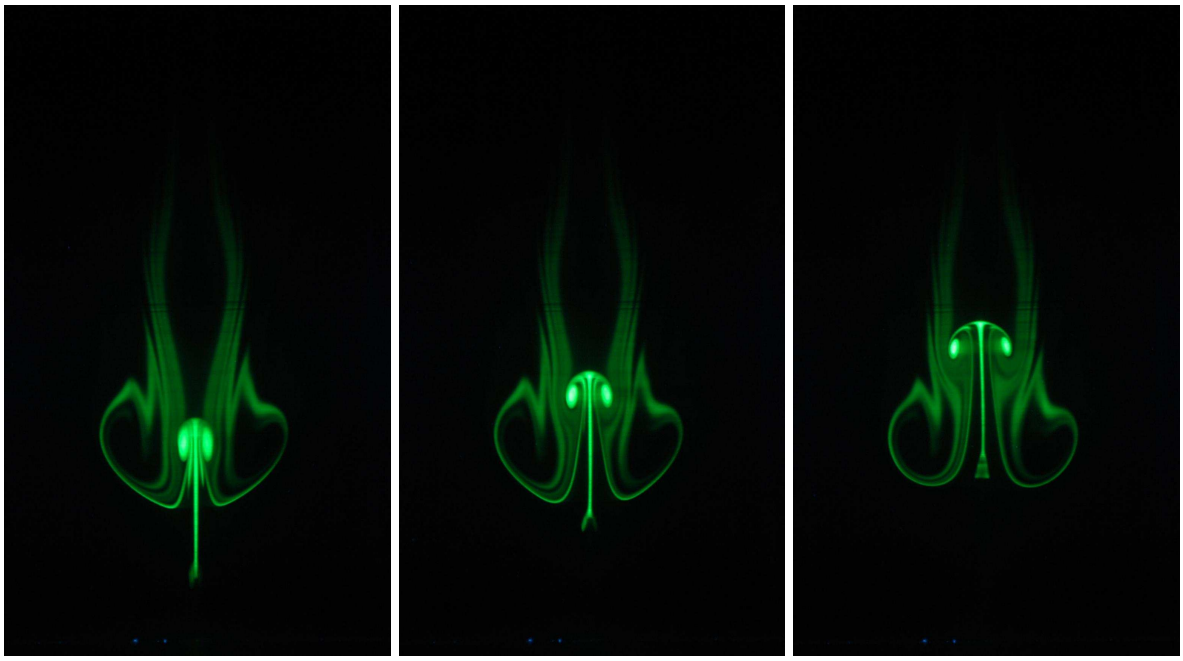

Figure 2: Temporal evolution of a strong vortex ring impacting the vortex breakdown and piercing through the bubble. $Re = 2000$.

Finally, a parallel is drawn between a light jet and a vortex ring generated at the bottom of the cylinder: strong vortex rings are able to pierce through the bubble, as shown on figure 2, whereas weak vortex rings are simply advected around the bubble.

Additionally, the mixing efficiency of this flow will be briefly mentioned. It has been studied quantitatively by measuring the temporal decay of the variance of the spatial dye distribution. The mixing time, required for homogeneization of the dye, scales on the slow molecular diffusive time for a perfectly axisymmetric flow. However, the presence of a small tilt of the end plates breaks the symmetry and strongly accelerates the mixing. In this case, the mixing time scales on the convective time and can be a few orders of magnitude lower even for small tilt angles.

References

[1] J. Dusting, J. Sheridan & K. Hourigan, A fluid dynamics approach to bioreactor design for cell and tissue culture, *Biotechnology and Bioengineering*, **94**, 1196–1208 (2006).

[2] P. Escudier, Observations of the flow produced in a cylindrical container by a rotating endwall. *Exp. Fluids*, **2**, 189–196 (1984).

[3] H. Husain, V. Shtern & F. Husain, Control of Vortex Breakdown by addition of near-axis swirl. *Phys. Fluids*, **15**, 271 (2003).

[4] L. Mununga, K. Hourigan, M. C. Thompson and T. Leweke, Confined Flow Vortex Breakdown Control using a small rotating disk. *Phys. Fluids*, **16**, 4750–4753 (2004).

[5] M. A. Herrada & V. Shtern, Control of Vortex Breakdown by Temperature Gradients. *Phys. Fluids*, **15**, 3468 (2003).

[6] M. P. Ismadi, P. Meunier, A. Fouras and K. Hourigan, Experimental control of vortex breakdown by density effects, *to appear in Phys. Fluids* (2011).

LARGE EDDY SIMULATION OF SWIRLING JET FLOW UNDERGOING VORTEX BREAKDOWN INCLUDING NOZZLE MODELING

Tobias Luginsland, Leonhard Kleiser
Institute of Fluid Dynamics, ETH Zurich, 8092 Zurich, Switzerland

1 Scientific background and objectives

Swirling jets undergoing vortex breakdown occur in many technical applications, e.g. vortex burners, turbines and jet engines. At the stage of vortex breakdown the flow is dominated by a conical shear layer and a large recirculation zone around the jet axis. This highly nonlinear flow state additionally features hysteresis behaviour, bistability, i.e. different flow states occuring at the same values of control parameters, and bifurcation. Despite decades of intense research there is still no consensus found about the underlying mechanism leading to this abrupt change of flow [1]. In their experimental investigation Liang & Maxworthy [2] suggest the existence of a pocket of absolute instability in the wake of the jet triggering a global mode overwhelming the whole flow. In a recent investigation [3] a co-rotating, counter-winding helical mode is found with its 'wave-maker' located in the inner region of the jet. A preceding investigation of our group [4] showed that our DNS/LES code CONCYL is capable of capturing the fundamental physics of swirling jets undergoing vortex breakdown, see also [5]. The results showed good qualitative agreement with experimental data for a self-excited and a forced jet. The fact that the breakdown occurred directly after the inflow plane was considered to possibly prevent the development of self-excited instabilities due to the presence of an inflow sponge layer.
To account for more realistic inflow boundary conditions, in the present work a rotating nozzle is included in the computational domain [6]. A Re=5000, Ma=0.6 swirling jet with the azimuthal velocity component as high as the streamwise component (swirl number S=1.0) is investigated by LES along the lines of [4]. The simulation is done on a domain with size $L_r \times L_z = 10R \times 20R$ in the radial and streamwise directions with a nozzle of length $L_n = 6R$ included, where R is the nozzle radius. The grid resolution is $N_\theta \times N_z \times N_r = 36 \times 180 \times 216$ grid points. Our work is in progress and preliminary results are presented and will be compared to recently published results in the literature.

2 Simulation methodology and Results

Our simulation code, recently parallelized for massively parallel architectures, solves the compressible Navier-Stokes equations in cylindrical coordinates [7]. Spatial derivatives are calculated using high-order finite difference schemes (up to 10th order) for the streamwise and radial directions while a Fourier spectral method is employed in the circumferential direction. Time integration is done applying a 4th-order 6th-stage LDDRK scheme developed for investigating aeroacoustics of jets [8]. As a subgrid scale model we use our in-house Approximate Deconvolution Model (ADM). Boundary conditions are chosen in analogy to [4] and the nozzle is modelled as an isothermal wall.
Figure 1 shows the development of $\langle\theta, t\rangle$-averaged profiles for all three velocity components. At the jet axis a deficit in the streamwise velocity develops, with the profile changing from jet- to wake-like within the downstream part of the nozzle indicating beginning vortex breakdown. At the same downstream position the azimuthal velocity profile start to deviate from the initial solid-body rotation. Behind the nozzle both velocity components are largest within the azimuthal shear layer accompanied with a rising radial velocity component related to the massive spreading of the jet. The recirculation is strongest around $z = 7.5R$ representing the core of the recirculation bubble, which has a length of about $2R$. Within the nozzle pressure and density (not shown) increase in the downstream direction, adapting to far-field values right behind it.
Instantaneous contours of the streamwise, w, and azimuthal, v, velocity components are plotted in figure 2. The local recirculation near the centerline is much stronger compared to the averaged data. The rapid breakup of the conical shear layers is visible. In the recirculation zone the fluid counter-rotates with respect to the mean flow, an effect also reported by Facciolo et al. [9]. Compared to results stated in [4] the spreading angle of the jet is larger.
An analysis of the instantaneous stagnation point location shows that it travels upstream, shifting up- and downstream around $z = 6.5R$ precessing around the jet axis in a counter-clockwise manner. Iso-surface plots of the pressure show a helical, counter-winding mode, co-rotating with the mean flow, similar to structures observed by Billant et al. [10] for the post-breakdown stage.

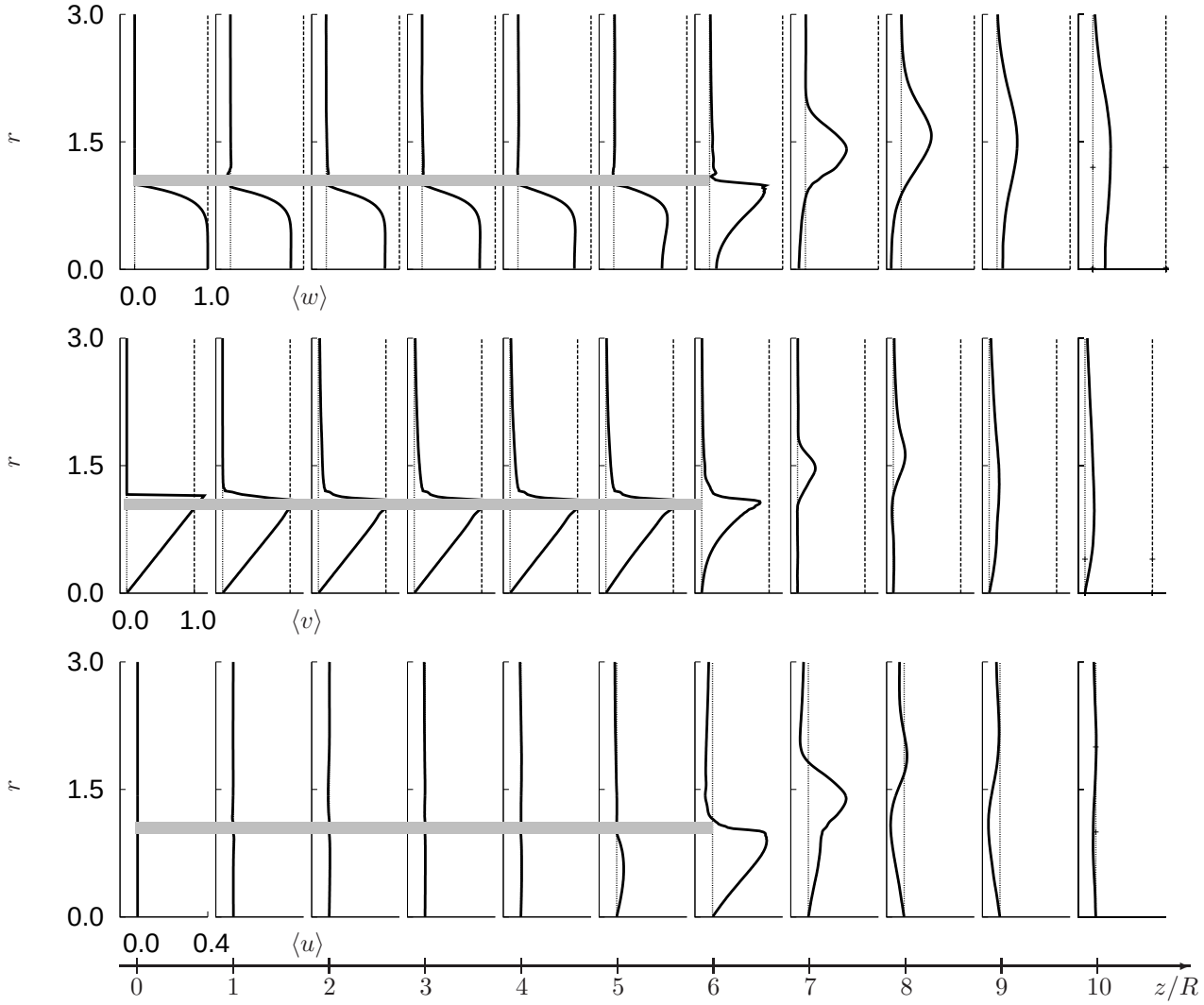

Figure 1: Axial development of mean streamwise, azimuthal and radial velocity (top to bottom). The grey bar indicates the position of the nozzle wall.

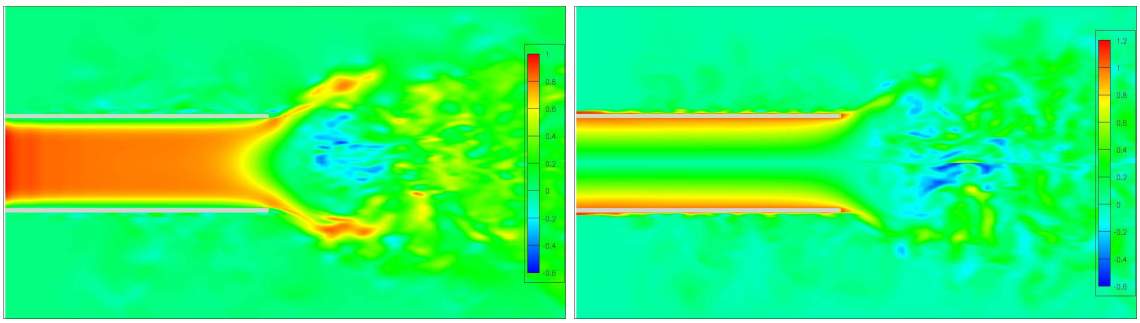

Figure 2: Contour plots of the instantaneous streamwise (left) and azimuthal (right) velocity at 20 flow-through times.

References

[1] O. Lucca-Negro and T. O'Doherty, *Prog Energy Combust Sci* **27**, 431–481 (2001).
[2] H. Liang and T. Maxworthy, *J. Fluid Mech* **525**, 115–159 (2005).
[3] K. Oberleithner, C. N. Nayeri, C. O. Paschereit and I. Wygnanski, *EFMC8* (2010).
[4] S. B. Müller and L. Kleiser, *Computers & Fluids* **37**, 844–856 (2008).
[5] S. B. Müller, *ETH Dissertation* **17375** (2007).
[6] S. Bühler, T. Luginsland, D. Obrist and L. Kleiser, *Proc. Appl. Math. Mech.* **10**, 443–444 (2010).
[7] T. Luginsland, S. Bühler, D. Obrist and L. Kleiser, *Proc. Appl. Math. Mech.* **10**, (2010), to appear.
[8] J. Berland, C. Bogey and C. Bailly, *Computers & Fluids* **224**, 637–662 (2007).
[9] L. Facciolo, N. Tillmark, A. Talamellil and P.H. Alfredsson *Phys. Fluid* **19**, 1–18 (2007).
[10] P. Billant, J.-M. Chomaz and P. Huerre *J. Fluid Mech* **376**, 183–219 (1998).

FAN TONE GENERATION IN AN ISOLATED ROTOR DUE TO UNSTABLE SECONDARY FLOW STRUCTURES

Daniel Wolfram[1], Thomas Carolus[2] & Michael Sturm[2]
[1] *Pollrich Ventilatoren GmbH, 41065 Mönchengladbach, Germany.*
[2] *University of Siegen, Departement of Fluid- and Thermodynamics, 57068 Siegen, Germany.*

Both centrifugal and axial fans are used in many applications like ventilation systems or cooling units and thus being subject of our everyday life. Due to official restrictions and the increasing consideration of comfort factors the acoustic performance of that kind of machines becomes more and more important. A typical acoustic spectrum of a fan consists of both broadband and tonal components, see figure 1. Often, the overall acoustic level is dominated by the tonal part, especially the tone at blade passing frequency (BPF) and higher harmonics. The source mechanism for the BPF noise of centrifugal fans typically refers to the interaction between the blade channel flow and guide vanes or the volute-cutoff. In case of an axial fan the rotor-stator interaction is often the source of BPF noise. For both types of fans an isolated rotor should not exhibit tonal noise at the blade passing frequency. However, measurements show the opposite. As shown by many authors [1, 2], the steady loading of the blades as well as the volume displacement by the moving blades can not be the source of the BPF noise for fans with a low characteristic circumferential Mach number. Thus, the detailed noise generating mechanism of the BPF noise of an isolated fan rotor is still unknown.

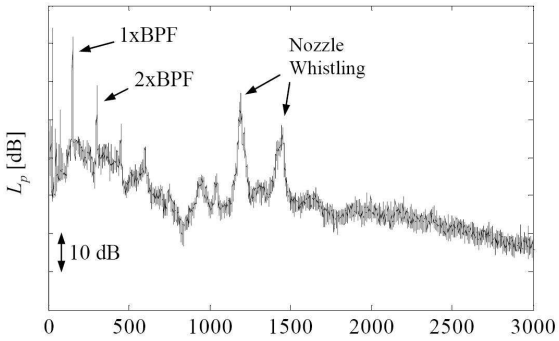

Figure 1: Noise spectrum of an isolated centrifugal impeller near design point, BPF tones and whistling tones are not related to each other [3]

The objective of this study is to characterize the BPF noise of a centrifugal fan in a controlled laboratory environment and eventually to shed some light on the source mechanism. For that purpose an isolated centrifugal fan in a large semi-anechoic room has been investigated with one-dimensional hot wire anemometry, flush mounted pressure transducers and microphones to measure the acoustic sound pressure. The acoustic mea-

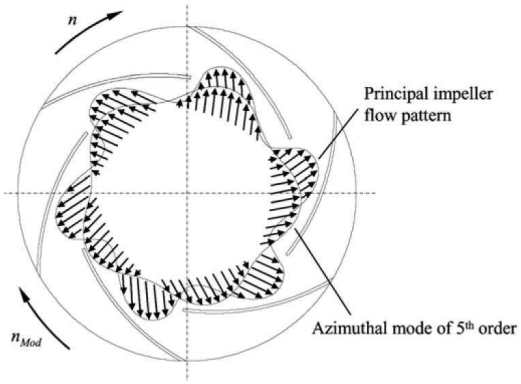

Figure 2: Example of a 5th order mode interfering with a 6th order principal flow pattern at the inflow (schematically)

surements show that the amplitude of the BPF tone varies more or less with time and hence indicate a slight unsteady source mechanism. A spectral decomposition reveals that the BPF noise is exclusively flow-induced. With the aid of a modal analysis azimuthal modes, i.e. highly coherent flow structures, have been detected, which are steady or at least quasi-stationary in respect to the laboratory system. These modes are believed to interact with the rotating blades and cause periodic blade force fluctuations at the BPF frequency, see figure 2.

However, the modal analysis is not able to identify any causality. Although the measurements indicate that the modes originate in the intake and are convected through the blade channels to the discharge of the impeller, a 3D unsteady numerical simulation using the hybrid SAS method has been performed to gain an insight into the detailed flow field. The simulation shows that the blades of the impeller and the friction of the rotating hub gradually impose a pre-swirl on the inflow and cause the formation of an unstable inlet vortex, see figure 3. This vortex takes a helical form with the vortex core varying slowly its position with respect to the impeller center. Compared to the blade speed the movement of the vortex is so slow that it can be considered to be quasi stationary, but simultaneously it explains the time varying BPF noise mentioned above. The dominated frequencies of the predicted blade pressure fluctuations at a monitored point on the blade agree well with the analyzed measured time signals. Seemingly, the simulation supports the hypothesis that came up with the measurements, figure 2. With the results of both the measurements and the numerical investigations the BPF noise of a centrifugal impeller can be traced back to the formation of an unstable inlet vortex that leads to quasi stationary secondary flow structures which interacts with the rotating impeller blades.

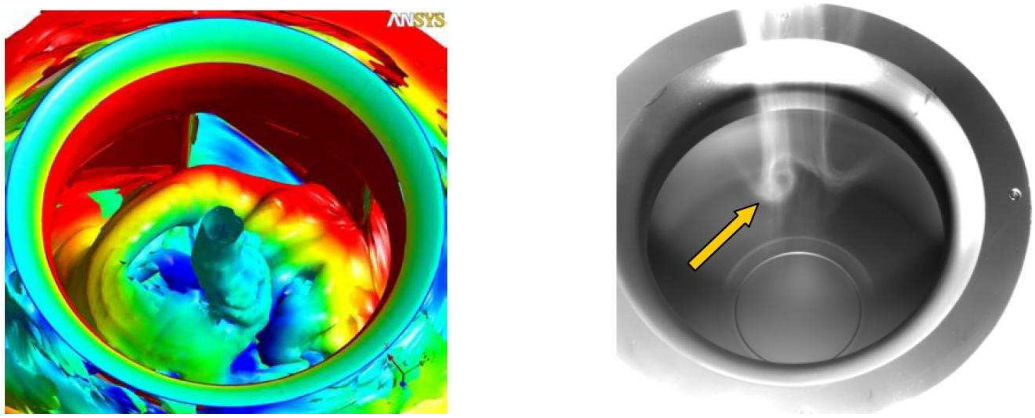

Figure 3: Vortex formation at impeller intake at arbitrary instances of time: CFD (left) and snapshot of a smoke filament (right)

In future the vortex generation mechanism should be investigated in more detail considering the relevant literature, e.g. [4]. A further research topic is related to the inflow structure of axial fans. It is of interest whether a similar phenomenon is responsible for blade tone harmonics observed in these machines.

References

[1] M. E. Goldstein, Aeroacoustics. *McGraw-Hill*, 1974.

[2] M. Roger, Noise in Turbomachines - Noise from moving surfaces. *VKI-Lecture Series 2000-02, von Karman Institute for Fluid Dynamics*, Belgium, 2000.

[3] D. Wolfram, Th. Carolus, Akustische Quellen bei gehäuselosen Radialventilatoren: Analyse, Modelle, Minderung (Acoustic sources in isolated centrifugal fans: Analysis, models, reduction). *Report No. F20910A by the Institut für Fluid- und Thermodynamik, Universität Siegen* , 2009.

[4] G. K. Batchelor, The theory of rotating fluids. *Cambridge University Press*, 1980.

SEGREGATION-BAND DYNAMICS IN PARTICLE-LADEN RIMMING FLOW

Peter J. Thomas[1] & Estelle Guyez[2]
[1] *Fluid Dynamics Research Centre, School of Engineering, Coventry CV4 7AL, UK.*
[2] *CEA DEN/DTN/SE2T/LITA, 17 rue des Martyrs, 38000 Grenoble, France.*

Rimming flow is the flow established inside a partially fluid-filled cylinder when it is rotated about a horizontal axis of rotation. While the cylinder is stationary the liquid rests in a quiescent pool within the cylinder. When the cylinder rotates the rising side of its inner surface drags out a film of liquid from the pool which then coats the inner cylinder wall above the pool. Rimming flow of homogeneous liquids can display a number of different, distinct flow states and it has been the subject of numerous studies in the past [1, 2].

In Refs. [3, 4] we investigated for the first time how the flow patterns of rimming flow are modified when successively increasing amounts of small particles are added to the liquid. During these experiments we observed that, soon after the cylinder begins to rotate, the particles segregate from the liquid and establish the new type of banding pattern shown in figure 1. The banding structure consists of a regular pattern of circumferential regions with, alternatingly, high particle concentrations and regions of very low particle concentrations - sometimes entirely free of particles. Our long-term observations, some lasting over four weeks, revealed that the banding pattern can drift very slowly along the axis of rotation revealing complex spatiotemporal behaviour [5, 6]. Here we summarize and discuss some of our recent work investigating the details of the band-drift dynamics.

Figure 2 displays examples of spatiotemporal diagrams illustrating typical aspects of the system dynamics in different regions of parameter space. The diagrams were constructed by analysing sequences of photographs of the type shown in figure 1. From each photograph of a sequence a pixel line was extracted horizontally across the cylinder (*c.f.* figure 1). The extracted lines were processed to display black at positions where a band is present and white for regions of low particle concentrations. The sequence of successive pixel-scan lines of each experiment were then composed into the spatiotemporal plots of figure 2.

Figure 2(a) shows results for an experiment in which the segregation bands drifted from positions 0 cm $< L <$ 13.5 cm towards the left end wall ($L = 0$ cm) and from positions 13.5 cm $< L <$ 27 cm towards the right end wall ($L = 27$ cm). The left-hand ordinate displays time t in terms of cylinder rotations t/T (T, cylinder rotation period) and the right-hand ordinate additionally shows time in terms of days. The figure reveals that it took the band initially located near $L \approx 12$ cm at $t/T = 0$ about 3000 cylinder rotations (0.5 days), to drift to the left endwall at $L = 0$ cm. In the experiments that resulted in figure 2(b) the drift direction is reversed and the bands drift from both endwalls towards the centre of the cylinder. Note the extremely slow drift velocities of the order of approximately 13.5 cm/25 days. Figure 2(c) displays data from an experiment with zig-zag band drift in the centre of the cylinder and band drift similar to that of figure 2(a) in the regions adjacent to the left and right endwall. For the experiment in figure 2(d) all bands initially drifted towards the endwalls for about 0.4 days. However, thereafter the system dynamics suddenly changed with the centrals bands becoming stationary while only the outermost bands continued to drift towards the endwalls. We have observed various other distinct drift modes extending from completely stationary banding structures, over other complex geometric patterns to entirely irregular band-drift patterns. We will consider for which conditions in parameter space the different band-drift modes are adopted and we will discuss the governing non-dimensional groups responsible for the drift-mode selection.

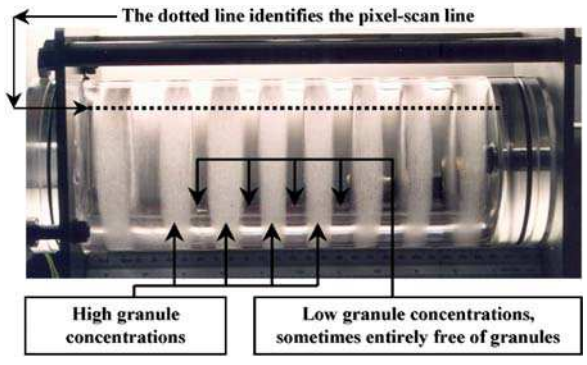

Figure 1: Head-on view of segregation-band pattern in partially fluid-filled, horizontally rotating circular cylinder (cylinder length, 27 cm; diameter, 10 cm).

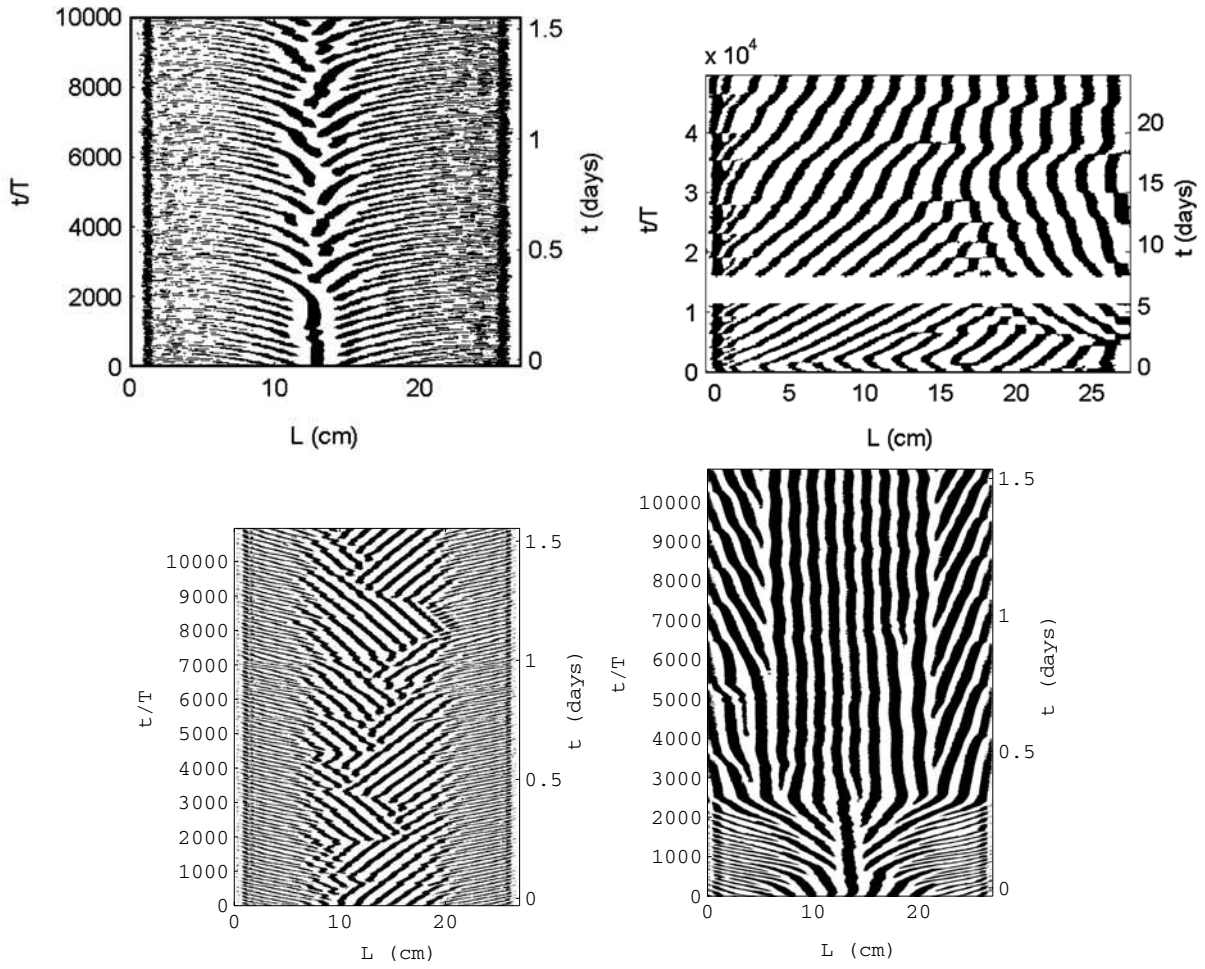

Figure 2: Spatiotemporal diagrams illustrating some typical drift modes of the segregation bands.

References

[1] S. T. Thoroddsen & L. Mahadevan, Experimental study of coating flows in a partially-filled horizontally rotating cylinder. *Exp. Fluids* **23**, 1–13 (1997).

[2] G. Seiden & P. J. Thomas, Complexity, segregation and pattern formation in rotating-drum flows. Submitted to *Rev. Mod. Phys.* (2011).

[3] O. A. M. Boote & P. J. Thomas, Effects of granular additives on transition boundaries between flow states of rimming flow. *Phys. Fluids* **11**, 2020–2029 (1999).

[4] P. J. Thomas, G. D. Riddell, S. Kooner & G. P. King, Fine structure of granular banding in two-phase rimming flow. *Phys. Fluids* **13**, 2720–2723 (2001).

[5] E. Guyez & P. J. Thomas, Spatiotemporal segregation-pattern drift in particle-laden rimming flow. *Phys. Rev. Lett.* **100**, 075401 (2008).

[6] E. Guyez & P. J. Thomas, Effects of particle properties on segregation-band drift in particle-laden rimming flow. *Phys. Fluids* **21**, 033301 (2009).

EUROMECH Colloquium 525, 21-23 June 2011, Ecully, France

Instabilities and transition in three-dimensional flows with rotation

CLUSTER FORMATION FOR INCOMPRESSIBLE VISCOUS FLUID/RIGID SOLID PARTICLE MIXTURES IN ROTATING CYLINDERS

Roland GLOWINSKI & Tsorng-Whay PAN
University of Houston, Department of Mathematics, Houston, TX 772004, USA

1. Problem presentation and previous results

In a previous publication (ref. [1]) the authors discussed the numerical simulation of particle cluster formation in a rotating cylinder containing a fluid/particles mixture, the fluid (resp., the particles) being incompressible, viscous and Newtonian (resp., rigid solid and spherical). More precisely, assuming that the gravity field is vertical, that the cylinder has a circular cross-section, that its rotation axis is horizontal, and that the particle density is larger than the fluid density, the simulation reported in [1] have shown, in particular, the following behavior:

Suppose that at time zero the fluid and the particles are at rest, the particles lying on the bottom part of the cylinder; suppose next that the cylinder starts rotating around its axis: if the angular velocity is large enough one observes the formation of particle clusters as shown in Figure 1(a) (borrowed from [1]). Figure 1(b) shows the projection of the particle population (160 particles here) on a vertical plane orthogonal to the rotation axis.

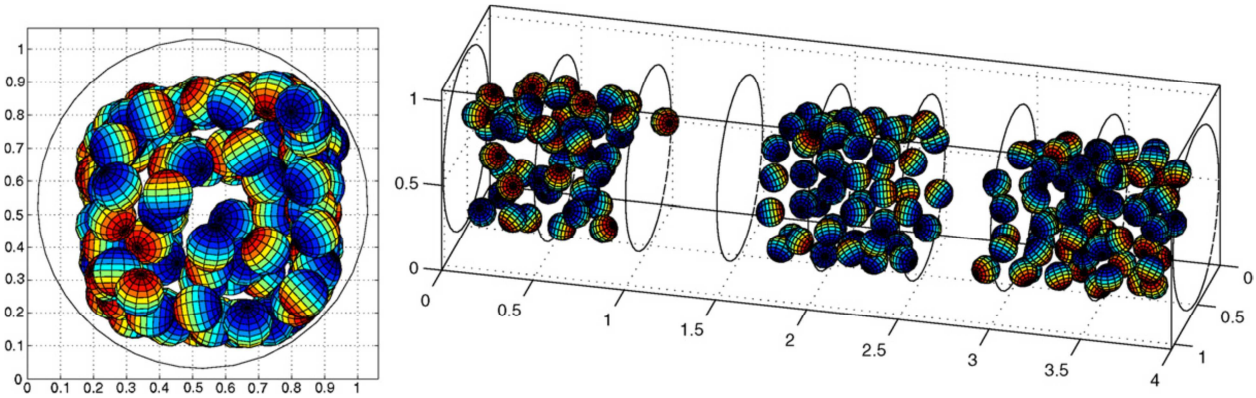

(a) (b)

Figure 1. Cluster formation in a rotating cylinder.

Actually, the simulation results reported in [1] agree with the experimental ones available in the literature (some of these references are given in [1]).

The computational methodology used in [1] relies on several ingredients, such as: finite element methods for the space discretization, time discretization by operator-splitting, a Lagrange multiplier based fictitious domain method allowing the fluid flow computations to be done in the full cylinder using a fixed grid, despite the fact that the physical flow region is a time variable subset of the full cylinder.

2. Objectives of the present study

Our objectives in this presentation are to go beyond [1] (still using the same computational methodology) by considering:

(i) The effect of the size of the particle populations on the formation of clusters.

(ii) The effect of gravity and fluid/particle density ratio on the formation of clusters.

Concerning (ii), our simulations strongly suggest that cluster formation does not take place in the ***neutrally buoyant*** case, that is, when the particles have the same density than the surrounding fluid. It is worth noticing that this result is in agreement with the results from laboratory experiments.

Reference

[1] PAN, T-W., R. GLOWINSKI, S. HOU, Direct numerical simulation of pattern formation in a rotating suspension of non-Brownian settling particles in a fully filled cylinder, *Computers and Structures*, **85**, (2007), 955–969.

STABILITY OF UNSTEADY FLOW IN A ROTATING TORUS

J.P. Denier[1], R.E. Hewitt[2], A.L. Hazel[2] & R.J. Clarke[3]
[1]*School of Mathematical Sciences, University of Adelaide, Adelaide 5005, Australia.*
[2]*School of Mathematics, University of Manchester, Manchester, M13 9PL, UK.*
[3]*Dept. of Engineering Science, University of Auckland, New Zealand.*

Abstract

We consider the temporal evolution of a viscous incompressible fluid in a torus of finite curvature; a problem first investigated by Madden and Mullin (1994), herein referred to as MM. The system is initially in a state of rigid-body rotation (about the axis of rotational symmetry) and the container's rotation rate is then changed impulsively. We describe the transient flow that is induced at small values of the Ekman number, over a time scale that is comparable to one complete rotation of the container. We show that (rotationally symmetric) eruptive singularities (of the boundary layer) occur at the inner or outer bend of the pipe for a decrease or an increase in rotation rate respectively. Moreover, there is a ratio of initial-to-final rotation frequencies for which eruptive singularities can occur at both the inner and outer bend simultaneously. We also demonstrate that the flow is susceptible to a combination of axisymmetric centrifugal and non-axisymmetric inflectional instabilities. The inflectional instability arises as a consequence of the developing eruption and is shown to be in qualitative agreement with the experimental observations of MM. Detailed quantitative comparisons are made between asymptotic predictions and finite (but small) Ekman number Navier–Stokes computations using a finite-element method.

1 Introduction

This work is directly motivated by the investigation of MM, which considered the internal flow induced by the sudden rotation of a toroidal container filled with an incompressible Newtonian fluid; the axis of rotation being the axis of rotational symmetry of the torus. Their work was largely experimental in nature, capturing the flow response by a combination of flow visualisation and LDV methods. In the initial stages an axisymmetric 'front' was observed at the outermost radius of the toroidal pipe. This front propagated radially inwards away from the wall, before propagating waves appeared in the around-torus direction, breaking the rotational symmetry of the flow. The rapid growth of these waves led ultimately to three-dimensional disordered flow (figure 19 of their paper presents a sequence of flow visualisation pictures that nicely captures the evolution, as obtained by a light sheet through the mid-plane of symmetry of the torus).

MM speculate that the origin and break-up of the inwardly propagating front has two potential sources (p. 241-242), a collisional boundary-layer phenomena and a centrifugal instability; however no detailed comparisons were possible to support either source.

Rather than restricting attention to the 'spin-up from rest' case considered by MM, we address a broader range of problems in which a transition is made from a rigid-body rotation at an initial frequency, Ω_i, to that at a second frequency, Ω_f, such that $|\Omega_i - \Omega_f| = O(1)$. This gives us a two-parameter problem (for a fixed torus curvature), with the flow governed by the rotation ratio $\Omega_r = \Omega_i/\Omega_f$ and an Ekman number $\mathrm{Ek} = \nu/(a^2\Omega_f)$, where a is the radius of the toroidal pipe.

Our aim is to clarify the physical origins of the fronts and waves observed in the experimental work of MM.

2 Main results and methodology

We take a two-stranded approach to this problem: (i) we consider the $\mathrm{Ek} \ll 1$ limit in detail and describe the resulting unsteady boundary layer that develops in the torus together with its linear stability properties, (ii) we validate the conclusions of the boundary-layer results by large-scale Navier–Stokes computations at small, but finite, values of Ek.

A non-axisymmetric wave instability near an eruption point

We first determine the unsteady, axisymmetric base flow that develops subsequent to an impulsive change in the rotation rate of the container. We then consider the linear stability of this base flow to perturbations that are non-axisymmetric, by considering a Fourier component in the around-torus (axial) direction.

The underlying base flow in the $\mathrm{Ek} \ll 1$ limit is axisymmetric, unsteady, and evolves to a finite-time singularity at either the outermost point or/and innermost point of the torus (depending on Ω_r). As one may anticipate, the boundary-layer singularity is associated with a localised eruption into the bulk flow at finite but small Ek; good quantitative agreement is found between the eruptive boundary-layer solutions and the

Navier–Stokes solutions. A key feature of the pre-eruption process is the introduction of inflexional velocity profiles in the dominant velocity component around the torus. We demonstrate the existence of an (inviscid) instability mechanism associated with these inflexional profiles prior to the eruption of the boundary layer. By computation of the unsteady evolution of a single Fourier mode (in the meridional cross section of the torus), in conjunction with the unsteady base flow, we demonstrate that the (local) asymptotic boundary-layer predictions are in agreement with the (global) finite-Ek response of the system.

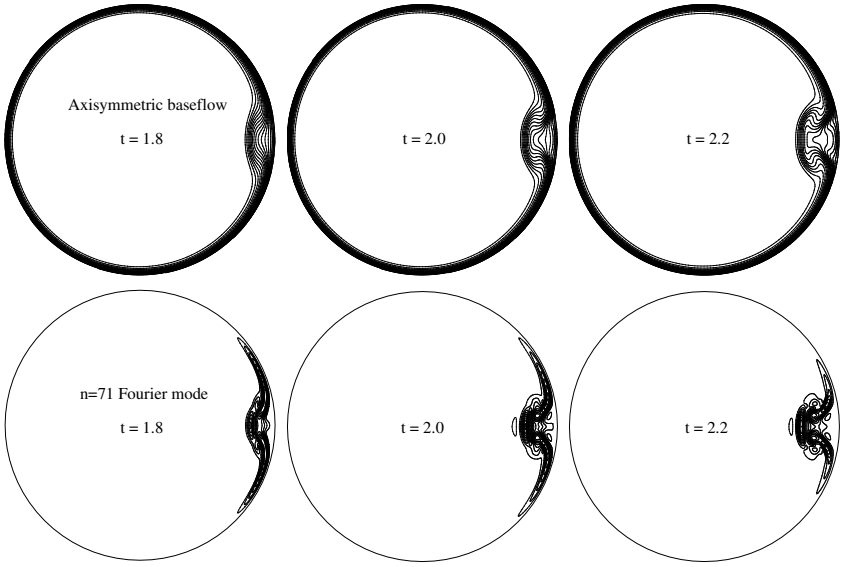

Figure 1: Contours of the axial (around torus) flow in the meridional cross section for Ek = 1/2000, $\Omega_r = 0$ (spin-up from rest) and the timescale shown is based on the final rotation frequency; the torus curvature is the value of the MM experimental configuration. Here we show the axisymmetric base flow and a non-axisymmetric Fourier mode (n being the around-torus wave number) of a linear disturbance. The disturbance becomes concentrated at the inflexion point induced by the eruption at the outermost point of the torus. In these cross sections, the axis of rotation is to the left of each image.

The results of our asymptotic analysis predict the peak growth rate is for perturbations with $n = k\varrho^{5/4}\mathrm{Ek}^{-1/2}$ (where $k \approx 0.1$ to 0.11) waves around the torus. Here ϱ is a dimensionless measure of the distance of the eruption point from the axis of rotation (on the pipe-radius lengthscale) and k is a weakly varying function of the slower timescale over which the baseflow varies. Thus, the inviscid local analysis leads to an axial (around the torus) wave number of $n \approx 50$ for the fastest growing mode (taking $k \approx 0.105$) when Ek = 1/1000. Extrapolation of the section of torus shown in figure 19 of MM leads to the estimate that $n \approx 60$ in their experimental work at approximately the same value of Ek.

The 'fronts' observed in the experimental work of MM correspond to the collisional eruption of the centrifugally induced meridional flow within the boundary layer. The subsequent unstable waves can, we claim, be qualitatively linked to an inviscid instability of the near-eruption flow that grows on a faster timescale than that at which the baseflow develops, and hence can be described by a local eigenvalue problem.

An axisymmetric centrifugal instability

If time permits we will also discuss the sensitivity of the unsteady flow to an (axisymmetric) centrifugal instability in the small time limit. In this case the growth of these modes is not governed by an eigenvalue problem because the timescale for the development of the disturbance is comparable to the timescale of the baseflow development. The development of these modes can therefore only be discussed in the context of an appropriate initial-value problem. Crucially, for $\Omega_r > 0$ these modes occur at the inner/outer-most radial position on the torus wall, whereas the inflexional modes above occur at the outer/inner-most points. The two instability mechanisms therefore remain largely isolated from each other; this is not true if $\Omega_r < 0$ however.

References

Madden, F. N. and Mullin, T. The spin-up from rest of a fluid-filled torus. *J. Fluid Mech.*, **265**, 217 (1994).

INSTABILITIES IN TAYLOR–COUETTE–POISEUILLE FLOW WITH POROUS WALLS

Denis MARTINAND[1], Nils TILTON[1] & Eric SERRE[1] & Richard M. LUEPTOW[2]
[1] *LM2P2 UMR 6181 CNRS Aix-Marseille Université, Marseille, France.*
[2] *Department of Mechanical Engineering, Northwestern University, Evanston IL, USA.*

We consider Taylor–Couette–Poiseuille flow developing between an outer, fixed, impermeable cylinder and a concentric, inner, rotating, permeable cylinder with radial suction, see figure 1. This system is useful for

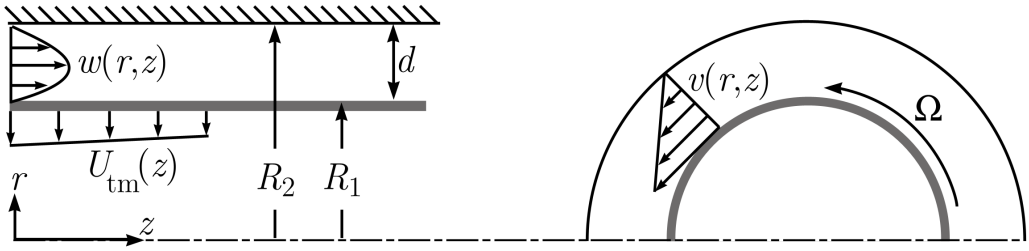

Figure 1: Sketch, not to scale, of the annular geometry and laminar base flow.

dynamic filtration because the shear due to the rotating cylinder and, in the case of supercritical flow, the Taylor vortices, wash contaminants away from the permeable cylinder and prevent fouling. The fluid mechanics of this system are not fully understood due to the coupling between the axial pressure drop, which drives the axial Poiseuille flow, and the transmembrane pressure difference which drives the suction. In addition to the filtration flux, this coupling induces axial variations of the velocity field. These variations eventually modify the nature of the subcritical flow which can evolve from suction to injection (cross flow reversal) or consume the whole axial flow (axial flow exhaustion). Moreover, owing to the axial and radial flows and their variations along the axial direction, the stability of this flow strongly departs from that of Taylor–Couette flow.

1 Analytical approach

Because filtrating devices utilize membranes with small permeability and suction, we propose an asymptotic solution to the subcritical flow assuming a slow axial variation of the velocity and pressure fields [1]. The transmembrane suction is coupled with the pressure through Darcy's law. The obtained analytical approximation correctly captures the axial variations of the velocity field, e.g. the two aforementioned possible behaviors. This laminar flow is then used as a base state to study the appearance of centrifugal instabilities in the form of Taylor vortices developing in the most common configuration, i. e. when the mean axial flow decreases downstream due to filtration but do not reverse. According to the theory of nonlinear global modes in slowly varying open flows [2], the unstable state is expected to form a front at the axial location where the flow undergoes a transition from local convective unstability to local absolute instability. This front acts as a wavemaker and selects the frequency of the vortices.

2 Numerical approach

These analytical results for the subcritical and supercritical flows are then compared with dedicated spectral direct numerical simulations implementing Darcy's law on the inner cylinder. These numerical simulations require some special care to correctly handle the axial and transmembrane flows, together with solving the pressure field, in order to avoid numerical noises prone to trigger uncontroled extrinsic instabilities.

3 Results

As seen in figure 2, global synchronized modes governed by local absolute instabilities are retrieved in numerical simulations. These numerical results, concerning for instance the features of these instabilities such as the location of the front or the frequency, are in good agreement with the analytical prediction based on previous

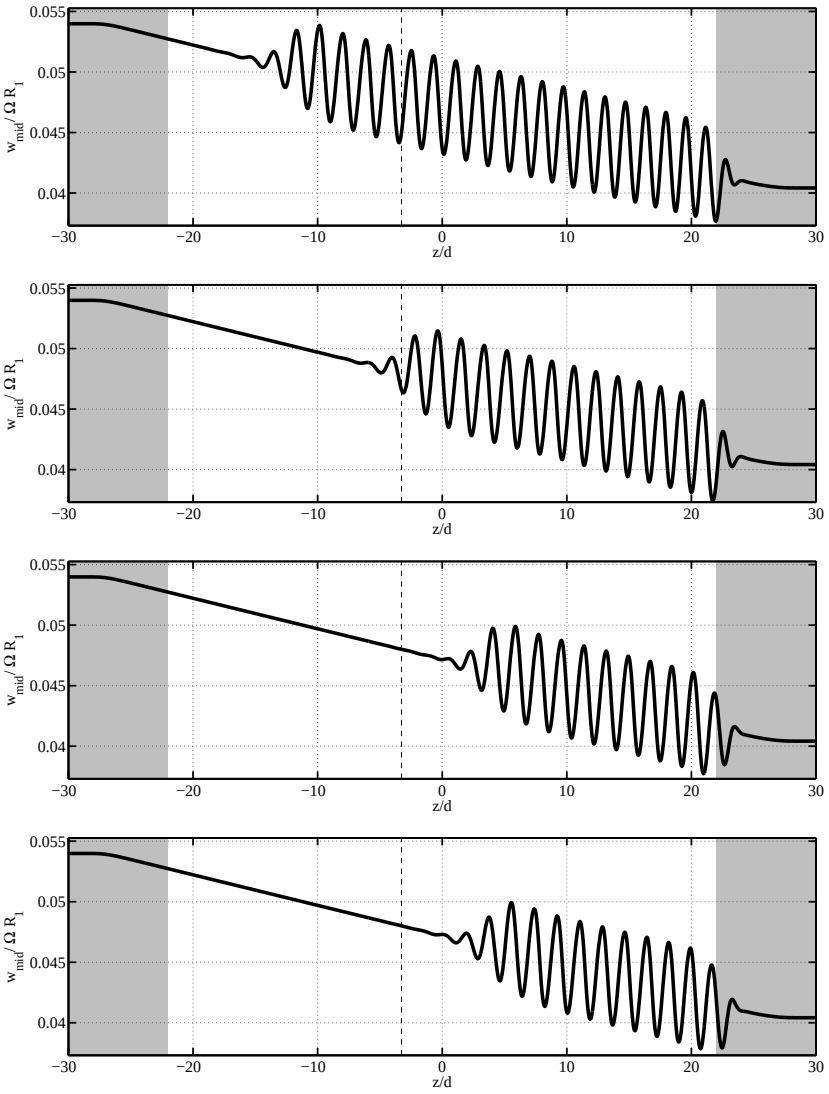

Figure 2: Temporal evolution of the axial velocity as a function of the axial coordinate, the rotating Reynolds number is set to 120, the axial Reynolds number varies from 4.32 (inlet) to 3.24 (outlet). (−−): Boundary between the locally convectively and absolutely unstable regions

results pertaining to the convective/absolute stability analysis of the Taylor–Couette–Poiseuille without radial flow and the axial evolution of the stationnary part of the total flow.

References

[1] N. Tilton, D. Martinand, E. Serre and R. M. Lueptow. Pressure-driven radial flow in a Taylor-Couette cell. *J. Fluid Mech.* **660**, 527–537 (2010).

[2] B. Pier, P. Huerre and J. M. Chomaz. Bifurcation to fully nonlinear synchronized structures in slowly varying media. *Physica D* **148**, 49–96 (2001).

SECONDARY INSTABILITY OF STRATIFIED EKMAN LAYER ROLL VORTICES

Nadia Mkhinini[1], Thomas Dubos[1], Philippe Drobinski[1]
[1] *Laboratoire de MÉtÉorologie Dynamoique / IPSL, École Polytechnique, Palaiseau*

We study the transition to turbulence of the Ekman flow in a linear density stratification, an exact solution of the Boussinesq equations occurring near boundaries in rotating fluids. The control parameters are the Richardson number $Ri = \frac{\delta^2 N^2}{G^2}$, the Reynolds number $Re = \frac{G\delta}{\nu}$ and the Prandtl number $Pr = \frac{\nu}{\kappa}$ where $\delta = \sqrt{2\nu/f}$ is the Ekman length, ν is the kinematic viscosity, f is the Coriolis parameter, G is the geostrophic velocity far from the lower boundary and κ is the thermal diffusivity. We consider $Re = 500$ and $Re = 1000$. In order to assess separately the effect the diffusion of momentum and heat, we consider two values of the Prandtl number : $Pr = 1$ and $Pr = 4$.

1 Nonlinear primary instability

The Ekman flow is subject to linear instability for $Ri < Ri_c(Re, Pr)$ where Ri_c depends very little on Pr (Brown, 1972). This instability develops into traveling Kelvin-Helmholtz roll vortices which we compute as a function of stratification as in Dubos et al. (2008). Fig. 1 presents the amplitude of the equilibrated vortices as measured by their kinetic, potential and total energy. While for $Pr = 1$ the roll amplitude vanishes at $Ri = Ri_c$ this is not the case at $Pr = 4$. So far only supercritical bifurcations had been identified in the Ekman layer stability diagram (Haeusser and Leibovich, 2003; Dubos et al., 2008). The subcritical bifurcation observed at $Pr = 4$ allows us to compute equilibrated vortices at $Ri > Ri_c$.

2 Linear secondary instability

Fig. 2 presents the growth rate σ_2 of infintesimal three-dimensional perturbations to the travelling rolls as a function of their horizontal wavenumber k_y. For $Ri = 0$ we recover at $k_y > 1$ the unstable modes identified by Dubos et al. (2008). New, less unstable modes branches are obtained for $0 < k_y < 1$. However as Ri increases the modes for $k_y > 1$ become less unstable, become dominated by the unstable modes for $k_y < 1$ and eventually disappear. For $Pr = 1$ the overall maximum growth rate decreases as Ri increases, but not for $Pr = 4$. This must be related to the fact that the roll vortices weaken as Ri approaches Ri_c if $Pr = 1$, but not if $Pr = 4$.

3 Conclusion

We have studied the influence of an ambient linear stratification on the secondary instability of the Ekman flow. This influence depends markedly on the Prandtl number. Our results reveal that the bifurcation at $Ri = Ri_c$ is subcritical $Pr = 4$. In this regime, finite amplitude vortices exist beyond $Ri = Ri_c$ and the growth rate of the secondary instability increases as the ambient stratification increases, instead of decreasing as occurs for $Pr = 1$ and as intuition suggests. A complementary study of the nonlinear development of the secondary instabilty is under way.

References

Brown, R. A. (1972). On the inflection point instability of a stratified Ekman boundary layer. *J. Atmos. Sci*, 29:850–859.

Dubos, T., Barthlott, C., and Drobinski, P. (2008). Emergence and secondary instability of ekman layer rolls. *J. Atmos. Sci*, 65(7):2326–2342.

Haeusser, T. M. and Leibovich, S. (2003). Pattern formation in the marginally unstable Ekman layer. *J. Fluid Mech.*, 479:125–144.

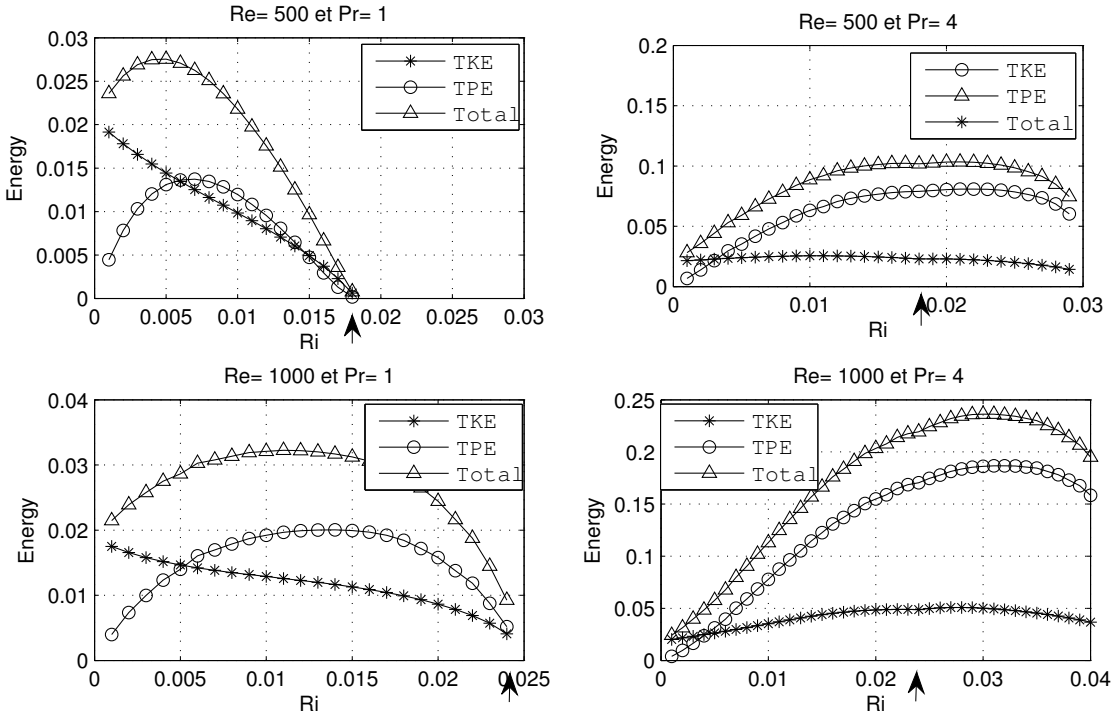

Figure 1: Energy of roll vortices as a function of ambient stratification. Arrows point to $Ri = Ri_c$

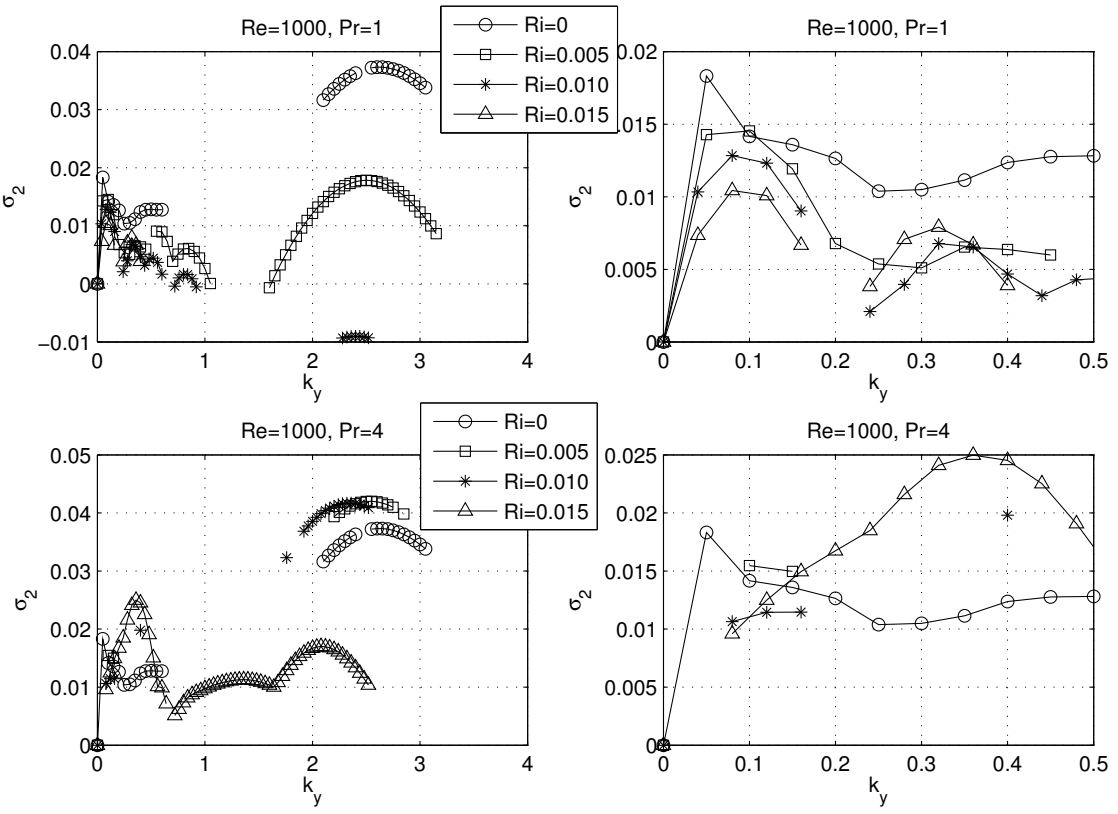

Figure 2: Growth rate σ_2 of secondary instability of Ekman roll vortices as a function of wave vector k_y (right : zoom)

A STUDY ON THE 3D INERTIAL INSTABILITY MECHANISM IN THE SUB-MESOSCALE OCEAN

Ayah LAZAR[1,2], Alexandre STEGNER[2] & Eyal HEIFETZ[1]
[1] *Department of Geophysics and Planetary Science, University of Tel Aviv, Tel Aviv 69978, Israel.*
[2] *Laboratoire de Météorologie Dynamique, CNRS, ENS, 24 Rue Lhomond, 75005 Paris, France.*

In the sub-mesoscale ocean vortices tend to be predominantly cyclonic [4]. Inertial instability (hereafter II), which is a centrifugal instability mechanism in the presence of the Coriolis force, is a destructive mechanism that acts only on anti-cyclones, and therefore is hypothesized to cause this asymmetry. Furthermore, since II is in fact the growth of the overturning vorticity, thus creating vertical mixing, it is expected to contribute to nutrient enrichment from the deep, affecting primary production and the oceanic carbon cycle.

Linear stability analysis [6] shows that three-dimensional unstable modes of parallel shear flow (without curvature) may have stronger growth rates than the standard two-dimensional barotropic modes when the absolute vorticity is negative, thus II is more significant than shear instability in the destruction of strong anticyclonic shear. For circular vortices (with curvature), vortex columns are unstable to 3D perturbations where the generalized Rayleigh discriment is negative $\chi(r) \equiv \left(\frac{1}{r}\partial_r(rV) + f\right)(2V/r + f) < 0$, where $V(r)$ is the azimuthal velocity and f the Coriolis parameter, which implies that the region of instability is in the anticyclone periphery [2]. Axis-symmetry seems to be a proper simplification, as it was shown by [1] that the growth rates of axis-symmetric disturbances are larger than non axis-symmetric ones, and the latter are completely stable above a relatively low cut-off azimuthal wave number. Recent fully non-linear numerical simulations show that the area of the instability is breached [5] into the anticyclone core from the outside [3] in the nonlinear phase.

However, for surface oceanic vortices, which are among the most energetic structures of the oceans, one should also take into account the thickness and the stratification of the thermocline. Both the shallow-water constraint and the stratification stabilize these intense anticyclones. The stratification induces a low vertical wave-number cutoff (smaller wavelength) [3, 5]. The small scale perturbations are more sensitive to the vertical dissipation and the growth rate of the unstable modes could be strongly reduced or vanish completely. We apply linear stability analysis to examine 3D II in a vertically confined and stratified, axis-symmetric, mean-flow. We define the dynamical parameters that govern the stability, and find the parameters, which are both insensitive to different vorticity profiles and are relatively easy to estimate from laboratory experiments and oceanic in situ measurements. These are the eddy Rossby number, characterized by the maximal azimuthal velocity and the radius at which this velocity is reached, $Ro = V_{max}/r_{max}f$, which turns out to be a more suitable parameter than, say, the normalized vorticity of the eddy; the aspect ratio, $\delta = h/R$ (which is small $\delta << 1$); the normalized stratification, $S = N/f$; and the vertical Ekman number, $E_k = \nu/fh^2$. In cases of strong stratification, we use the Burger number to combine both the aspect ratio and the stratification. We solve the problem analytically for a Rankine vortex (see figure 1a). For other vorticity profiles an eigenvalue decomposition is used, which we confirmed by recalculating for the Rankine vortex. We map the parameter space (see figure 1b), and corroborate our findings (see figure 2) with large-scale laboratory experiments studies, performed at the LEGI-Coriolis platform.

References

[1] P. Billant and F. Gallaire. generalized rayleigh criterion for non-axisymmetric centrifugal instabilities. *Journal of Fluid Mechanics*, 542:365–379, 2005.

[2] R. C. Kloosterziel, G. F. Carnevale, and P. Orlandi. Inertial instability in rotating and stratified fluids: barotropic vortices. *Journal of Fluid Mechanics*, 583:379, July 2007.

[3] R. C. Kloosterziel, G. F. Carnevale, and P. Orlandi. Saturation of inertial instability in rotating planar shear flows. *Journal of Fluid Mechanics*, 583:413, July 2007.

[4] Walter Munk, Laurence Armi, Kenneth Fische, and F. Zachariasen. Spirals on the sea. *Proceedings: Mathematical, Physical and Engineering Sciences*, 456(1997):1217–1280, May 2000.

[5] Riwal Plougonven and Vladimir Zeitlin. Nonlinear development of inertial instability in a barotropic shear. *Physics of Fluids*, 21(10):106601, 2009.

[6] Shinichiro Yanase, Carlos Flores, O. Métais, and J.J. Riley. Rotating free-shear flows. I. Linear stability analysis. *Physics of Fluids A: Fluid Dynamics*, 5(November):2725, 1993.

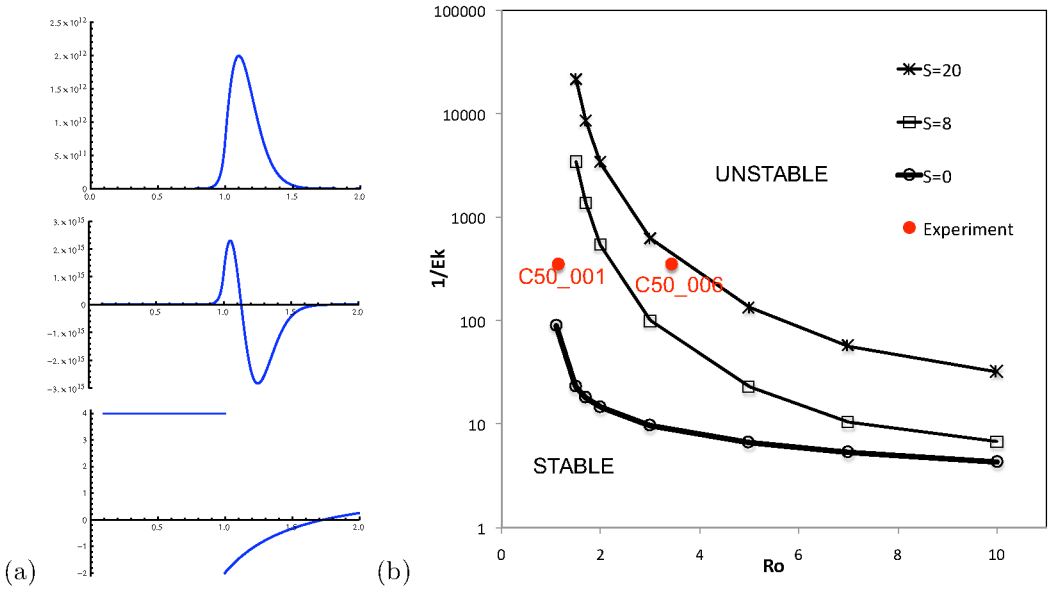

Figure 1: Panel (a) - First (top) and second (middle) horizontal modes for a sample Rankine vortex ($Ro = -3$). This is the solution of a modified bessel equation of order unity inside the vortex and of imaginary order outside. On the bottom is the χ parameter, and it is evident that the instability, in both modes, is localized to the area where $\chi < 0$. Panel (b) - Marginal stability curves ($\sigma = 0$) - on the $(1/E_k, |Ro|)$ plane, for three stratification values $S = 0, 8, 20$ and $\delta = 0.2$. Not shown are curves for different types of non-isolated vortices, which on this parameter space, are very close to the ones shown for the Rankine vortex. The parameters of experiments $C50\_001$ and $C50\_006$ from the experiments performed at the LEGI-Coriolis platform are both marked with red dots. Both are with $\delta = 0.2$ and S 8, which means that $C50\_001$ should be stable and $C50\_006$ should be unstable as they are on either side of the marginal stability curve. See figure 2 for the results.

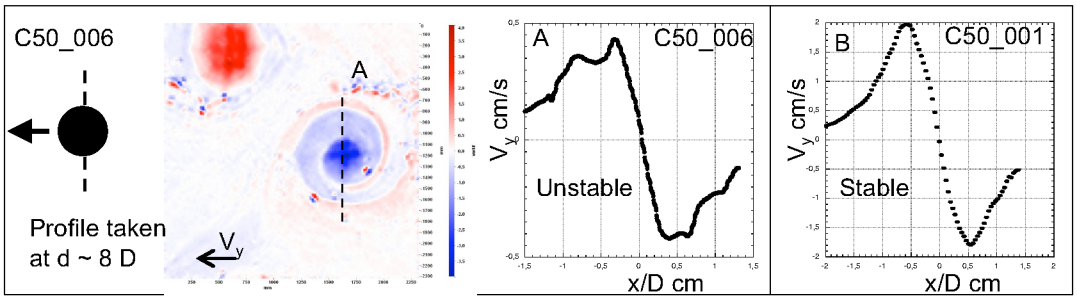

Figure 2: A good case study for II is expected in Island wakes, where the forcing that generates the anticyclones is strong. Then they are created, but destructed far more rapidly than their cyclonic counterparts in the wake. For that reason, we conducted experiments of island-wake vortices instability on the 14-meter diameter rotating platform at the LEGI-Coriolis in Grenoble with quantitative PIV measurements of the wake flow. On the left, vorticity field of experiment $C50\_006$ calculated from the PIV. The cylinder and its direction is shown schematically. Small scale patterns that can easily be seen with dye cannot be detected by 2D PIV measurements, therefore the signature of the II is extracted by the mesoscale evolution of individual eddies, in this case the velocity profiles of anticyclones taken when the vortex is at a distance of eight times the diameter of the cylindrical island model (in experiment $C50\_006$ the profile is taken where the line A is indicated). Panel (A) and (B) show the velocity profiles for experiments $C50\_006$ and $C50\_001$ respectively. Experiment $C50\_001$ is predicted by its place on the stability diagram (1b) to be stable and indeed, the anticyclone in this experiment is unperturbed. Experiment $C50\_006$ is predicted to be unstable and indeed the anticyclone is perturbed at the edges, where the parameter $\chi < 0$ (the cyclones, not shown, in all cases are unperturbed as the instability is asymmetric).

SLOSHING MODES AND SINGULAR INERTIAL MODES IN A CYLINDRICAL TANK ROTATING AROUND ITS AXIS

David Fabre, Jérôme Mougel & Laurent Lacaze
Institut de Mécanique des Fluides de Toulouse, Université de Toulouse / CNRS

1 Introduction

The problem of sloshing of a liquid in a partially filled tank is relevant to many fields in engineering. The particular case where the tank is rotating is relevant, for instance, to the fuel tanks of satellites and spatial launchers. It is known that the fluid motion occurring in these tanks can have a destabilizing effect on the motion of the vehicle, so a prediction of the properties of these motions is highly desirable. The problem is also relevant to the tides in a closed lake or internal basin.

Here we consider the case of a partially filled cylindrical tank rotating around this axis. It is well known that in this case, a steady solution corresponds to a solid-body rotation of the liquid with a parabolic free surface. Previous investigations [3, 4] mostly studied the modes and stability of small oscillations in the inviscid case. A striking result is that the nature of the problem and of its solutions sharply varies with the ratio of the relative frequency of the eigenmode (i.e. with respect to the rotating frame) to twice the rotation rate. When this parameter is larger than 2 or smaller than -2, the problem is elliptic and admits well-defined eigenmodes which do not penetrate deeply into the fluids. On the other hand, when this parameter is within the interval $[-2, 2]$, the problem is hyperbolic, and nothing guaranties the existence of regular eigenmodes. Regular eigenmodes were actually identified in this range in particular cases : they have a different structure, more akin to the tidal waves first investigated in the shallow-water theory of Lord Kelvin. The works dealing with the viscous problem [1] seem to have been limited to the case of axisymmetric waves.

In this work we investigate the problem with three methods : a shallow-water theory, a semi-analytical method where the solutions are expanded in series of special functions, and a finite-difference solution of the viscous problem. The results are compared with previous works. A striking result is the discovery, in the hyperbolic case (as defined above), of a new set of viscous eigenmodes with a pecular structure, akin to the singular inertial modes found in other geometries such as spherical shells [5] or the atmosphere of rotating stars [2].

2 Base flow, Stability equations and resolution methods

We consider a cylindrical recipient partially filled with water and rotating around its axis. We note R the radius of the container, Ω the rotation rate and g the acceleration of gravity. It is a classical exercise to demonstrate that the free surface takes, at equilibrium, a parabolic shape defined by

$$z = h(r) \equiv h_0 + \frac{\Omega^2 r^2}{2g} - \frac{\Omega^2 R^2}{4g}, \tag{1}$$

where h_0 is the average depth of the water ; more precisely the depth that the same volume of water would fill in the recipient if the rotation was stopped. We investigate the linear stability properties of this flow by considering eigenmodes with the form $\hat{u}(r, z)e^{im\theta}e^{\sigma t}$, where r, θ, z are cylindrical coordinates, m is an azimuthal wavenumber and $\sigma = \sigma_r + i\sigma_i$ a complex frequency. These eigenmodes have to be computed as nontrivial solutions of an eigenvalue problem which can be written in the following symbolic form :

$$\mathcal{A}\hat{u} = \sigma\mathcal{B}\hat{u}. \tag{2}$$

Three methods of resolutions are used to tackle this problem. The first method is a shallow-water theory which allows to reduce the problem to a single, second-order equation which turns out to have analytical solution in terms of hyperbolic functions. This method is by nature limited to the case where the aspect ratio $\chi = h_0/R$ of the tank is small (but viscosity may be included with an ad-hoc modeling).

The second method, which is also limited to the inviscid case, consists of finding semi-analytical solutions expanded over a basis of functions with separable variables, with the following form (for the pressure component):

$$p(r, z) = \Sigma_{j=1}^{\infty} X_j \frac{\cosh(k_j z)}{\cosh(k_j h_0)} J_m(\xi_j r), \tag{3}$$

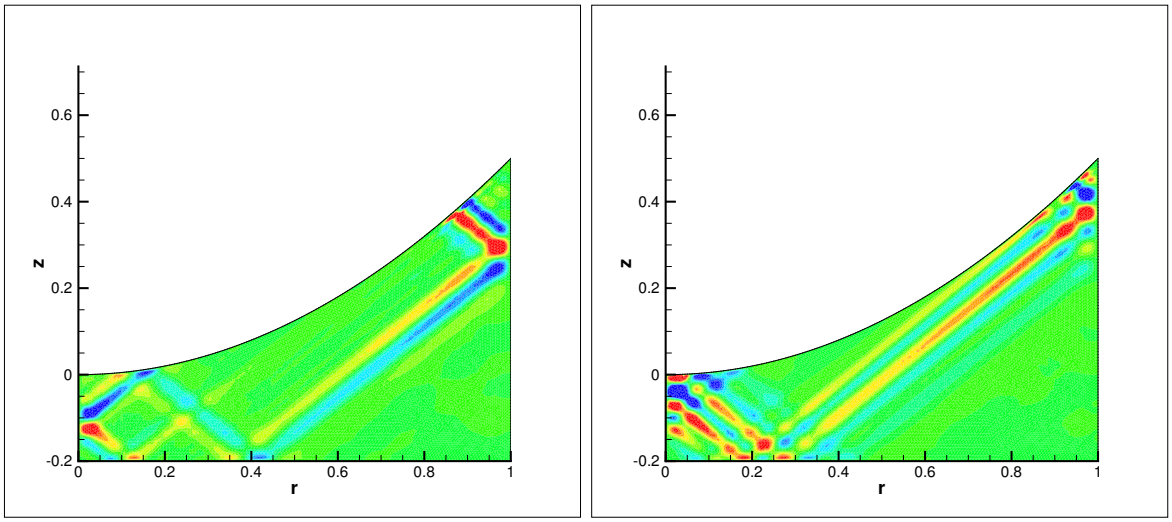

Figure 1: Exemples of singular eigenmodes in a tank with a parabolic surface

Where J_m is a Bessel function, k_j, ξ_j are vertical and radial "wavenumbers" which have to be taken among a discrete set of characteristic values, and X_j are amplitude coefficients to be solved for. Such an expansion automatically satisfies the boundary conditions at the bottom and outer boundary. Truncation of this series to a finite N and imposition of the free-surface condition at N points leads system of equations for the N amplitudes X_j, which admits nontrivial solutions for a discrete set of eigenvalues.

The third method consists of discretizing the set of partial differential equations formed by the eigenvalue problem with a finite element methods. We do this by means of the software FreeFem++. This method allows to consider the general, viscous problem.

3 Results

Before considering the general case, we consider three situations where a comparison between our three methods of resolution (and with previous work) is possible. The first particular case corresponds to weak rotation. In this case, the eigenmodes belong to two distinct sets. The first ones are "pure sloshing modes" identical to those existing in a non-rotating container. The second ones are "pure inertial modes" which are identical to those existing in a cylindrical container with a flat, rigid surface. The second particular case corresponds to weak aspect ratio h_0/R and allows use of the shallow-water approximation. The third particular case corresponds to large aspect ratio h_0/R. In this case inviscid solutions can be found in closed form [3]

We then consider the general, viscous case. In addition to the modes already identified in the litterature, we evidence a new set of eigenmode solutions with a singular structure, akin to the singuliar modes existing in spherical shells [5] or the atmosphere of rotating stars [2]. The structure of these modes is concentrated along "rays" forming a closed pattern in the geometry. Figure 1 shows sample specimens of such modes.

References

[1] H. F. Bauer and W. Eidel. Axisymmetric natural damped frequencies of a viscous liquid in a circular cylindrical container- an alternative semi-analytical solution. *Forschung im Ingenieurwesen*, 65:191–199, 1999.

[2] B. Dintrans and M. Rieutord. Oscillations of a rotating star: a non-perturbative theory. *Astron. Astrophys.*, 354:86–98, 2000.

[3] J. W. Miles. Free surface oscillations in a rotating tank. *Phys. Fluids*, 2:297–305, 1959.

[4] J. W. Miles and B. A. Troesh. Surface oscillations of a rotating liquid. *ASME J. Appl. Mech.*, 28:491–496, 1961.

[5] M. Rieutord and L. Valdettaro. Inertial waves in a rotating spherical shell. *J Fluid Mech.*, 341:77–99, 1999.

FLOW INSTABILITIES IN A VERTICAL DIFFERENTIALLY ROTATING CYLINDRICAL ANNULUS WITH A RADIAL TEMPERATURE GRADIENT

Innocent MUTABAZI, R. GUILLERM, A. PRIGENT, V. LEPILLER, S. MALIK
LOMC, FRE31O2, CNRS-Universit du Havre, 53 rue Prony, 76058 Le Havre Cedex, France.

1 Introduction

Flow in a differentially rotating cylindrical annulus with a radial temperature gradient is encountered in many industrial applications [1]. It has been investigated experimentally and numerically by few authors [2, 3, 4, 5, 6]. For small values of the control parameter,away from the boundaries, the base flow has two velocity profiles each of which is unstable. The rotation induces circular Couette flow which is potentially unstable to centrifugally driven perturbations leading to longitudinal vortices. The radial temperature gradient induces a baroclinic vertical flow (ascending near the hot surface and descending near the cold one). This flow has a velocity profile with an inflexion point and it is potentially unstable to transverse oscillatory perturbations. The present study is concerned with experimental and linear stability analysis of this flow when the driving forces (control parameters) are increased in magnitude.

2 Experimental setup and stability analysis

The experimental setup consists of two coaxial cylinders of height $L = 55.9\,cm$ and a gap $d = 0.5\,cm$. The aspect raio of the system is $\Gamma = 111.8$ and the radius ratio$\eta = 0.8$. The inner cylinder is rotating at angular frequency Ω while the outer cylinder is fixed. Inside the inner cylindrical tube was circulating a water low maintained at controlled temperature T_1 and the outer cylinder was immersed into a large thermal bath maintained at controlled temperature T_2. The working fluid is a deionized water with a kinematic viscosity $\nu = 10^{-}2\,cm^2/s$ at $T = 295K$. The flow is described by three control parameters : the Prandtl number $Pr = \nu/\kappa$, the Grashof number $Gr = \alpha\delta T g d^3/\nu^2$ which measures the magnitude of the temperature gradient on the flow and the Taylor number $Ta = (\Omega a d/\nu)(d/a)^{1/2}$ related to rotation and therefore counting for centrifugal effects. The flow was visualized by adding a suspension of Kalliroscope AQ1000 in 2% by volume. To visualize the temperature fields, we seeded the flow with SR25C5W thermochromic liquid crystals from Hallcrest of about by 0.05%. They occur in form of encapsulated spheres of mean diameter $75m$ and their response time to a temperature change is about $3ms$. These particles have also been used to determine the velocity components, using a Basler IEEE-1394 camera, by tacking pictures of the cross section with a time delay of 82 ms.

2.1 Experimental results

A radial temperature gradient imposed on the cylindrical surfaces of the flow annulus induces a large convective cell with particules ascending near the hot wall and descending near the cold one. For a fixed value of Grashof number, we have increased the rotation rate until we obtained a bifurcation to a new state formed of pattern of helicoidal vortices (Figure 1-a). All critical states are represented in the diagram (Gr, Ta) in Figure 1-b. For chosen state, we have measured the velocity field and the temperature in the cross section (Figure 2).

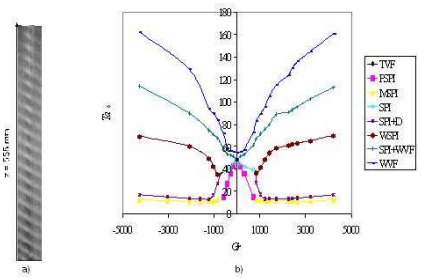

Figure 1: a) Pattern obsevred for $Ta = 24$ and Gr=706. b) Diagram of bifurcations in the plane Gr, Ta).

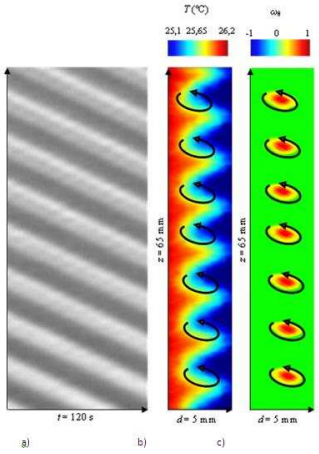

Figure 2: a) Space-time diagram of the pattern obsevred for Ta= 24 and Gr=706. b) Temperature distribution in the gap, c) Vorticity distribution in the gap.

2.2 Linear stability analysis

The flow is governed by the Navier-Stokes equations, energy equation and mass conservation equations written in cylindrical coordinates together with no-slip boundary conditions and isothermal cylindrical surfaces. Neglecting the end effects near the top and bottom plates, the base flow velocity profile is $\vec{v} = V(r)\vec{e}_\theta + W(r)\vec{e}_z$ where $V(r)$ and $W(r)$ are the circular Couette profile and the baroclinic axial velocity component respectively; their expressions can be found in [5]. We have performed linear stability of this flow assuming an infinite length of the system. We found that critical modes are nonaxisymmetric oscillating vortices. The variation of critical values of Ta with Gr are in a very good agreement with experimental ones. The corresponding state diagrams are well superimposed.

3 Conclusion

We have performed thourough investigation of stability of the flow between differentially rotating annulus with a radial temperature gradient. We have found a good agreement between experimental results, those from linear stability analysis and from numerical simulations [7].

References

[1] F. Kreith, Convection Heat Transfer in rotating systems, in *Advances in Heat Transfer* **5**, Academic Press NY, 129 (1968).

[2] H.A. Snyder, S.K.F. Karlsson, Experiments on the stability of Couette motion with a radial thermal gradient, *Phys. Fluids.* **7**(10), 1696 (1964).

[3] P.D. Weidman and M. E. Ali, On the stability of circular Couette flow with a radial heating, *J. Fluid Mech.***2**20, 53 (1990).

[4] D.C. Kuo, K.S. Ball, Taylor-Couette flow with buoyancy: onset of spiral flow, *Phys. Fluids* **9**, 2872 (1997).

[5] V. Lepiller, A. Goharzadeh, A. Prigent and I. Mutabazi, Weak temperature gradient effect on the stability of the circular Couette flow, *Euro.Phys. J. B* **61**, 445 (2008).

[6] R. Guillerm, Etude expérimentale des instabilits thermo-hydrodynamiques dans un systme de Couette-Taylor, *Thèse de doctorat de l'Université du Havre* (2010).

[7] D.H. Yoon, C.W.Kang, K.S. Yang and I. Mutabazi, Effect of radial temperature gradient on Taylor vortex flow, 16^{th} Int. Couette Taylor Workshop, Princeton 9-11 September 2009

MULTIVARIATE DATA ANALYSIS METHODS FOR DETECTING BAROCLINIC WAVE INTERACTIONS IN THE THERMALLY DRIVEN ROTATING ANNULUS

Thomas von Larcher[1], Uwe Harlander[2] & C. Egbers[2]
[1] *Institute for Mathematics, Freie Universität Berlin, Germany.*
[2] *Dept. of Aerodynamics and Fluid Mechanics, Brandenburg University of Technology Cottbus, Germany*

1 Motivation

Since the pioneering studies by R. Hide in the fifties of the last century [4], the elegant laboratory set-up of the differentially heated, rotating cylindrical gap of fluid is used by many authors to study the stability as well as the transition of fully 3D wavy flow patterns. They evolve from the release of potential energy through baroclinic instability that occur due to a radial temperature gradient and rotation. A vertically and horizontally sheared mean flow develops from which regular and complex wave flow patterns of different wave number can then emerge. These wave flows are called baroclinic waves due to the underlying instability mechanism, and the flow regimes, that develop in the annulus, depend mainly on two forcing parameters, i.e. on the temperature difference ΔT and on the angular velocity Ω. Note that the fluid viscosity is also a key parameter (e.g., [1]), but is kept fix in the experiments.

The rotating annulus, though being subject to detailed investigations since more than four decades, is still of interest not only in recent experimental research with respect to atmospheric sciences but also in the development of new numerical models where it then can be used as reference for the validation of new model concepts. For this purpose, the set-up might be particularly suited due to its relative simple geometry as well as due to the well definable forcing parameters. On the other hand, a rich flow behaviour is found that is either steady or time-dependent (e.g., [2], [5], [6]). The latter one, for example, undergoes changes in the wave amplitude or shape and also more types of complex flow patterns are known to exist, driven by e.g., wave-wave interactions and wave-mean flow interactions.

Our experimental set-up, described in detail in [7], is one of only few exclusive reference experiments within the priority program 'Multiple Scales in Fluid Mechanics and Meteorology' (MetStröm), that focus on the development of spatiotemporal, multiple scales numerical model concepts, see *http://metstroem.mi.fu-berlin.de.*

2 Data analysis methods

In our experimental study, we make use of non-intrusive measurement techniques of a quite different nature to better understand the transition from the regular wave regime to the quasi-chaotic regime at high rotation rates and to reveal the underlying dynamic processes of complex wave flow patterns. While the high accurate Laser-Doppler-Velocimetry (LDV) and Particle Image Velocimetry (PIV) is used for the acquisition of high resolution velocity data, a high sensitive thermographic camera, which resolution allows for resolving fine scale structures, measures time series of temperature distribution at the surface. These techniques allow us to detect the flow dynamics in the subsurface, as well as the dynamics of the surface flow.

Both time series data are analyzed by using multivariate statistical techniques. While the LDV data sets are studied by applying the Multi-Channel Singular Spectrum Analysis ($M-SSA$), the temperature data sets are analyzed by applying the Empirical Orthogonal Functions (EOF). In addition, the temperature data are processed in a way to become comparable to the LDV data, i.e. reducing the size of the data set in such a manner that the temperature measurements would imaginary be performed at equidistant azimuthal positions only. This approach initially results per se in a great loss of information. But applying the $M-SSA$ to the reduced temperature data sets enables us not only to compare the different data analysis methods but also to reclassify the results yielded with the LDV data analysis.

2.1 Exemplary analysis of a particular data set

An exemplary analysis run of one particular temperature data set is shown in figure 1. The dominating regular wave pattern of azimuthal wave number m=3 has three vortices of lower temperature at the inner (cooler) sidewall and three relative warm regions near the outer (warmer) sidewall, see figure 1a. The narrow jet-stream circumventing the eddies transports heat and momentum. Figure 1b shows a spatio-temporal plot of the processed data. The drift rate of the dominating mode m=3 is determined to $0.025^{\mathrm{rad}}/_{\mathrm{s}}$. That wave mode is also found in the first component of the data reconstruction using the (EOF 1 and 2) of the ($M-SSA$), see figure 1c. At this parameter point, no higher mode than m=3 is found.

3 Objectives

Our work presented here is based on a previous experimental study on baroclinic wave interactions by [3] who apply multivariate, statistical data analysis methods to velocity data. In addition, we use temperature data as well as velocity data, which are measured at the same parameter points but –unfortunately– not synchronous. The use of different data acquisition techniques allow us to match not only the information coming from the analysis of temperature and velocity data but also to match the analysis of the surface flow and of subsurface flows. For example, the results of the (EOF) analysis of velocity and temperature data can be used to calculate the turbulent radial heat flux ($v'T'$), which is a key parameter for understanding the observed flow phenomena (v' (T') denotes the deviation from the mean velocity (temperature)).

With the use of the statistical analysis tools, we gain the knowledge of the variability of the flow regimes particularly in the transition between regular wave modes of different azimuthal wave number as well as in the transition to quasi-chaotic flow. Our work is a continuation of the efforts of the authors and colleagues to reach these goals and it should be regarded as part of an overall operation.

References

[1] J.S. Fein and R. L. Pfeffer, An experimental study of the effects of Prandtl number on thermal convection in a rotating, differentially heated cylindrical annulus of fluid. *J. Fluid Mech.* **75**, 81–112 (1976).

[2] W.-G. Früh and P. L. Read, Wave interactions and the transition to chaos of baroclinic waves in a thermally driven rotating annulus. *Phil. Trans. R. Soc. Lond. A* **355**, 101–153 (1997).

[3] U. Harlander, Th. von Larcher, Y. Wang and C. Egbers, PIV- and LDV-measurements of baroclinic wave interactions in a thermally driven rotating annulus. *Experiments in Fluids* **10.1007/s00348-009-0792-5**, 1-13 (2009).

[4] R. Hide, An experimental study of thermal convection in a rotating fluid *Phil. Trans. Roy. Soc. Lond. A* **250**, 441–478 (1958).

[5] P. L. Read and M. J. Bell and D. W. Johnson and R. M. Small, Quasi-periodic and chaotic flow regimes in a thermaly-driven, rotating fluid annulus. *J. Fluid Mech.* **238**, 599–632 (1992).

[6] B. Sitte and C. Egbers, Higher order dynamics of baroclinc waves. In: Physics of Rotating Fluids, G. Pfister and C. Egbers (eds.), Springer, 355–375 (2000).

[7] Th. von Larcher and Ch. Egbers, Experiments on transitions of baroclinic waves in a differentially heated rotating annulus. *Nonlin. Proc. in Geophys.* **12**, 1033–1041 (2005).

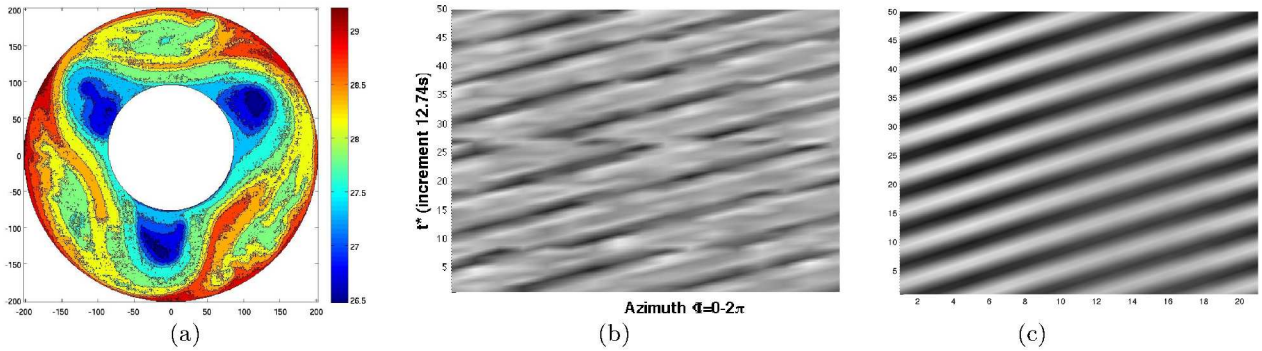

(a) (b) (c)

Figure 1: Exemplary analysis of a regular wave flow of wave number m=3. (a) View of surface temperature distribution, unit [°C], (b) merge plot of temperature time series processed at 20 equidistant locations on mid radius, the anomaly at $t^* \approx 27$ results from a malfunction during data acquisition, unit [°C]. (c) Reconstructed time series using EOF 1 and 2 computed of the temperature data set.

DYNAMICS OF FLOWS WITH HELICAL SYMMETRY

Maurice ROSSI[1,2], Ivan DELBENDE[1,3] & Benjamin PITON[1,3]
[1] *Université Pierre et Marie Curie-Paris 6 (UPMC)*
[2] *IJLRA-UPMC, 4 place Jussieu, case 162, 75232 Paris Cedex 05, France*
[3] *LIMSI-CNRS, BP 133, 91403 Orsay Cedex, France*

1 Context and objectives

Rotating devices such as propellers, wind turbines, helicopter rotors are known to develop a system of helical vortices in their wake. These structures result from the rapid roll-up of the vorticity sheet continuously generated at the trailing edge of the rotating blades. Very often, these flows display a helical symmetry, meaning that they are, at least locally, invariant through combined axial translation of distance Δz and rotation of angle $\theta = \Delta z/L$ around the same z-axis. The helix pitch $2\pi L$ is then a spatial period of the flow. In the literature, the analytical [1, 2] and numerical [3] works describing stationary helical vortices have been mostly restricted to helical vortex filaments and patches in inviscid situations with the vorticity always pointing along helical lines of pitch $2\pi L$. However, wake vortices form through the roll-up of the trailing vorticity sheet, and viscous diffusion eventually leads to continuous distributed vorticity distributions within the vortex cores, such as Gaussian. Moreover, a distribution of axial velocity may also be present, which has always been disregarded in the literature.
The objective of the current study is to simulate the viscous dynamics of helical vortex systems without the above restrictions. We present here an original DNS code [4] which solves the incompressible Navier–Stokes equations with enforced helical symmetry at fixed pitch $2\pi L$. The three-dimensional equations are reduced to a modified two-dimensional unsteady problem which can be solved via a generalised vorticity/streamfunction formulation. The code is thus able to take 3D vortex curvature and torsion effects into account while the resolution is of a 2D type, allowing for finer grids, higher Reynolds numbers and longer integration times.

2 Results

In this framework, we study the long-time (or equivalently far-wake) dynamics of systems with 2 and 3 helical vortices regularly spaced along a cylinder of radius R. Figure 1 shows the time evolution of the distance between two interacting helical vortices (when cut in a plane perpendicular to their common axis) for different values of the reduced pitch L. At high pitch ($L/R > 2$), one recovers the classical picture of pure 2D vortex merging ($L = \infty$), yet with larger evolution time scales. At smaller pitch (see $L/R = 0.8$) a quite different type of vortex merging occurs which involves neighbouring spires, as shown in figures 2 and 3. The conditions on vortex pitch and core size leading to one type of merging or to the other as well as the associated transition are investigated. Helically symmetric flows are also produced by natural instability of axisymmetric jets, wakes and trailing vortices. DNS of the nonlinear saturation of such instabilities are presented here in the case of the Batchelor vortex. We retrieve the different behaviours observed when the swirl parameter is varied [5], and we present new results concerning the saturation of viscous centered modes [6].

References

[1] J. C. Hardin, The velocity field induced by a helical vortex filament. *Phys. Fluids* **25**(11), 1949–1952 (1982).

[2] P. A. Kuibin and V. L. Okulov, Self-induced motion and asymptotic expansion of the velocity field in the vicinity of a helical vortex filament. *Phys. Fluids* **10**, 607–614 (1998).

[3] D. Lucas and D. G. Dritschel, A family of helically symmetric vortex equilibria. *J. Fluid Mech.* **634**, 245–268 (2009).

[4] I. Delbende, M. Rossi and O. Daube, DNS of flows with helical symmetry. Submitted to *Theoret. Comput. Fluid Dynamics* (2011).

[5] I. Delbende and M. Rossi, Nonlinear evolution of a swirling jet instability. *Phys. Fluids* **17**(4), 044103 (2005).

[6] S. Le Dizès and D. Fabre, Large-Reynolds-number asymptotic analysis of viscous centre modes in vortices. *J. Fluid Mech.* **585**, 153–180 (2007).

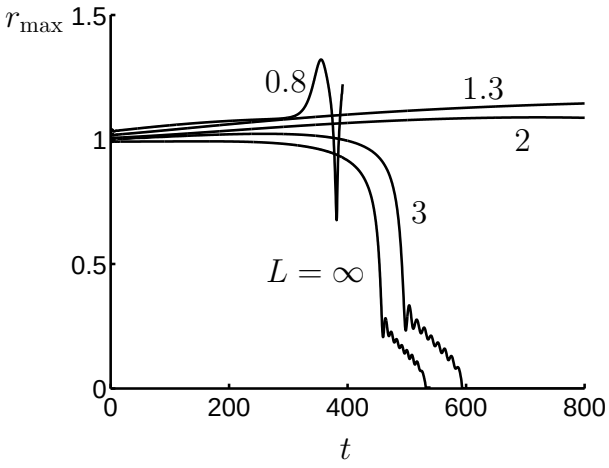

Figure 1: Merging of two helical vortices at $Re = \Gamma/\nu = 10000$ for different values of the reduced pitch L: time evolution of the distance $r_{\max}$ of one of the vortices from the axis. Initially, the helical vortices have circulation $\Gamma = 1$, core size $a = 0.2$ and are on a cylinder of radius $R = 1$.

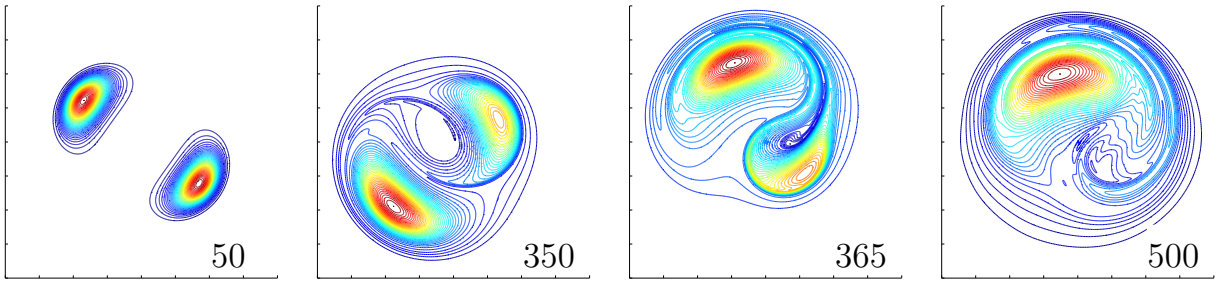

Figure 2: Merging of two helical vortices at pitch $L = 0.8$ at $Re = 10000$. Initially, the helical vortices have circulation $\Gamma = 1$, core size $a = 0.2$ and are on a cylinder of radius $R = 1$. Snapshots of the helical vorticity component for different times in a plane perpendicular to the helix z-axis.

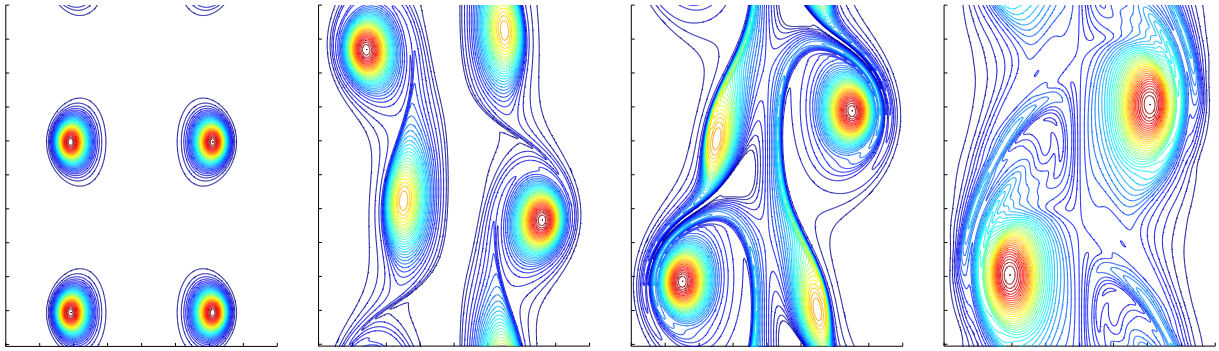

Figure 3: Same as 2 but viewed in a meridian plane.

SPATIO-TEMPORAL DEVELOPMENT OF INSTABILITIES IN HELICAL VORTICES

H. Bolnot, S. Le Dizès & T. Leweke
IRPHE, CNRS & Aix-Marseille University, 49 rue Joliot-Curie, F-13013 Marseille France

In aeronautics, the dynamics of helical vortices are of interest for many applications. For instance, helicopter wakes exhibit a global transition to the Vortex Ring State (VRS) in steep descent regimes which can lead to a loss of control and crash the apparatus. This transition could be associated with an instability phenomenon and we will argue that it is due to the change of nature from convective to absolute of the pairing instability. For wind turbines, instabilities are also known to be responsible for the turbulence in the far wake. Understanding the spatio-temporal development of the different instabilities is therefore also important in this context. In this work, we consider the particular instability that leads to vortex pairing and address our results in both context of wind turbines and helicopter.

Numerical simulations have shown that several instabilities can occur in helical wakes. Both the three-dimensional elliptic instability and the two-dimensional pairing instability were found to play an important role in helicopter as well as wind turbine wakes (Leishman *et al.* [1], Walther *et al.* [2]). However, the theoretical results known about the stability properties of a helical vortex wake were established for only few model cases: a helical filament (Widnall [3]) or in the limit of large wavenumbers (Okulov [4], Okulov and Sørensen [5]). For the pairing instability, which requires to take into account the geometry of the vortex core, a systematic analysis of the absolute/convective nature of the instability was performed numerically in the case of an array of straight vortices (Brancher and Chomaz [6]) but has still to be done for a helical vortex wake.

In order to focus on the development of the pairing instability and filter out all other instabilities, the helical wake is represented by an array of axisymmetric vortex rings. For small helix pitches, this provides a good approximation of the azimuthal vorticity field, as shown in Figure 1. The instabilities developing along the array of vortex rings are characterized in detail. The linearized Navier-Stokes equations for the perturbations are discretized by means of a spectral method, in order to describe the spatio-temporal evolution of the wave packet generated by a localized initial perturbation. The temporal growth rate of the pairing instability is obtained as a function of the perturbation propagation speed for the different parameters ($\frac{a_0}{R}$, $\frac{a_0}{h}$, Re) of the system. A conclusion is eventually made on the different flow configurations that could lead to the Vortex Ring State, which arises when unstable perturbations (with a positive growth rate) propagate upstream faster than the advection speed of vortices. For wind turbine configurations, the distance (behind the rotor plane) at which the pairing instability initiates will be determined as a function of the parameters, which represents a major issue in the design of wind turbine farms.

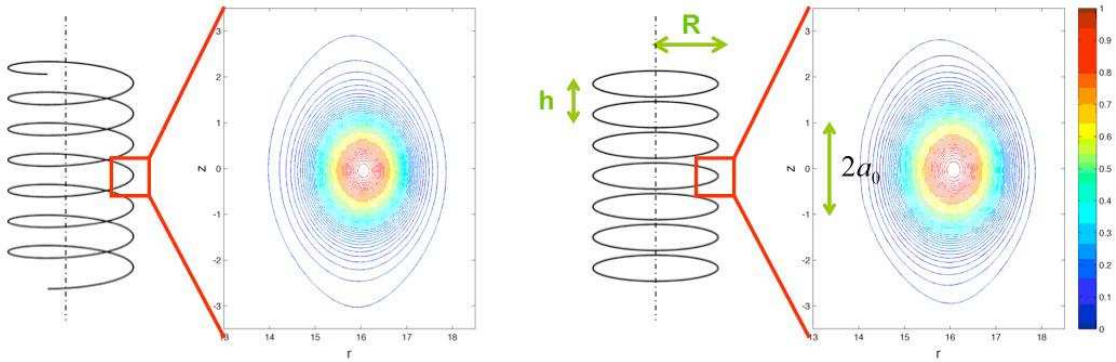

Figure 1: Sketches and azimuthal vorticity contours of a helical vortex (left) and of a vortex rings array (right). The initial condition in both cases is a Gaussian vortex of core radius a_0 and with no axial velocity. Simulations were run for $\frac{a_0}{R} = \frac{1}{16}$ and $\frac{a_0}{h} = \frac{1}{8}$ at $Re = \frac{\Gamma}{2\,\pi\,\nu} = 500$. The helical vortex is computed by forcing the flow to have a helical symmetry (see Delbende [7]).

In parallel with this theoretical approach, experimental results concerning helical wakes will be presented. The characteristics of the wake behind a rotor for different tip speed ratios, defined as the tip speed over the external speed $TSR = \frac{V_{tip}}{V_{ext}}$, are analyzed qualitatively as well as quantitatively.

The facility used here is a closed loop water channel in which an external field can be imposed to the rotor. This free surface channel has a test section of $38 * 50 * 150\ cm^3$ and generates a constant incoming velocity (less than 1 % of turbulence) up to 100 cm/s. A visual access is available on the 5 sides of the test section. The

rotor diameter is 16 *cm* and its rotational speed can be varied up to 10 *rps*. The sense of rotation determines whether the rotor accelerates the fluid (helicopter climb regime) or if it produces a counter flow (helicopter descent regimes and wind turbines configuration). Qualitative observations of the wake are made through dye visualizations, either by injecting a line of fluorescein upstream of the rotor plane or by painting directly the surface of the blades at the tip location in order to visualize the center of the tip vortices which evolves in the wake downstream as shown in Figure 2(a). A quantitative analysis of the wake is also performed thanks to Stereo Particle Image Velocimetry (SPIV). The vortical structure developing in the wake is identified precisely by calculating the characteristics of the vortices (position, core size, circulation, axial velocity) as a function of their age. For instance, Figure 2(b) shows a three-dimensional reconstruction of the vorticity field obtained by interpolating azimuthally the phase-averaged vorticity calculated in a plane containing the rotor axis.

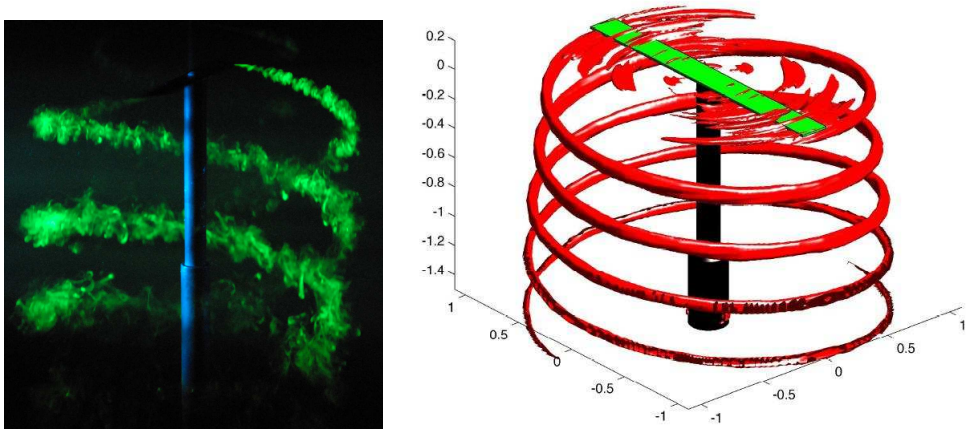

(a) (b)

Figure 2: (Left) Dye visualization of the wake illuminated in volume in climb regime at $TSR = 4.5$ The incoming velocity as well as the induced velocity of the rotor are oriented downwards. (Right) Isocontour of vorticity of the 3D wake in climb regime at $TSR = \frac{V_{tip}}{V_{ext}} = 10$ (with $V_{tip} = 100\ cm/s$, $V_{ext} = 10\ cm/s$ and Reynolds number based on the chord and the tip speed $Re = 15000$).

These experimental results are eventually compared with the numerical predictions concerning the threshold of the transition leading to VRS for helicopter configurations and the distance at which the pairing instability occurs in the case of wind turbine wakes.

This work is supported by EUROCOPTER S.A.S. through a doctoral grant (contract no. IPEC 0187N/2009).

References

[1] Bhagwat M.J. Leishman J.G. and Ananthan S. The vortex ring state as a spatially and temporally developing wake instability. *J. American Helicopter Society*, 49 (1), 2004.

[2] Walther J.H. *et al.* A numerical study of the stability of helical vortices using vortex methods. *J. Phys. Conf Series*, 75:012034, 2007.

[3] Widnall S.E. The stability of a helical vortex filament. *J. Fluid Mech.*, 54:641–663, 1972.

[4] Okulov V.L. On the stability of multiple helical vortices. *J. Fluid Mech.*, 521:319–342, 2004.

[5] Okulov V.L. and Sørensen J.N. Stability of helical tip vortices in a rotor far wake. *J. Fluid Mech.*, 576:1–25, 2007.

[6] Brancher P. and Chomaz J.M. Absolute and convective secondary instabilities in spatially periodic shear flows. *Phys. Review Letters*, 78:658–661, 1997.

[7] Delbende I. DNS of vortices with helical symmetry. *Proceedings of the* 8^{th} *Euromech Fluid Mechanics Conference*, 2010.

DEVELOPMENT OF HELICAL VORTEX THEORY

Valery OKULOV
Department of Mechanical Engineering and Center for Fluid Dynamics,
Technical University of Denmark, 2800 Kgs. Lyngby, Denmark; E-mail: vaok@mek.dtu.dk

The main goal of the current communication is to attract attention to the thriving theory of helical vortices which are 2-D from Euler's consideration and looks from this point of view like "plane" flows (fig. 1a) but with additional uniform rotation of a plane pattern of the flow along fixed axis (fig. 1b). However, from Lagrange's point of view the 2-D helical vortices induce strong 3-D motion of fluid particles (fig. 1c) [1].

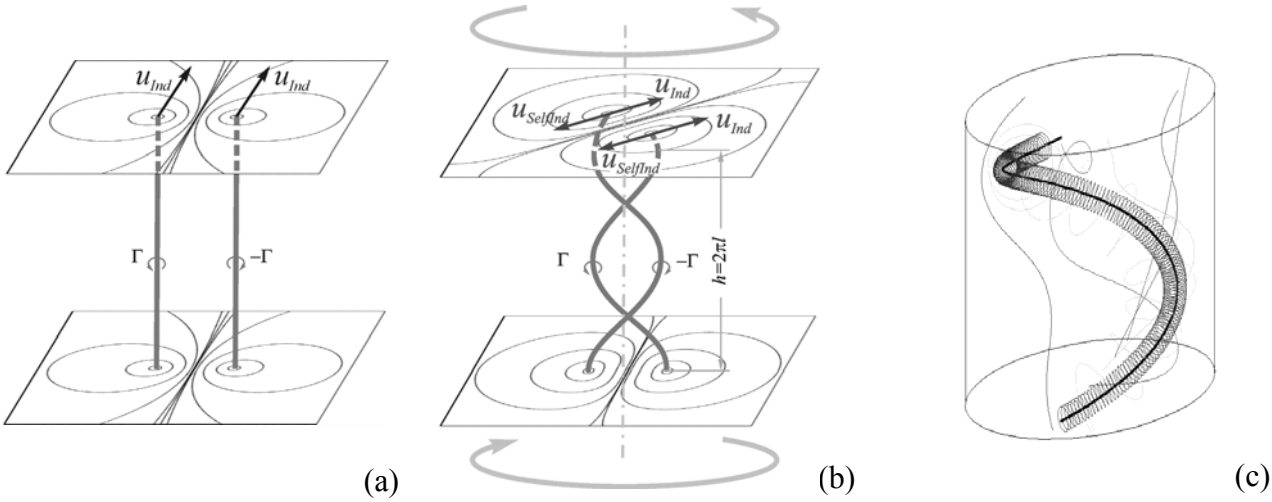

Figure 1. Examples of 2-D flows with rectilinear (a) and helical vortices (b);
3-D paths of fluid particles induced by single helical vortex filament in a cylinder (c).

At present the theory of 2-D helical vortex dynamics are based on various analytical components, which holds true for all values of the helix pitch, such as (i) the 2-D Biot-Savart law for helical filaments represented by Kapteyn series [2] or rewriting in a form with singularity separation [3] (fig. 2); (ii) solutions of helical vortex tubes with finite core, governed by series expansion of helical multipoles [4]; (iii) relations between the induction of vortex filaments and the self-induced velocity of helical vortex tubes [5] resulting in a closed analytical solution of the helix motion [6]; (iv) analytical representation of Goldstein's solution for the circulation of a helical vortex sheet in equilibrium [7]; (v) Kelvin's N-gon stability problem of point vortices generalized to multiple helical vortices [6, 8].

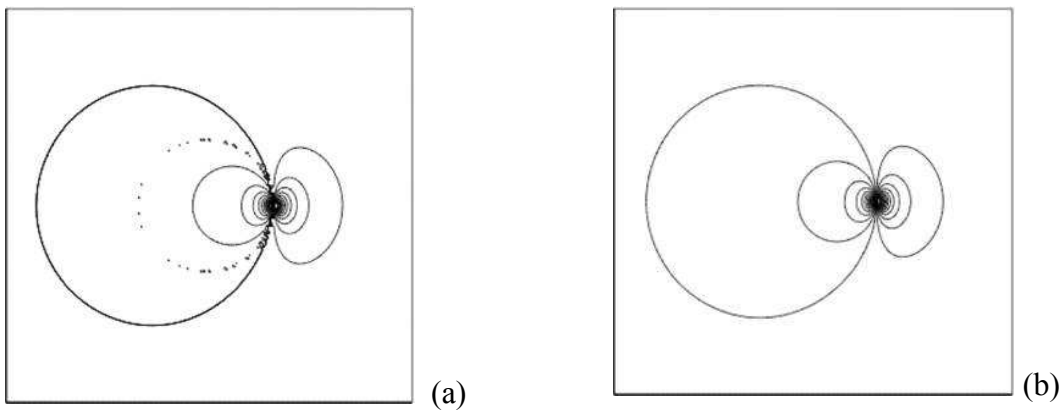

Figure 2. Isolines of the azimuthal velocity field induced in cross-section by helical vortex filament:
(a) inaccurate simulation by finite part of the Kapteyn series with unreal singularities on cylinder supporting the helix;
(b) accurate simulation after separation of the singularity along the helix filament in the Kapteyn series [3].

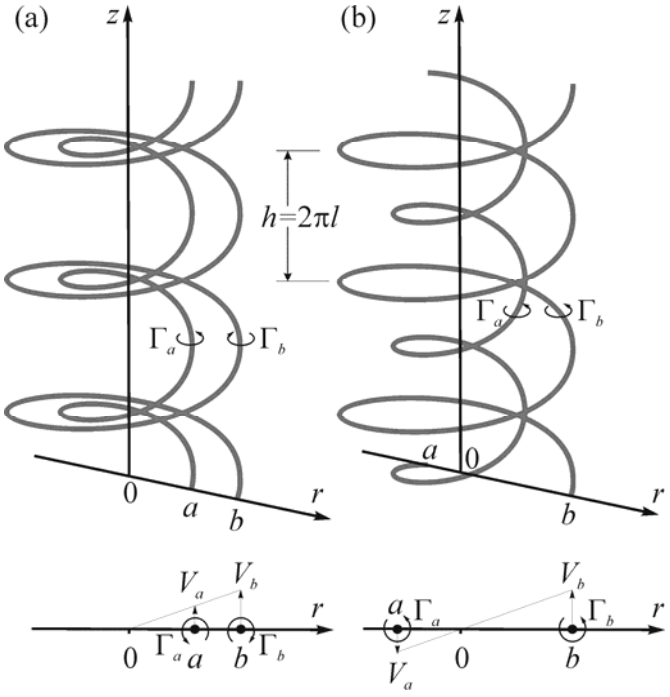

Figure 3. Two possibilities for equilibrium of helical vortex pairs and its prototypes from point vortex pairs: (a) centre or axis of rotation lies on the same hand from both point vortices; (b) centre of or axis rotation lies between ones

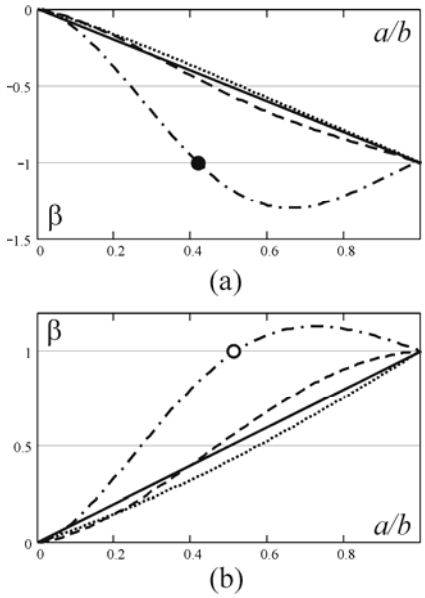

Figure 4. The circulation ratio β of the two helical vortices in equilibrium rotation as function of their relative proximity for different values of helical pitch *h*: 1.5 (dash-dotted lines); 2(dashed lines); 5 (dotted lines); infinity (solid lines). Circle and point indicate equilibrium of the helical pairs with different levers.

An important result of the 2-D helical vortex theory is that the vorticity submitted to the helical symmetry does not vary along a trajectory of fluid particles. It coincides with conclusion of point vortex dynamics but in contrast of the plane one, where the total vortex motion consists of the mutual induction of other point vortices, for helix case in additional to an induced flow field due to induction from the other helical vortices on the surroundings a self-induction of the helical vortex should be included too. In result of this difference unexpressed applications of the 2-D helical vortex dynamics were established. For example figs. 3 and 4 demonstrate how the two helical vortices (vortex pair) with the same or opposite circulations but different levers can be in equilibrium rotation which is impossible for two point vortices. In the presentation it was also shown how the assumption of helical symmetry in the context of 2-D helical vortices can be exploited to analyze and model various cases of rotating flows.

References

[1] Alekseenko S.V., Kuibin P.A., Okulov V.L. Theory of Concentrated Vortices: An Introduction. Springer (2007)
[2] Hardin, J.C.: The velocity field induced by a helical vortex filament. Phys. Fluids 25, 1949–1952 (1982)
[3] Okulov, V.L.: Determination of the velocity field induced by vortex filaments of cylindric and weak conic shapes. Russ. J. Eng. Thermophys. 5(2), 63–75 (1995)
[4] Fukumoto, Y., Okulov, V.L.: The velocity field induced by a helical vortex tube. Phys. Fluids 17(10), 107101 (2005)
[5] Boersma, J., Wood, D.H.: On the self-induced motion of a helical vortex. J. Fluid Mech. 384, 263–280 (1999)
[6] Okulov, V.L.: On the stability of multiple helical vortices. J. Fluid Mech. 521, 319–342 (2004)
[7] Goldstein, S.: On the vortex theory of screw propellers. Proc. R. Soc. Lond. A 123(792), 440–465 (1929)
[8] Okulov, V.L., Sørensen, J.N.: Stability of helical tip vortices in a rotor far wake. J. Fluid Mech. 576, 1–25 (2007)

A UNIFIED CRITERION FOR THE CENTRIFUGAL INSTABILITY OF VORTICES AND SWIRLING JETS

Paul Billant[1], Francois Gallaire[2]
[1]*LadHyX, CNRS-Ecole Polytechnique, F-91128 Palaiseau, France.*
[2]*LFMI, EPFL, 1015 Lausanne, Switzerland.*

It is well known that swirling jets can become centrifugally unstable like pure vortices but with a different azimuthal wavenumber selection. The Leibovich and Stewartson [1] criterion is a generalization of the Rayleigh criterion to swirling jets: it is a sufficient condition for instability with respect to perturbations with both large axial and azimuthal wavenumbers. We have relaxed the large azimuthal wavenumber assumption in this criterion and obtained a new criterion that is valid whatever the azimuthal wavenumber and whatever the magnitude of the axial flow: from zero (pure vortex) to finite values (swirling jets). The new criterion recovers the Leibovich-Stewartson criterion when the azimuthal wavenumber is large and the Rayleigh criterion when the azimuthal wavenumber is finite [2]. The criterion is confirmed by comparisons with numerical stability analyses of various classes of swirling jet profiles. In the case of the Batchelor vortex, it provides more accurate results for perturbations with finite azimuthal wavenumbers than the Leibovich-Stewartson criterion (figure 1). The criterion shows also that a whole range of azimuthal wavenumbers are destabilized as soon as a non-zero axial velocity component is present in a centrifugally unstable vortex.

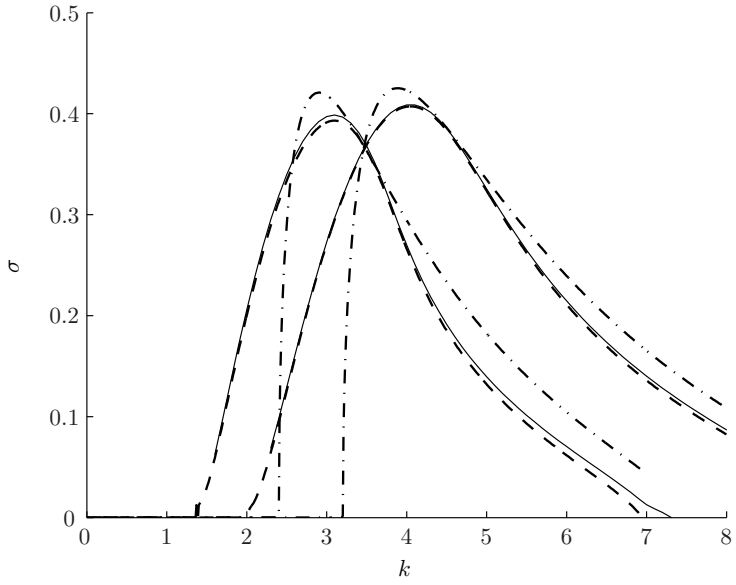

Figure 1: Growth rate as a function of the axial wavenumber k for the Batchelor vortex for the swirling parameter $q = 0.8$ and the azimuthal wavenumbers $m = -6$ and $m = -8$ (from left to right). Solid line: exact result, dashed line: present criterion, dashed-dotted line: Leibovich & Stewartson criterion.

References

[1] S. Leibovich & K. Stewartson A sufficient condition for the instability of columnar vortices. *J. Fluid Mech.* **126**, 335–356 (1983).

[2] P. Billant & F. Gallaire Generalized rayleigh criterion for non-axisymmetric centrifugal instabilities. *J. Fluid Mech.* **542**, 365–379 (2005).

TRANSITION CHARACTERISTICS OF A SWIRLING ANNULAR FLOW

Arturo Héctor GONZÁLEZ ARAYA[1]
[1] *Lehrstuhl für Fluidenergiemaschinen, Ruhr Universität, Bochum, Germany*

1 Introduction and scope of the work:

The subject of this paper is transition of a **swirling annular flow** induced by the Tollmien-Schlichting mechanism which is characterised by waves propagating with a certain speed in the shear flow. One of the outstanding characteristics of this flow is the helical shape of its streamlines. Flows with such streamlines are very difficult to successfully simulate with CFD, as the Reynolds stress tensor has a strong anisotropy [1]. The object of this work is to try to gain insight into the physical features both in qualitative and quantitative terms through studying the bifurcation characteristics of this flow on the verge of transition. The focus of our attention is on the shape of the Reynolds stress tensor, for which the relevant properties of the bifurcating solution of the nonlinear equation of motion for disturbances to the basic flow are examined. A set of (nonlinear) differential equations governing the dynamics of disturbances in a swirling flow is derived for the flow in the annular gap between concentric circular cylinders. The analysis is undertaken for the swirling flow when an axial pressure gradient (parameterized by Re, Reynolds number), a rotation of the outer cylinder (parameterized by S_a, rotation number) and the axial translation of the inner cylinder (parameterized by T_w, translation number) act simultaneously to maintain the swirling flow.

2 Outline of the method of Stewartson and Stuart to gain an understanding of the influence of flow parameters in this problem

The starting point of our work is a linear stability analysis for the flow described above. To this end it is necessary to derive the nonlinear equations of motion for the flow in which the pressure is eliminated as an unknown. The system of equations derived is referred to as the **extended Orr-Sommerfeld and Squire equations** which together with the continuity equation lead to the following equation system which is written in matrix notation $\mathscr{D}\mathbf{v} = \mathscr{N}$:

$$\mathscr{D} = \begin{pmatrix} D_{OSr} & D_{OS\varphi} & D_{OSx} \\ D_{Sqr} & D_{Sq\varphi} & D_{Sqx} \\ D_{Cor} & D_{Co\varphi} & D_{Cox}. \end{pmatrix}, \mathbf{v} = \begin{pmatrix} v_r \\ v_\varphi \\ v_x \end{pmatrix}, \mathscr{N} = \begin{pmatrix} \mathscr{N}_{OS} \\ \mathscr{N}_{Sq} \\ \mathscr{N}_{Co} \end{pmatrix} \tag{1}$$

Here D_{OS}, D_{Sq}, D_{Co}, $\mathbf{v}$ and $\mathscr{N}$ represent the operator in the classical Orr-Sommerfeld equation, Squire equation, continuity equation, velocity disturbance and nonlinear terms in the radial, azimuthal, and streamwise directions respectively.
When the velocity disturbance is considered small the nonlinear terms can be neglected and the equation system above becomes the classical eigenvalue problem with which it is possible to determine the neutral stability surface of the flow.

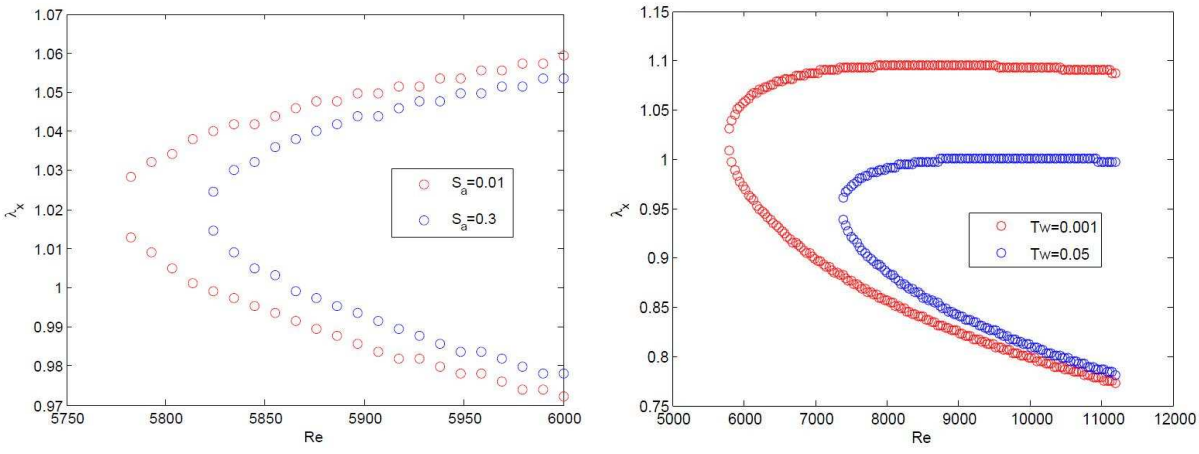

Figure 1: Neutral surfaces for a swirling annular flow.

The diagrams above demonstrate the stabilizing effect of both the rotation of the outer cylinder from $Sa = 0.01$ to $Sa = 0.3$ and the axial translation of inner cylinder from $Tw = 0.001$ to $Tw = 0.05$.
The figures of projections of these neutrally stable curves were evaluated numerically through MATLAB-programs.
Following the steps developed by Stewartson and Stuart for a weakly nonlinear theory, elementary waves centered around the neutral stability curve which were determined in the linear stability theory are used as part of a wave packet which for large times is described as superposition of several elementary waves moving with the group velocity and whose amplitude varies slowly. The slow variation of the amplitude is designated here as **B**. The wave packet has the following form:

$$\mathbf{v} = A_N(y)\exp[i\Theta_N]exp[\omega_{Ni}t] + c.c.. \tag{2}$$

$$\Theta_N(r,\varphi,x) = (\lambda_{Nx}x + n_{N\varphi}\varphi + \omega_N t) \tag{3}$$

Here the frecuency ω_N is permitted to be complex, the wavenumber λ_{Nx} is real whereas n_φ may assume only real integer values. The subscript N denotes values on the surface of neutral stability and i the imaginary part. The above form of the wave involves the identification of a small amplitude parameter ϵ_A with the temporal growth rate ω_{Ni} of the wave packet.
When the departure of the parameters of the flow (Re, Sa and Tw) is small relative to those of the neutral stability surface, the growth rate ω_{Ni} can be approximated by its Taylor expansion through the flow parameters [2].

$$\epsilon_A = \omega_{Ni} = d_{Re}|Re - Re_N| + d_{S_a}|S_a - S_{aN}| + d_{T_w}|T_w - T_{wN}| \tag{4}$$

With the help of this parameter it is possible to define new scales in the problem solving the nonlinear problem with the method of multiple scales. An asymptotic expansion is introduced for the velocity perturbation v as well as the extension of the partial derivatives of the equations in the new scales [3].

$$\mathbf{v} \simeq \epsilon_A^{\frac{1}{2}}\mathbf{v}_1 + \epsilon_A\mathbf{v}_2 + \epsilon_A^{\frac{3}{2}}\mathbf{v}_3 + o(\epsilon_A^{\frac{3}{2}}) \tag{5}$$

By substitution of (5) in (1) yields a new system of equations which is sorted according to the order of the approximations. In the compact matrix-operator notation these may be written as follows:

$$\begin{aligned} O(\epsilon_A^{\frac{1}{2}}) &: \mathscr{D}\mathbf{v}_1 = (RHS)_1 = 0. \\ O(\epsilon_A) &: \mathscr{D}\mathbf{v}_2 = (RHS)_2 \\ O(\epsilon_A^{\frac{3}{2}}) &: \mathscr{D}\mathbf{v}_3 = (RHS)_3 \end{aligned} \tag{6}$$

The solution for $\mathbf{v}_1$ is sought in a product form as follows:

$$\begin{aligned} \mathbf{v}_{1r} &= B_r(New\ scales)A_{Nr}(y)\exp[i\Theta_N] + c.c \\ \mathbf{v}_{1\varphi} &= B_\varphi(New\ scales)A_{N\varphi}(y)\exp[i\Theta_N] + c.c \\ \mathbf{v}_{1x} &= B_x(New\ scales)A_{Nx}(y)\exp[i\Theta_N] + c.c \end{aligned} \tag{7}$$

Formulating the solvability condition for the equations to the orders $O(\epsilon_A)$ and $O(\epsilon_A^{\frac{3}{2}})$ in (6) , which involves determining the solution of adjoint problem of original eigenvalue problem, one of the three equations necessary for the evolution equation of the amplitude B can be obtained.
The remaining equations for B can be obtained through the continuity equation and determining the direction of flow of kinetic energy in the fluctuation motion, matching the ratio of the partial derivatives of the kinetic energy to new scales with the ratio of the partial derivatives of ω_{Ni} to the wave numbers of the problem.
Besides it is expected that the form of the Reynolds stress tensor in the wall-normal direction is given by components of the tensor product of (A_{Nr}; $A_{N\varphi}$; A_{Nx}), with itself.

References

[1] Rocklage-Marliani, G.; Schmidts, M.; Vasanta Ram, V.I.: *Three-dimensional laser-Doppler velocimeter measurements in swirling turbulent pipe flow*; Flow, Turbulence and Combustion Vol. **70**, 43-67, 2003.

[2] Huerre, P. and Rossi, M.: Hydrodynamic Instabilities of Open Flows. In Godreche and Mannville (Eds.) *Hydrodynamic and Nonlinear Instabilties*, Cambridge University Press, Cambridge, UK, 1998.

[3] Stewartson, K. and Stuart, J. T.: *A nonlinear instability theory for a wave system in plane Poiseuille flow.*; J. Fluid Mech. **48**: 529-545, 1971.

AXISYMMETRIC VORTEX BREAKDOWN IN CONSTRICTED PIPES

François GALLAIRE[1], Philippe MELIGA[2]
[1] *Laboratory of Fluid Mechanics and Instabilities, Ecole Polytechnique Fdrale de Lausanne CH-1015 Lausanne, Switzerland.*
[2] *M2P2, UMR-6181 CNRS IMT, 38, Rue Frdric Joliot-Curie 13451 MARSEILLE Cedex 13, France.*

We investigate numerically and theoretically the axisymmetric vortex breakdown occurring in a contracting pipe of finite extension, i.e. the transition from a smooth columnar state to a breakdown state exhibiting a recirculation bubble. Velocity distributions are prescribed at the pipe inlet under the form of Batchelor vortices with uniform axial velocity and variable levels of confinement. A numerical continuation technique is developed to follow the branches of nonlinear steady solutions when varying the swirl parameter. In the most general case, for Re=500, vortex breakdown occurs abruptly owing to a subcritical, global instability of the non-parallel, viscous columnar solution, and results in the coexistence of multiple stable solutions over a finite range of swirl. For highly confined vortices, a second scenario prevails, where the flow transitions smoothly from the columnar to the breakdown state without any instability. These results are reminiscent of those obtained by [2] and [1] where slip is allowed at the wall.

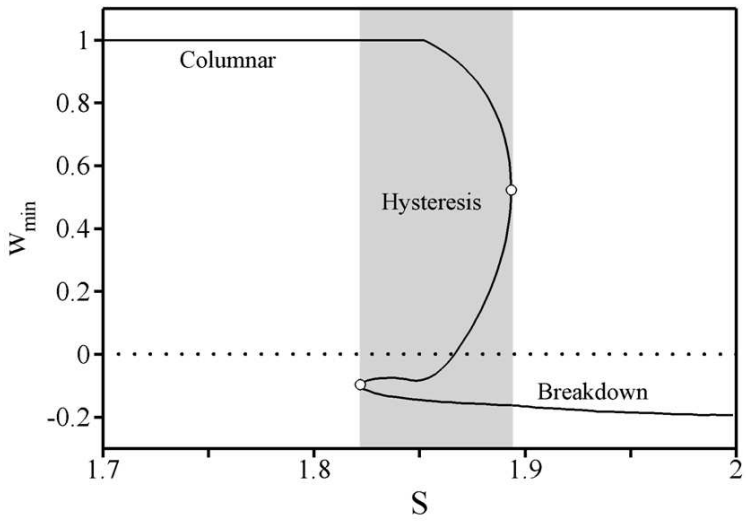

Figure 1: Bifurcation diagram illustrating the onset of vortex breakdown as the swirl is increased. The minimum axial velocity u_{min} is plotted as a function of the swirl - $Re = 500$.

The effect of a low flow rate jet positioned at the pipe wall is then characterized in the perspective of control. Its effectiveness is evaluated in light of three practically meaningful criteria, namely the ability of the control to optimize either the stability domain or the topology of the columnar state, and its ability to alleviate hysteresis. For each criterion, an optimal jet position is determined from nonlinear simulations.

The results are in good agreement with those issuing from an weakly nonlinear asymptotic expansion of the Navier- Stokes equations, which yields two normal forms describing the two saddle-node bifurcations underlying the fold structure of the bifurcation. The open-loop control enters as a forcing term in the resulting amplitude equations.

References

[1] P. S. Beran and F. E. Culick, The role of non-uniqueness in the development of vortex breakdown in tubes,*J. Fluid Mech.* **242**, 491–527 (1992).

[2] J.M. Lopez, "On the bifurcation structure of axisymmetric vortex breakdown in a constricted pipe"*Phys. Fluids* **6**, 3683–3693 (1993).

INFLUENCE OF PISTON POSITION ON THE SCAVENGING AND SWIRLING FLOW IN TWO-STROKE DIESEL ENGINES

A. Obeidat[1], S. Haider [1], K. E. Meyer [1], T. Schnipper [1] S. Mayer[2] & J. H. Walther[13]
[1] *Department of Mechanical Engineering, Technical University of Denmark, DK-2800 Kgs. Lyngby, Denmark*
[2] *MAN Diesel & Turbo, Teglholmsgade 41, DK-2450 Copenhagen SV, Denmark*
[3] *Chair of Computational Science, ETH Zurich, CH-8092 Zurich, Switzerland*

1 Introduction

We study the effect of piston position on the in-cylinder swirling flow in a low speed large two-stroke marine diesel engine model. We are using Large Eddy Simulations in OpenFOAM, with three different models for the turbulent flow: a one equation model (OEM), a dynamic one equation model (DOEM) and Ta Phuoc Loc's model (TPLM). The simulated flows are grid-independent and they are computed in situations analogous to two different piston positions where the air intake ports are uncovered 100% and 50%, respectively. We find that the average flow inside the cylinder changes qualitatively with port closure from a Burgers vortex profile to a solid body rotation while the axial velocity changes from a wake-like profile to a jet-like profile. The numerical results are compared with measurements in a similar geometry [3] and we find a good agreement between simulations and measurements. Furthermore, we consider the unsteady flow and identify a dominant frequency in a power spectrum based on velocity which we show is due to precession of the vortex core, and compare with measurements of the unsteady flow obtained with Laser Doppler Anemometry.

2 Numerical methods

We study the swirling flow numerically using large eddy simulations [6, 5]. We apply three different models. The one equation eddy model where the kinetic energy k is solved while another scale is estimated [7, 1, 5, 4, 6], the dynamic k-equation eddy-viscosity model, where the model constants are recalculated during the simulation rather than to be pre-calculated [2, 5, 6] and the Ta Phouc Loc model, which is based on the velocity-vorticity (v-ω) formulation of the Navier-Stokes equations, where two spatial filters are used [8, 9].

3 Computational domain and results

The computational domain is shown in Fig. 1 (a). Flow enters uniformly at an oblique angle which ensures the overall in-cylinder swirling flow as shown in Fig. 1 (b) [3]. All the results are obtained by simulating the flow on a grid with 8 million cells.

(a) (b)

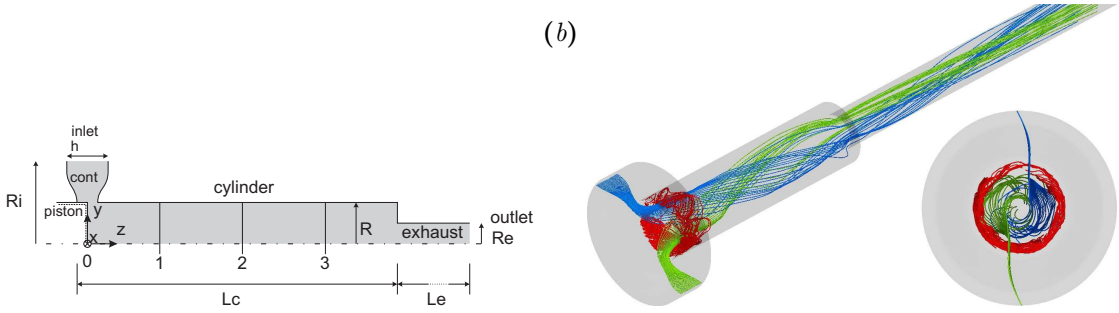

Figure 1: (a) Sketch of the cylindrical computational domain shown in grey shades, in the case where the piston covers the intake ports by 50%. Flow enters radially through the horizontal inlet section and exits through the vertical outlet. Notice that the exhaust is shortened in the figure. Data are extracted at the enumerated cross-sectional planes marked by z_i, and $R = 9.5$ cm. (b) Visualization of the three-dimensional time average streamlines (in blue and green colors) of the mean-field for the 100% open port case. Notice the 'braided' separation region shown by red streamlines and the modest pitch of the flow in the main cylinder. The small inset shows the swirling motion of the streamlines

Fig. 1 (*b*) shows the time average stream lines for the 100% open port case. The results shown in Fig. 2 demonstrate that the simulations capture the wake and jet like profiles of the axial velocity but both are not as pronounced as in the experimental results.

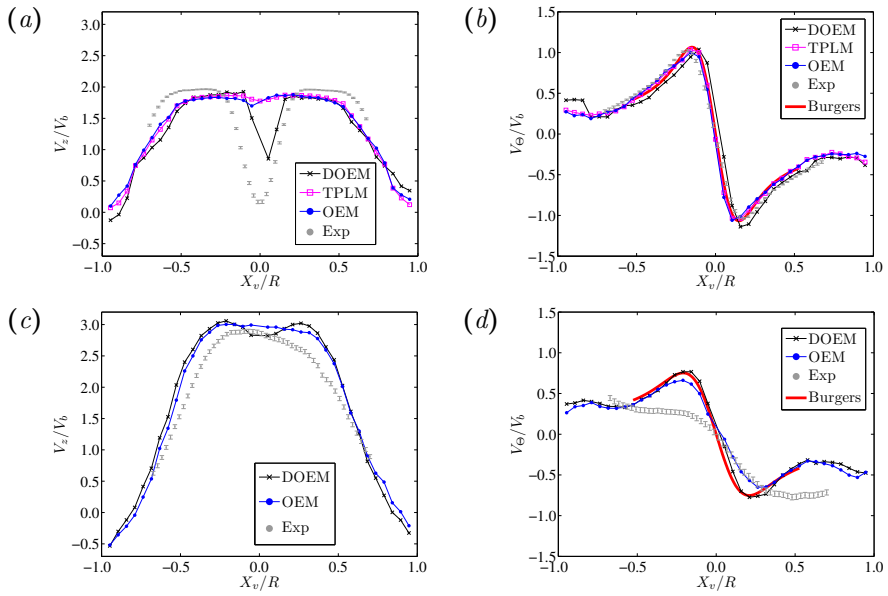

Figure 2: (*a,b*) Time averaged axial and tangential velocity profiles for the 100% open ports, (*c,d*) Time axial and tangential velocity profiles for the 50% open ports, at the axial position $z1/2R = 0.96$.

References

[1] L. Davidson. Large-Eddy Simulations: A dynamic one-equation subgrid model for three-dimensional recalculating flows. In *In 11th International Symposium on Turbulent Shear Flow*, pages 3:26.1–26.6, 1997.

[2] M. Germano, U. Piomelli, P. Moin, and W. Cabot. A dynamic subgrid-scale eddy viscosity model. *Phys. Fluids*, 3:1760–1765, 1991.

[3] S. Haider, A. Obeidat, K. E. Meyer, and J. H. Walther. Particle image velocimetry of swirling flow in a pipe. *J. Mar. Sci. Technol.*, submitted, 2011.

[4] Thomas J. R. Hughes, Luca Mazzei, Assad A. Oberai, and Alan A. Wray. The multiscale formulation of large eddy simulation: Decay of homogeneous isotropic turbulence. *Phys. Fluids*, 12(2):505–512, 2001.

[5] M. Lesieur, O. Metais, and P. Comte. *Large Eddy Simulations of Turbulence*. Cambridge University Press, 2005.

[6] Roland Schiestel. *Modeling and Simulation of Turbulent Flows*. John Wiley & Sons, 2007.

[7] U. Schumann. Subgrid Scale Model for Finite Difference Simulations of Turbulent Flows in Plane Channels and Annuli. *J. Comput. Phys.*, 18:376–404, 1975.

[8] L. Ta Phuoc. Modèles de sous maille appliqúes aux ecoulements instationnaires décollés. In *Proceedings of the DRET Conference: Aérodynamique Instationnaire Turbulente-Aspects Numériques et Expérimentaux*, pages 1–38, Orsay, France, 1994. Lab. d'Informatique pour la Mecanique et les Sciences de l'Ingénieur. Centre Natonal de la Recherche Scientifique.

[9] C. Tenaud, S. Pellerin, A. Dulieu, and L. Ta Phuoc. Large eddy simulations of a spatially developing incompressible 3D mixing layer using the **v**-ω formulation. *Computers & Fluids*, 34:67–96, 2005.

ON THE RELATION BETWEEN THE EQUATIONS FOR LARGE-EDDY SIMULATION OF TURBULENT FLOW AND FOR WEAKLY NONLINEAR EVOLUTION OF DISTURBANCES FOR FLOWS IN TRANSITION

Venkatesa Iyengar VASANTA RAM[1],
[1] *Institut für Thermo- und Fluidynamik, Ruhr Universität, Bochum, Germany.*

1 Summary

The work submitted herewith is based on the author's attempt to unveil the relationship between the equations for large-eddy simulation of turbulent flow (LES) and those for weakly nonlinear evolution of disturbances on the route to transition according to the nonlinear stability theory of Stewartson and Stuart [1]. Two flow examples in which three-dimensionality and rotation exercise significant effects on transition have been chosen for the purpose of illustrating the nature of this relationship. These are:

- The swirling flow between concentric circular cylinders with a rotating inner cylinder and an imposed axial pressure gradient, and
- The plane channel flow on a rotating system undergoing transition under the influence of the Coriolis force.

The relationship brought out by the study may be summarised in words as follows:

The amplitude evolution equation may be interpreted as one governing the slow modulation of the amplitude of a wave packet of disturbances under the influence of **Reynolds-stress like terms**. The **profiles of the Reynolds-stress like terms** in the wall-normal direction are given by those of the products of the fluctuating velocity components on the surface of neutral stability according to the classical linear stability theory.

2 Basic ideas of the two approaches

- **Large-eddy simulation** The basic idea in large-eddy simulation is a division of the turbulent motion in the flow into one with widely differing scales, viz. **large eddies**, and **small-scale motion** or **the rest**. Averaging of the equations of motion is performed only over scales of the latter, a procedure that filters out details of the **small-scale motion** leaving equations for the **filtered quantities** in which, however a **sub-grid scale stress tensor** appears, see eg. [2], [3]. There arises a necessity for a closure hypothesis.
- **Nonlinear stability Theory** The nonlinear stability theory of Stewartson and Stuart [1] seeks the **bifurcating solution** of the complete equations of motion when the flow parameter assumes values **just beyond transition**. The formalism of their method can be understood in terms of **multiple scales**, see eg. [5]. At values of the flow parameters just beyond transition, the classical linearized equations of motion for small-amplitude disturbances yield exponentially growing disturbances, however with a growth rate that remains small when the departure of the flow parameters from those on the surface of neutral stability is small. The slow growth rate for amplification of disturbances from linear theory may be associated with further scales of time and length entering the problem and suited to account for the effects from the nonlinearities (**Reynolds stres like terms**) that were ignored in the linear theory. The solution of the **nonlinear problem** is sought in a form closely related to the wave-form of disturbances according to linear stability theory, but with an amplitude that gets modulated by the nonlinearities in the problem. The approach results in a nonlinear matrix equation that describes the **amplitude evolution in terms of the newly introduced scales**.

3 Outline of the work

- **Step 1: Solution of the classical linearized problem for small-amplitude disturbances**

  1. Starting from the set of nonlinear equations of motion for the disturbance, solutions of the equations for infinitesimally small disturbances in the flow in question are obtained by a suitable numerical method, see eg. [4]. The classical eigenvalue problem thus posed has nontrivial solutions only when a certain **dispersion relation** of the problem is fulfilled which we write in conventional notation symbolically as follows:

– For the swirling annular flow with rotation of the inner cylinder and small gap width this is $\omega = \omega(\lambda_x, n_\varphi; Ta, S_i)$, where Ta is the **Taylornumber** and S_i is a **swirl parameter**.
– For the plane channel flow on a rotating system this is $\omega = \omega(\lambda_x, \lambda_z; Re, Ro)$, where Re and Ro are the **Reynoldsnumber** and the **Rotation number** respectively.

The dispersion relations for infinitesimally small disturbances yield the **surface of neutral stability** which is a surface in the space of the flow parameters, i.e. (Ta, S_i) or (Re, Ro) as the case may be, on which the **imaginary part of the frequency**, denoted ω_i, is zero.

2. From the solution of the classical eigenvalue problem, the solution for the propagation of a disturbance for arbitrary initial conditions is obtained as a Fourier-superposition of wave-modes for which the velocity disturbance $\mathbf{u}$ may be written in the form $\mathbf{u} = \mathbf{a}(y)\exp[i\Theta] +$ c.c.. Here, y is the co-ordinate normal to the walls, and the column vector $\mathbf{u}$ and the phase Θ are as follows:
   – In the swirling annular flow: $\mathbf{u} = (u_r, u_\varphi, u_x)^T$; $\Theta(x, \varphi, t) = (\lambda_x x + n_\varphi \varphi - \omega t)$.
   – In the plane channel flow: $\mathbf{u} = (u_y, u_z, u_x)^T$; $\Theta(x, z, t) = (\lambda_x x + \lambda_z z - \omega t)$;

   Here the wave-number pair (λ_x, n_φ), or (λ_x, λ_z) or as the case may be, are real but the frequency ω is permitted to be complex. Values on the entire real axis are permissible for λ_x, λ_z whereas n_φ may assume only real integer values.
3. For initial conditions that generate waves that remain close to the surface of neutral stabilty, the classical linear theory leads to the result that the form of the wave-packet for long times and at large distances from the source assumes a form similar to that of a single mode. The components of this (column) vector, written as a diagonal matrix $\mathbf{U}$ may be written in a coordinate system travelling with the wave-packet as $\mathbf{U}_N = \mathbf{A}_N(y)\exp[i\Theta_N]\exp[\omega_{Ni}t] + c.c.$. Here the subscript N denotes values on the surface of neutral stability and i the imaginary part. It is seen that a wave-packet has a growth rate given by ω_{Ni}, which depends upon the departure of the flow parameters from those on the surface of neutral stability, (Ta_N, S_{iN}) or (Re_N, Ro_N).

- **Step 2: Extension of the solution to the classical linearized problem to weakly nonlinear evolution of disturbances according to the method of Stewartson and Stuart**

1. The method of Stewartson and Stuart examines solutions for flow parameters in the neighbourhood of the surface of neutral stability when ω_{Ni} is small but > 0. Following Stewartson and Stuart, [1], we introduce an **amplitude parameter**, ϵ_A, that is small and defined for the two flows as a linear combination of the departures of the flow parameters from their values on the surface of neutral stability. The **amplitude parameter** ϵ_A is defined through:
   – for the swirling annular flow: $\epsilon_A = \omega_{Ni} = d_{Ta}|Ta - Ta_N| + d_{Si}|S_i - S_{iN}|$, and
   – for the plane channel flow: $\epsilon_A = \omega_{Ni} = d_{Re}|Re - Re_N| + d_{Ro}|Ro - Ro_N|$.
2. A solution for the nonlinear problem is sought in the form $\mathbf{U} \simeq \mathbf{B}\mathbf{A}_N \exp[i\Theta_N] + c.c$ where the diagonal matrix $\mathbf{B}$ is a function of the set of newly introduced scales. The elements of the diagonal matrix $\mathbf{U}$ - these are (B_r, B_φ, B_x), or (B_y, B_z, B_x) as the case may be - may be regarded as the components of the **filtered velocity disturbance**.
3. A **solvability condition** yields the **amplitude evolution equations** (nonlinear matrix equations) for $\mathbf{B}$ for the flow problems in question. Their relationship to LES will be discussed at EC525.

References

[1] Stewartson, K. and Stuart, J. T.: A nonlinear instability theory for a wave system in plane Poiseuille flow, *J. Fluid Mech.* **48**: 529-545 (1971).

[2] Lesieur, M.: *Turbulence in Fluids*. Kluwer Acad. Publishers, 1997, Third Revised and Enlarged Edition, Fluid Mechanics and its Applications **40**.

[3] C. Meneveau, C. and Katz, J.: Scale-Invariance and Turbulence Models for Large-Eddy Simulation. In *Annual Rev. Fluid Mech.*, **32**, 1-32, 2000.

[4] Schmid, P. J. and Henningson, D. S.: *Stability and Transition in Shear Flows*. Springer, Berlin, 1990, Applied Mathematical Sciences **142**.

[5] Huerre, P. and Rossi, M.: Hydrodynamic Instabilities of Open Flows. In Godreche and Mannville (Eds.) *Hydrodynamic and Nonlinear Instabilties*, Cambridge University Press, Cambridge, UK, 1998.

INERTIA-GRAVITY WAVES DURING THE TRANSITION TOWARDS GEOSTROPHIC TURBULENCE WITHIN A BAROCLINIC CAVITY

Anthony RANDRIAMAMPIANINA
Laboratoire Mécanique, Modélisation et Procédés Propres, UMR 6181 CNRS, Technopôle Château-Gombert. 38, rue F. Joliot-Curie. 13451 Marseille cedex 20, France.

1 Introduction

The transition to disordered behaviour in the form of 'Baroclinic Chaos' provides an important prototypical form of chaotic transition in fluid dynamics. This is of particular geophysical relevance in the context of understanding the origins of chaotic behaviour and limited predictability in the large-scale atmospheres of terrestrial planets and in the oceans. For many years, the differentially-heated, rotating cylindrical annulus, "the baroclinic cavity", has proved a fruitful means of studying fully-developed, nonlinear baroclinic instability in the laboratory. Transitions within the regular wave regime follow canonical bifurcations to low-dimensional chaos [1], but disordered flow appears to emerge via a different mechanism involving small-scale secondary instabilities [2]. In previous laboratory experiments of baroclinic waves, such fluctuations have been associated with a flow regime termed *Structural Vacillation* which is regarded as the first step in the transition to fully-developed geostrophic turbulence. Subsequent development within this so-called 'transition zone' leads to the gradual and progressive breakdown of the initially regular wave pattern into an increasingly disordered flow, ultimately leading to a form of stratified 'geostrophic turbulence'. Here we present an analysis which focusses on the small-scale features.

2 The numerical model and the case discussed

The physical model is that of the experimental rig used at the university of Oxford, UK ([3], [4]), filled with a liquid defined by a Prandtl number $Pr = 16$. It is composed of two vertical coaxial cylinders of inner radius $a = 4.5cm$ and outer radius $b = 15.cm$, held at constant temperature difference, $\Delta T = T_b - T_a = 2K$ and enclosed by two horizontal insulating rigid lids separated by a distance $d = 26.cm$. The whole cavity rotates around the central axis with $\Omega = 1.25rad/s$. The Navier-Stokes and energy equations coupled via the Boussinesq approximation are solved using a pseudo-spectral collocation-Chebyshev Fourier method associated with a second order time scheme.

3 Results

3.1 Structural Vacillation

The results are consistent with the structural vacillation observed in the laboratory, characterized by a spatio-temporal behaviour. While the large scale of the flow persists, here with a dominant azimuthal wavenumber $m = 3$, the flow does show noticeable irregular fluctuations at small scales which are going to progressively destroy the regularity of these main cells. This is illustrated by the streaklines shown at different heights of the cavity in figure 1.

3.2 Inertia gravity waves

Unlike a previous study using air as working fluid [2] where the driven mechanism resulted from a radial Rayleigh-Bénard rotating convection due to high centrifugal accelerations, the dynamics of the observed structural vacillation is mainly governed by inertia-gravity waves developing on top of large-scale baroclinic instabilities [5]. The small-scale structures appear spontaneously as soon as the large-scale regular waves occur, and indeed satisfy the characteristic dispersion relation given in [6]. These fluctuations are found to behave like the travelling waves emitted by thermal boundary layer instability determined as inertia-gravity waves for the value of Prandtl number considered here, according to analytical studies [7]-[8]. Moreover, a recent similar numerical study carried out at the university of Oxford UK [9], but considering a higher Prandtl number fluid, confirmed that these small-scale fluctuations correspond to inertia-gravity waves. A space-time map of the temperature along the azimuth at fixed radius and height during about three fundamental periods of the large-scale motion is displayed in figure 2, showing the perturbations attached to the $m = 3$ large-scale structure.

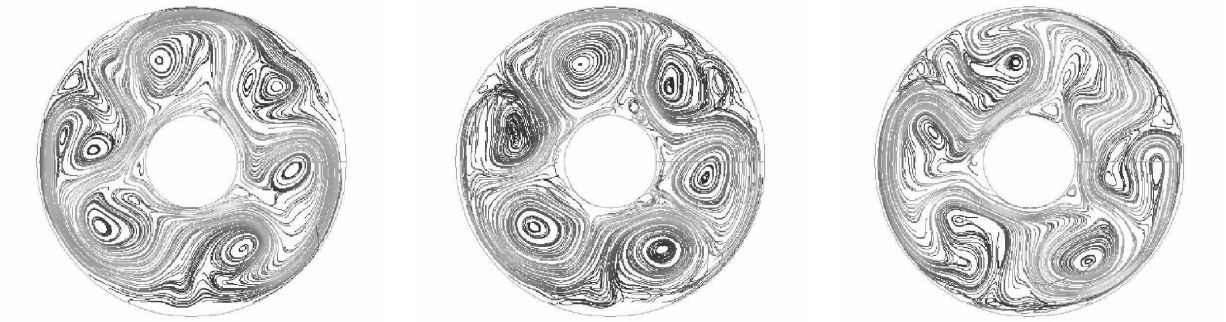

Figure 1: Instantaneous streaklines at different heights of the cavity

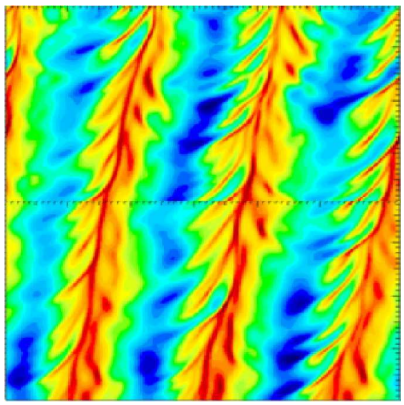

Figure 2: Space-time map of the temperature along the azimuth at fixed radius and height.

References

[1] A. Randriamampianina, W.-G. Früh, P. Maubert & P. L. Read, Direct Numerical Simulation of bifurcations to low-dimensional chaos in an air-filled rotating baroclinic annulus, *J. Fluid Mech.* **561**, 359-389, 2006.

[2] P. L. Read, P. Maubert, A. Randriamampianina & W.-G. Früh, Direct Numerical Simulation of transitions towards Structural Vacillation in an air-filled, rotating, baroclinic annulus, *Phys. Fluids* **20**, 044107, 2008.

[3] R. D. Wordsworth, P. L. Read & Y. H. Yamazaki. Turbulence, waves and jets in a differentially heated annulus experiment. *Phys. Fluids* **20**, 126602, 2008.

[4] R. D. Wordsworth, Theoretical and experimental investigations of turbulent jet formation in planetary fluid dynamics. *Ph. D Thesis*, **Linacre College, Oxford University (UK)**, 2009.

[5] Plougonven R. & Snyder C., Inertia-gravity waves spontaneously generated by jets end fronts. Part I: different baroclinic life cycles, *J. Atmos. Sciences* **64**, 2502-2519, 2006.

[6] Fritts D. C. & Alexander M. J., Gravity wave dynamics and effects in the middle atmosphere, *Reviews Geophys.* **41**, 1 / 1003, 2003.

[7] A. E. Gill and A. Davey, Instabilities of a buoyancy-driven system. *J. Fluid Mech.* **35**, 775-798, 1969.

[8] R. F. Bergholz, Instability of steady natural convection in a vertical fluid layer. *J. Fluid Mech.* **84**(4), 743-768, 1978.

[9] T. N. L. Jacoby, P. L. Read, P. D. Williams & R. M. B. Young, Generation of inertia-gravity waves in the rotating thermal annulus by a localised boundary layer instability. *Geophys. Astrophys. Fluid Dyn. (to appear).*

EXPERIMENTAL INVESTIGATION OF TRANSITION TO TURBULENCE IN A MAGNETIC OBSTACLE

Farzaneh SAMSAMI, Andre THESS & Yuri KOLESNIKOV
Institute of Thermo- and Magnetofluiddynamics, Faculty of Mechanical Engineering, Ilmenau University of technology, Germany.

1 Abstract

We present an experimental study about the structure of the flow in the movement of an electrically conducting fluid past a localized magnetic field,which has been called magnetic obstacle. We studied the sequences of vortex generation and the structure of bifurcations in the flow of eutectic alloy GaInSn. The flow is shown to undergo really complicated phenomena. Here we will try to introduce these phenomena.

2 Introduction

In practical applications we always deal with the nonideal, i.e. confined and nonhomogenous magnetic fields. There are many applications in which we combine such a magnetic field with the liquid metal flow and benefits from the interaction force which is called Lorentz force. This force can be used as an active force to drive the fluid flow, in a pump or stirrer, or as a passive force in measurement devices. The liquid metal flows under the influence of confined non-homogeneous magnetic fields, so called magnetic obstacle [1] is hardly understood. There are some literatures who try to discover the secrets of the magnetic obstacle [1]– [4] but they all suffer from the lack of experimental evidences and the transition to turbulence is still obscure. In the obove references the authors demonstrated that the flow pattern in a magnetic obstacle is really more complex than in the wake behind an ordinary hydrodynamical body. Votyakov et al. [1] showed that The flow will undergo two bifurcations (rather than one) and will involve up to six (rather than just two) vortices. The fluid flow is predicted to be stable and free of vortices at high velocities. By decreasing the flow rate, inner vortices and later on the six-vortex pattern will appear. This is in contrast to what we know from ordinary hydrodynamics in which vortex generation will be amplified by increasing flow rate. They also predicted the appearence of two bifurcation and related them to the appearence of the vortices, see figure 1. In this letter we will present the experimental results of the transition to turbulence in a magnetic obstacle.

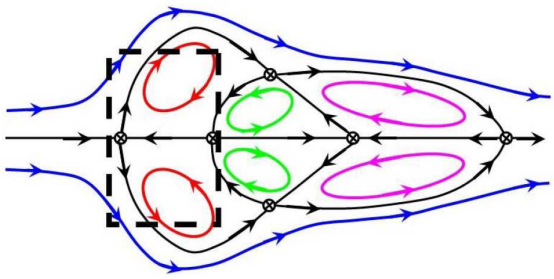

Figure 1: Topology of the predicted fluid flow as mentioned in [1].

3 Experimental set up

A 1200mm long channel with a rectangular 100mm × 25mm cross section made of Plexiglas is used in this experiment. The channel is filled up with 10mm GaInSn and has one Hartmann wall, one free surface and two side walls.The maximum intensity of the magnetic field in the Hartmann wall and in the free surface will be 0.4T and 0.2T accordingly and the related Hartmann number will be Ha = 110.6. The 20mm × 30mm × 40mm permanent magnet is installed on a moving rail beneath the channel which has the course of 850mm (figure 2). The distance between the magnet and the Hartmann wall is 8 mm. The experimental set up enables us to move the magnet with constant velocities varying from 5mm.s^{-1} to 80mm.s^{-1}, i.e. Re = 125 – 2000. The streamlines has been illuminated using gas bubbles generated due to the reaction of the acid HCl and GaInSn oxide on the free surface. A camera which moves with the magnet has been used to record the vortex generation sequences.

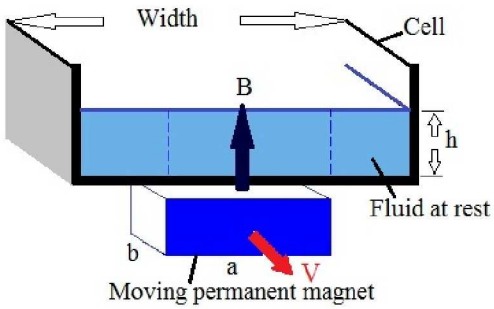

Figure 2: Sketch of channel and permanent magnet arrangement for this experiment.

4 Result and discussion

As the velocity and hence the Re Number changed, we observed different behaviours inside the magnetic field region and in downstream. These includes formation of bifurcations or their suppression, vortex shedding behind the magnet, symmetry breakdown, dupplication of vortices and also a behaviour that looks like intermittency. Two of the pictures taken during this investigation is shown in figures 3 and 4. In this figures a magnet indicatior shows the end position of the magnet. Notice that all the pictures do not have the same scale.

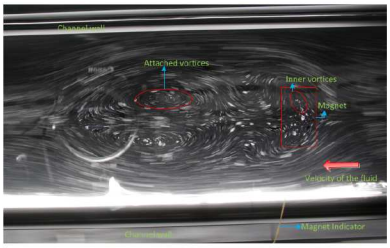

Figure 3: Transient 6 vortex structure at Re = 1000

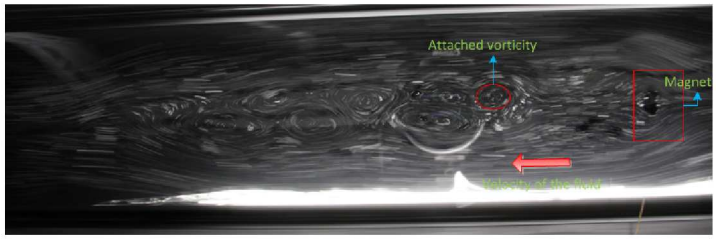

Figure 4: A street of vortices at Re = 1500

5 Conclusion

A new complicated phenomena that shows the features of the turbulent flow has been discovered. The vast number of turbulent phenomana that are visible in the fluid flow past a magnetic obstacle make it worth investigating in order to achieve a better understanding of magnetic obstacle or even turbulence.

6 Acknowledgment

The authors express their gratitude for financial support by the Deutsche Forschungsgemeinschaft.

References

[1] E. V. Votyakov, Y. Kolesnikov, O. Andreev, E. Zienicke, A. Thess, Structure of the wake of a magnetic obstacle. *Phys. Rev. Lett.* **98**, 144504 (2007).

[2] E. V. Votyakov, E. Zienicke, Y. Kolesnikov, Constrained flow around a magnetic obstacle. *J. fluid Mech.* **610**, 131–156 (2008).

[3] O. Andreev, Y. Kolesnikov, A. Thess, Experimental study of liquid metal channel flow under the influence of a non-uniform magnetic field. *Phys. fluids* **19**, 039902 (2007).

[4] E. V. Votyakov, S.C. Kassinos, On the analogy between streamlined magnetic and solid obstacles. *Phys. fluids* **21**, 097102 (2009).

EXPERIMENTAL INVESTIGATION ON TORQUE SCALING IN TURBULENT TAYLOR-COUETTE FLOW

Merbold S.[1], Egbers C.[1]
[1]*Department of Aerodynamics and Fluid Mechanics, Brandenburg University of Cottbus, Germany,*

1 Angular momentum flux and torque in Taylor-Couette

The concentric rotating Taylor-Couette flow (TC) is a well known system of instabilities in fluid dynamics (see Fig. 1a). In this work the transitions between different three dimensional flows of counter- and corotating Taylor-Couette flow and its dependence on different parameters is investigated. Depending on the rotation rate of the cylinders, one is able to create a linear stable (like pipe) or unstable flow (like Rayleigh-Bénard convection). From this background one can see TC flow as a link between Rayleigh-Bénard and pipe flow. [1, 2] also compare these three systems by an analytical derivation. It is possible to calculate the heat flux J_θ for Rayleigh-Bénard [3] , a transverse u_z flux J_{u_z} for pipe flow, and angular momentum flux J_ω for Taylor-Couette flow, which have a similar analytical form [1]. The Analogy of these three systems is obvious. For the example of Taylor-Couette-flow this flux is given as

$$J_\omega = r^3(< u_r\omega >_{A,t} -\nu\partial_r < \omega >_{A,t}), \tag{1}$$

where $< ... >_{A,t}$ denotes a spacial temporal average over a cylindrical surface of height L at radius r. Analytically, J_ω has to be independent of all radii ($\partial_r J_\omega = 0$). So it is of great interest to quantify the angular momentum flux J_ω as a parameter for the flow. At the wall the magnitude of J_ω corresponds to the torque the fluid works on the cylinders: Thus the dimensionless torque $G = T/(2\pi L\rho\nu^2) = \nu^{-2}J_\omega$ can be used to quantify the angular momentum flux J_ω. So the scaling of the torque with the rotation rate of the system gives the scaling of the angular momentum flux [2]. How the Torque scales for different Rotation numbers of the inner and outer cylinders needs to be investigated.

2 Experiments in Taylor-Couette flow

Figure 1a shows a sketch of the experimental apparatus used in the present investigations. Both cylinders can rotate independently and relative to each other with Reynolds numbers of inner (1) and outer rotation (2) $Re_{1,2} = R_{1,2}\omega_{1,2}(R_2 - R_1)/\nu$ of order of 10^3 up to 10^5 for a radius ratio $\eta = R_1/R_2 = 0.5$. This includes single rotations of both cylinders as well as co- and counterrotation. The end plates of the concentric cylinder gap are also able to rotate separately at an aspect ratio up to $\Gamma = (R_2 - R_1)/L <= 20$. As working fluid its used a silicone oil with a kinematic viscosity of $\nu = 0.65 \cdot 10^{-6}m^2/s$. The outer cylinder is made out of glass to enable optical measurements and is located inside a water box to keep the experiment isothermal. The inner cylinder is devided in three sections (Fig. 1b) where the middle section is constructed to measure the torque T the fluid interacts on the rotating cylinder wall. The two end sections are used to reduce the influence of the top and bottom end plates.

We use Particle Image Velocimetry (PIV) to measure the axial-radial and radial-azimuthal velocity fields (see Fig. 2) and to characterize different instabilities and flow patterns inside the cylinder gap. Laser Doppler Anemometry (LDA) is used to measure time series of the turbulent flow at different positions. The radial-azimuthal time dependent velocity field is measured in a second Taylor-Couette apparatus by LDA and PIV. This one has the identical geometry as the one used for torque measurements and is equipped with a transparent end plate attached to the outer cylinder. The azimuthal boundary layer profiles of inner and outer cylinder are also measured for different inner and outer Reynolds numbers. The measured velocity fields (i.e. angular velocity profiles see Fig.3) and the torque at inner cylinder are compared to verify equation (1). The radial conservation of the angular momentum flux ($\partial_r J_\omega = 0$) can be checked for turbulent Taylor-Couette flows.

Financial support by Deutsche Forschungsgemeinschaft (DFG FOR1182 EG100/15-1) is gratefully acknowledged.

References

[1] Eckhardt, B., Grossmann, S., Lohse, D.: Fluxes and energy dissipation in thermal convection and shear flows. *Europhys. Lett.* **78**:24001, 2007.

[2] Eckhardt, B., Grossmann, S., Lohse, D.: Torque scaling in turbulent Taylor-Couette flow between independently rotating cylinders. *J. Fluid Mech.* **581**:221-250, 2007.

[3] Grossmann, S., Lohse, D.: Scaling in thermal convection: a unifying theory. *J. Fluid Mech.* **407**:27-56, 2000.

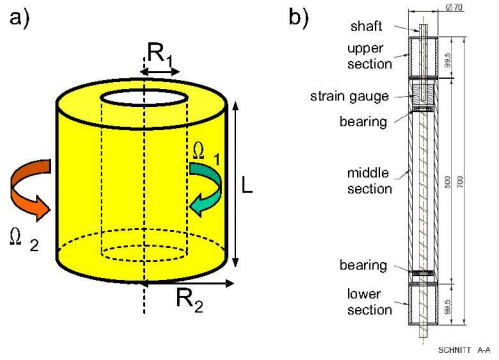

Figure 1: (a) Shematic drawing of the Taylor-Couette-system, $R_1 = 35mm, R_2 = 70mm, \eta = 0.5, Gamma = 20$ (b) Drawing of the inner cylinder with torque measuring unit

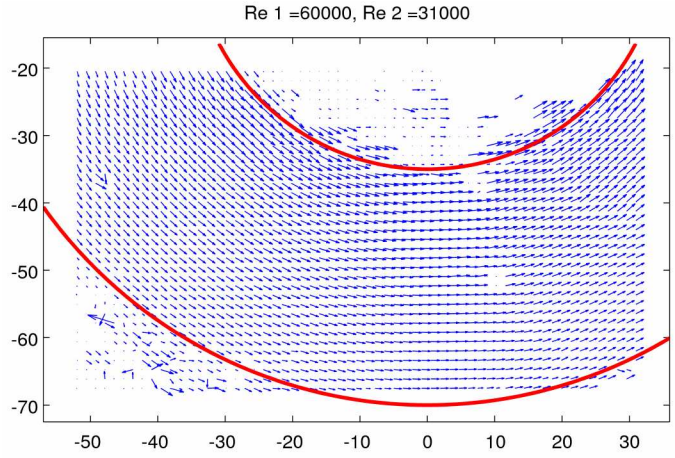

Figure 2: Radial-Azimuthal velocity field from PIV measurement for $Re_1 = 6 \cdot 10^4, Re_2 = 3.1 \cdot 10^4$

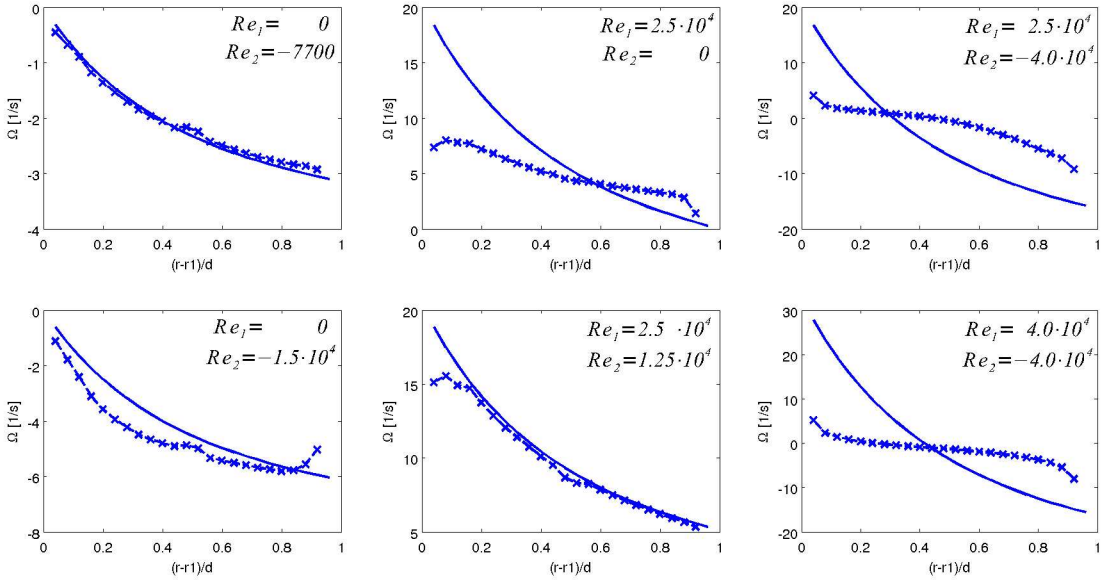

Figure 3: Angular velocity Ω over dimensionless gap width $(r - R_1)/d$. Temporal and azimuthal averaged over circular segments of $\pi/2$ (crosses) for different pairs of rotation Reynolds numbers Re_1, Re_2. The solid line indicates a two dimensional Couette-profile $\Omega = Ar + B/r$ in comparision to the measured profiles.

EXPERIMENTAL EVIDENCE OF A PHASE TRANSITION IN A TURBULENT SWIRLING FLOW

P.-P. Cortet[1,2], A. Chiffaudel[1], F. Daviaud[1], B. Dubrulle[1] & E. Herbert[1]
[1]*CEA, IRAMIS, SPEC, CNRS, Groupe Instabilités & Turbulence, 91191 Gif-sur-Yvette, France*
[2]*Laboratoire FAST, CNRS, Univ. Paris-Sud, Univ. Pierre-et-Marie-Curie, Bât. 502, Campus universitaire, 91405 Orsay, France*

Phase transitions are ubiquitous in physical systems and generally are associated to symmetry breakings. Symmetry breaking also governs transition to turbulence, that usually proceeds, as the Reynolds number Re increases, through a sequence of bifurcations breaking successively the various symmetries of the flow [1]. Finally, at large Re, it is commonly admitted that all the broken symmetries are restored in a statistical sense. However, recent studies have disturbed this vision raising intriguing features such as finite lifetime turbulence [3] and possible existence of turbulent transitions [4, 5, 6]. Consequently, despite turbulent flows are intrinsically out-of-equilibrium, one may wonder whether the observed transitions can be interpreted in terms of phase transitions. In this work [7], we introduce a susceptibility to symmetry breaking in a von Kármán turbulent flow and investigate its evolution as Re increases from 150 to 10^6 using stereoscopic Particle Image Velocimetry (SPIV). We observe a divergence of susceptibility at a critical Reynolds number $Re = Re_\chi \simeq 90\,000$ which sets the threshold for a turbulent "phase transition". Moreover, this divergence is associated with a peak in the amplitude of the fluctuations of the flow instantaneous symmetry.

Our experimental setup consists of a Plexiglas cylinder filled up with water-glycerol mixtures. The fluid is mechanically stirred by a pair of coaxial impellers rotating in opposite directions (Fig. 1(a)). SPIV measurements provide time series of the 3 velocity components in a meridian plane. Denoting the impellers rotation frequencies f_1 and f_2, the control parameters are the Reynolds number $Re = \pi(f_1 + f_2)R^2/\nu$, where ν is the fluid viscosity, and the rotation number $\theta = (f_1 - f_2)/(f_1 + f_2)$, which controls the asymmetry of the forcing conditions.

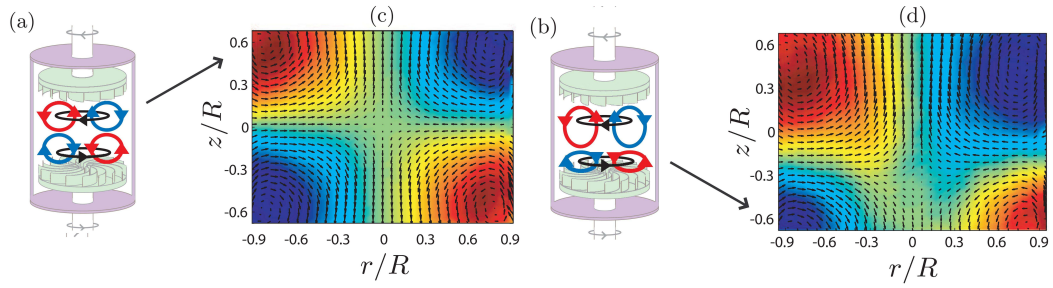

Figure 1: (a) and (b) Flow topologies and (c) and (d) corresponding experimental maps of mean velocity field at $Re = 800\,000$ for (c) $\theta = 0$ ($\overline{I} = 0$) and (d) $\theta = -0.0147$ ($\overline{I} < 0$). The color maps the azimuthal velocity u_φ whereas the arrows map the (u_r, u_z) field.

When $\theta = 0$, the experimental system is symmetric with respect to any $\mathcal{R}_\pi$-rotation exchanging the two impellers (Figs. 1(a) and (c)): the problem conditions are invariant under π-rotation around any radial axis passing through the center of the cylinder. When $\theta \neq 0$, the experimental system is no more $\mathcal{R}_\pi$-symmetric, the parameter θ measuring of the distance to the exact $\mathcal{R}_\pi$-symmetry. Depending on θ, the flow can respond by displaying different symmetries (Fig. 1): (i) the exact $\mathcal{R}_\pi$-symmetric flow composed of two toric recirculation cells separated by an azimuthal shear layer located at the equator, when $\theta = 0$; (ii) an asymmetric two-cells flow, the shear layer being closer to the slowest impeller, when $\theta \neq 0$. In order to quantify the distance of the flow to the $\mathcal{R}_\pi$-symmetry, we use the normalized and space-averaged angular momentum $I(Re, \theta, t)$ as order parameter: $I(t) = \frac{1}{\mathcal{V}} \int_\mathcal{V} r dr d\varphi dz \, \frac{r u_\varphi(t)}{\pi R^2 (f_1+f_2)}$ where $\mathcal{V}$ is the volume of the flow. An example of time variation of $I(t)$ at $\theta = 0$ in the turbulent regime is provided in Fig. 2(Left). Then, using this ensemble averaged order parameter, we define a susceptibility of the flow to symmetry breaking as: $\chi_I = \partial \overline{I}/\partial\theta|_{\theta=0}$.

In the laminar case, when $\theta = 0$, $\overline{I} = 0$ due to the symmetry of the flow. In contrast, as θ drifts away from 0, the value of the angular momentum $\overline{I}$ becomes more and more remote from zero as the asymmetry of the flow grows. The symmetry parameter $\overline{I} = I(t)$ evolves linearly with θ (Fig. 2(c)) and the susceptibility is $\chi_I \simeq 0.24$. Increasing the Reynolds number, one expects to reach fully developed turbulence around $Re = 10\,000$. Therefore, even when $\theta = 0$, the $\mathcal{R}_\pi$-symmetry is of course broken for the instantaneous flow. However, as usually observed for classical turbulence, this symmetry is restored for the time-averaged flow. Then, as in the case of the laminar flow, when θ is varied, we observe the breaking of the $\mathcal{R}_\pi$-symmetry of the mean flow. In Fig. 2(c), we see that, at $Re = 800\,000$, in the close vicinity of $\theta = 0$, $\overline{I}(\theta)$ evolves actually much more rapidly with θ than in the laminar case. Therefore, turbulence seems to enhance dramatically the sensitivity of the flow to symmetry breaking. In Fig. 2(a), we see that the susceptibility actually grows by more than two orders of magnitude between $Re = 150$ and $Re \simeq 90\,000$, before decreasing by a factor 4 between

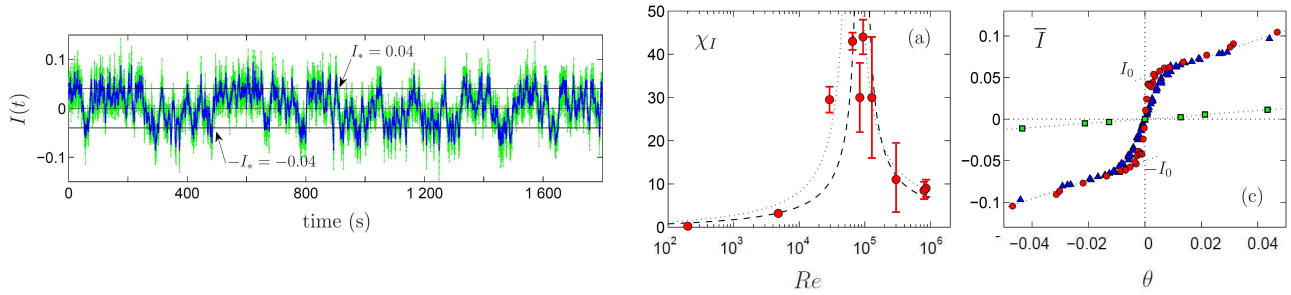

Figure 2: Left: Angular momentum $I(t)$ as a function of time for $Re = 43\,000$ and $\theta = 0$. Green dots are PIV data sampled at 15 Hz and blue dots correspond to 1 Hz low-pass filtered data. Eye-guiding lines have been drawn at $I(t) = \pm I_* = \pm 0.04$. Right (a): Susceptibility χ_I as a function of Re at $\theta = 0$; (c) angular momentum $\overline{I}$ as a function of θ for $Re = 150$ (green $\square$), $Re = 65\,000$ (red $\circ$) and $Re = 800\,000$ (blue $\triangle$).

$Re \simeq 90\,000$ and $Re = 800\,000$. These results suggest a critical divergence for $\chi_I(Re)$ near $Re = Re_\chi \simeq 90\,000$.

For higher $|\theta|$, we observe a crossover in the curve $\overline{I}(\theta)$ very close to $\theta = 0$, at $|\theta_r| \simeq 0.9\,10^{-3}$, for $Re = 65\,000$ (Fig. 2(c)). For $|\theta| > |\theta_r|$, we recover the laminar slow evolution of $\overline{I}$ with θ which is quite independent of Re at large Re, so that we can extrapolate this linear behaviour to $\theta = 0$. This extrapolation describes the ideal behaviour at critical $Re = Re_\chi$ if χ_I diverges: a jump of $\overline{I}$ between $-I_0$ and $+I_0$ where $I_0 \simeq 0.05$. This can be interpreted as a spontaneous "turbulent momentization" I_0 at $\theta = 0$ by analogy with the spontaneous magnetization M_0 at zero external field for ferromagnetism in the usual para-ferromagnetic transition.

A signature of this momentization can be seen on the instantaneous angular momentum $I(t)$ for Re near the peak of susceptibility and $\theta = 0$ (Fig. 2Left). Indeed, one observes that $I(t)$ does not remain near zero (its mean value) but shows a tendency to lock preferentially on the plateaus $\pm I_*$ with $I_* \simeq I_0$. The global angular momentum actually fluctuates very much along time with two separate time scales: fast fluctuations related to "traditional" small scale turbulence and time intermittencies corresponding to residence time of few tens of seconds. If one performs a time average over one of these intermittent periods only, one obtains a time localized "mean" flow, which breaks spontaneously the symmetry, analogous to what is obtained for true mean flows when $\theta \neq 0$. The previous experimental results set a strong connection between the spontaneous symmetry fluctuations of the flow near the peak of susceptibility and the mean flow response to the system symmetry breaking: the interpretation of the large fluctuations of $I(t)$ in terms of multistability suggests that the strong observed linear response of the mean flow (Fig. 2(c)) with respect to θ in the close vicinity of $\theta = 0$ is the result of a temporal mixing between the metastable states in different proportions.

Despite bifurcations with symmetry breaking are commonly found in natural turbulent flows, the corresponding theoretical tools are still today not well settled. Existing studies of phase transitions in the presence of fluctuations generally considers systems in which an external noise is introduced [8] and not intrinsically fluctuating systems. Our turbulent system, in which we access both to the spatiotemporal evolution of the states and the mean thermodynamic variables, appears as a a unique tool to study out-of-equilibrium phase transitions in strongly fluctuating systems.

References

[1] P. Manneville, *Dissipative Structures and Weak Turbulence*. Academic Press, Boston, (1990).

[2] B. Hof, *et al.*, Finite lifetime of turbulence in shear flows . *Nature* **443**, 59-62, (2006).

[3] F. Chillá, *et al.*, Long relaxation times and tilt sensitivity in Rayleigh Benard turbulence. *Eur. Phys. J. B* **40**, 223-227, (2004).

[4] R. Stevens, *et al.*, Transitions between Turbulent States in Rotating Rayleigh-Bénard Convection. *Phys. Rev. Lett* **103**, 024503, (2009).

[5] P. Tabeling, *et al.*, Probability density functions, skewness, and flatness in large Reynolds number turbulence. *Phys. Rev. E* **53**, 1613-1621, (1996).

[6] P.-P. Cortet, *et al.*, Experimental Evidence of a Phase Transition in a Closed Turbulent Flow. *Phys. Rev. Lett.* **105**, 214501, (2010).

[7] N. G. van Kampen: *Stochastic Processes in Physics and Chemistry*. North-Holland Personal Library, Elsevier, Amsterdam, (1981).

EXCITATION OF INERTIAL MODES IN A CLOSED GRID TURBULENCE EXPERIMENT UNDER ROTATION

Cyril Lamriben[1], Pierre-Philippe Cortet[1], Frédéric Moisy[1] & Leo R. M. Maas[2]
[1]*Laboratoire FAST, CNRS UMR 7608, Université Paris-Sud, Université Pierre-et-Marie-Curie, Bât. 502, Campus universitaire, 91405 Orsay, France,*
[2] *Royal Netherlands Institute for Sea Research, P.O. Box 59, 1790 AB Texel, The Netherlands*

Translating a grid in a closed volume of fluid is a convenient way to generate an approximately homogeneous and isotropic turbulence when a compact system is needed, e.g. when experiments are performed in a rotating frame [1, 2, 3, 4]. Such flow excited by a grid translation is, in general, composed of a superposition of (i) a reproducible flow (determined through ensemble averaging) and (ii) a non-reproducible turbulent flow. In the presence of background rotation, both of these two flow components may excite inertial waves [5], which propagate because of the restoring nature of the Coriolis force. The excited inertial waves are respectively (i) reproducible —and therefore detectable in the ensemble average— and (ii) non-reproducible —detectable in the individual realizations only— [6]. In a closed container, inertial waves may appear in the form of standing inertial modes, which are the eigenmodes of the container geometry [7, 8]. Excitation of inertial modes in grid-generated turbulence has been first observed by Dalziel [1] and are also visible in the experiments of Morize and Moisy [9] and Moisy *et al.* [10]. They have been characterized by Bewley *et al.* [3], who found good agreement between the measured frequencies and the numerical results of Maas [8].

We investigate here the structure of these inertial modes and we explore to what extent they may be reduced [6]. A square water tank is mounted on a rotating platform, and velocity fields in a vertical plane are measured using a corotating Particle Image Velocimetry system. Two grid configurations have been used: a "simple" grid, of mesh size 40 mm, and a "modified" grid, on the top of which a set of inner sidewalls is attached. We demonstrate that, in the latter configuration, the amount of energy stored in the inertial modes is drastically reduced compared to the former one.

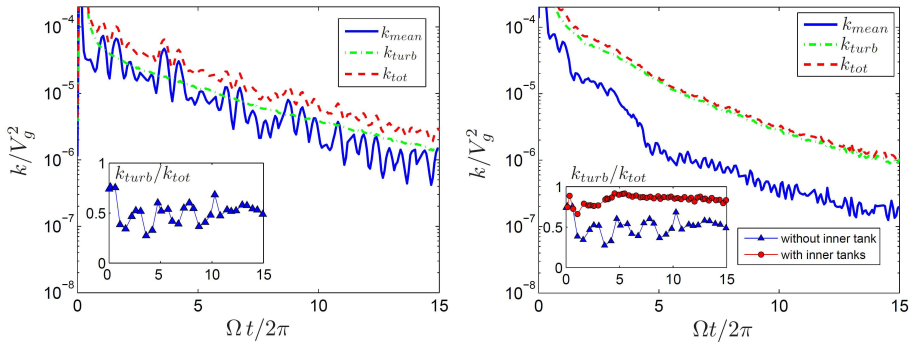

Figure 1: Total (dashed), mean (continuous) and turbulent (dashed-dotted) kinetic energies as a function of the number of tank rotations $\Omega t/2\pi$ from 40 realizations performed at $\Omega = 0.84$ rad s^{-1}. Left: simple grid. Right: modified grid with inner tanks. Inset: Ratio of turbulent to total kinetic energy as a function of $\Omega t/2\pi$.

We make use of the standard Reynolds decomposition to separate the reproducible inertial modes from the turbulence, $\mathbf{u}(\mathbf{x},t) = \mathbf{U}(\mathbf{x},t) + \mathbf{u}'(\mathbf{x},t)$, where the ensemble average $\mathbf{U}(\mathbf{x},t) \equiv \overline{\mathbf{u}}(\mathbf{x},t)$ is computed over 40 independent decay experiments. We compute the kinetic energies associated to each flow component, namely $k_{tot}(t) = \langle \overline{\mathbf{u}^2}(\mathbf{x},t) \rangle$, $k_{mean}(t) = \langle \mathbf{U}^2(\mathbf{x},t) \rangle$, and $k_{turb}(t) = \langle \overline{\mathbf{u}'^2}(\mathbf{x},t) \rangle$. The time evolution of these 3 energies is shown in Fig. 1(a), for an experiment performed at a rotation rate of $\Omega = 0.84$ rad s^{-1}. Both the energy of the total and the mean flow show, superimposed to their overall decay, marked oscillations corresponding to the inertial modes. On the other hand, the turbulent energy shows a monotonic decrease.

In the inset of Fig. 1(a), we plot the ratio of the turbulent to the mean energy : we see that turbulence represents only $50 \pm 10\%$ of the energy in the flow. This quite low ratio indicates that the energy injected with the simple grid configuration is evenly distributed among the reproducible inertial modes and the "true turbulence". It is therefore questionable to consider this turbulence as freely decaying, because of the possible energy transfer from the inertial modes to the turbulence. The oscillations in Fig. 1(a) have been analysed in details by computing the temporal spectrum of the ensemble-averaged flow $\mathbf{U}(\mathbf{x},t)$. The spectrum shows a series of peaks for frequencies σ in the range $[0, 2\Omega]$, as expected for inertial modes. By performing a band-pass filtering of $\mathbf{U}(\mathbf{x},t)$ at the peak frequencies, it is possible to extract the spatial structure of each inertial mode. The two dominating modes, of vertical wavenumber unity, are shown in Fig. 2, with associated frequencies perfectly matching the numerical predictions of Maas [8].

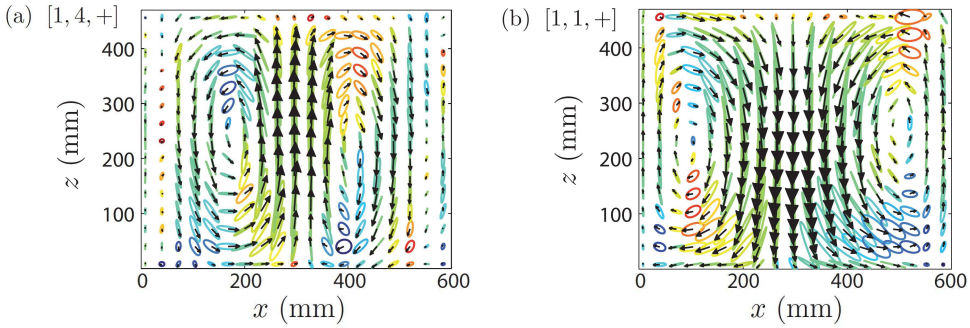

Figure 2: Spatial structure of the 2 dominating inertial modes. The ellipses show the velocity orbit, and the arrows illustrate the velocity field at a given arbitrary phase of the oscillation. The color traces the ellipticity $-1 < \epsilon < 1$.

In the modified grid configuration, a set of three parallelepipedic PVC tanks, each consisting in 4 vertical sidewalls, without top and bottom walls, is attached on the top of the grid. Since our grid is translated from the bottom to the top, the inner tanks are *upstream* of the grid, so that the volume of working fluid is the same as in the simple grid configuration. The time evolution of the 3 kinetic energies is shown in Fig. 1(b) for this modified configuration. In comparison with Fig. 1(a), the oscillations due to the inertial modes are strongly reduced, both for the mean and the total kinetic energies. We also see that the turbulent kinetic energy is now significantly larger than the one of the ensemble-averaged flow. This can be better seen in the inset of Fig. 1(b), showing that turbulence contains, after a transient of about one tank rotation, approximately $85 \pm 5\%$ of the total kinetic energy, a value much larger than the 50% obtained with the simple grid configuration. This result proves the efficiency of the modified grid to strongly reduce the production of inertial modes, and therefore to generate a turbulence which is presumably closer to the idealized situation of a free decay.

The present results suggest that the standard assumption of statistical homogeneity may not be appropriate to describe decaying rotating turbulence in a closed container, confirming the findings of Ref. [3]. This calls for the development of new theoretical tools to describe the interaction of turbulence with reproducible inertial modes. However, we have also shown that careful changes in the geometry of the grid allow us to strongly reduce the excitation of reproducible inertial modes, and hence to achieve a nearly "pure" rotating turbulence state. This modified configuration therefore suggests that it is indeed possible to investigate the properties of freely decaying homogeneous turbulence in confined geometry.

References

[1] S. B. Dalziel, Decay of rotating turbulence : some particle tracking experiments. *Appl. Sci. Research* **49**, 217-244 (1992).

[2] C. Morize, F. Moisy, M. Rabaud, Decaying grid-generated turbulence in a rotating tank. *Phys. Fluids* **17**, 095105 (2005).

[3] G. P. Bewley, D. P. Lathrop, L. R. M. Maas, K. R. Sreenivasan, Inertial waves in rotating grid turbulence. *Phys. Fluids* **19**, 071701 (2007).

[4] P. J. Staplehurst, P. A. Davidson, S. B. Dalziel, Structure formation in homogeneous freely decaying rotating turbulence. *J. Fluid Mech.* **598**, 81 (2008).

[5] P.-P. Cortet, C. Lamriben, F. Moisy, Viscous spreading of an inertial wave beam in a rotating fluid. *Phys. Fluids* **22**, 086603 (2010).

[6] C. Lamriben, P.-P. Cortet, F. Moisy, L. R. M. Maas, Excitation of inertial modes in a closed grid turbulence experiment under rotation. *Phys. Fluids* **23**, 015102 (2011).

[7] A. D. McEwan, Inertial oscillations in a rotating fluid cylinder. *J. Fluid Mech.* **40**, 603 (1970).

[8] L. R. M. Maas, On the amphidromic structure of inertial waves in a rectangular parallelepiped. *Fluid Dyn. Res.* **33**, 373 (2003).

[9] C. Morize, F. Moisy, Energy decay of rotating turbulence with confinement effects. *Phys. Fluids* **18**, 065107 (2006).

[10] F. Moisy, C. Morize, M. Rabaud, J. Sommeria, Decay laws, anisotropy and cyclone-anticyclone asymmetry in decaying rotating turbulence. *J. Fluid Mech.* **666**, 5 (2011).

GRID TURBULENCE IN SOLID BODY ROTATION

Presenting P. Orlandi,
Dipartimento di Ingegneria Meccanica e Aerospaziale
Università La Sapienza, Via Eudossiana 16, I-00184, Roma

1 Introduction

Isotropic turbulence is generated in wind tunnels by an uniform stream going through a solid grid. After an anisotropic region the flow becomes isotropic, and decays in the streamwise direction with a power law $(x_1/M)^{-m}$. In a laboratory it is rather difficult to investigate the effects of the solid body rotation on the power law decay. The study is easier in numerical experiments with three periodic directions and a synthetic isotropic turbulence at $t = 0$ which decays as t^{-m}. The power law m changes with the rotation number $N = 2\Omega L/U$, the inverse of the Rossby number used in geophysical flows. In this setup the initial conditions are different from those in real experiments. However in the experiments even the grid rotates and therefore the inlet conditions may change with the rotation rate.

In the present study the Navier-Stokes equations in a rotating frame are solved in a domain with dimensions $12\pi \times 2\pi \times 2\pi$ respectively in the streamwise, and in the other two homogeneous directions. Radiative boundary conditions at $L_1 = 12\pi$ allow the disturbance to exit from the computational domain. At the inlet an analytical velocity distribution $U_l = \delta_{1l} + A_l \sin(fx_2)\sin(fx_3) + A_R(x_2, x_3)$ is assigned, with $A_1 = 0$, $A_2 = A_3 = 0.25$ and $A_R = 0.01$. The solidity of the grid is $M = 2\pi/f$. This inlet condition is not isotropic having a turbulent stress $\langle u_2 u_3 \rangle \neq 0$ which should go to zero at a distance x_1/M to have an isotropic turbulent flow, further downstream decreasing as $(x_1/M)^{-m}$. The simulations are performed at a Reynolds number, which, for non rotating conditions close to the exit, has $R_\lambda = O(10)$ and $m = 2.5$. Several simulations were performed with fixed $f = 8$ and N varying from 1 to 10. Note that these values correspond to rotation rates higher than those achieved in laboratory experiments (Jacquin *et al.*[1]).

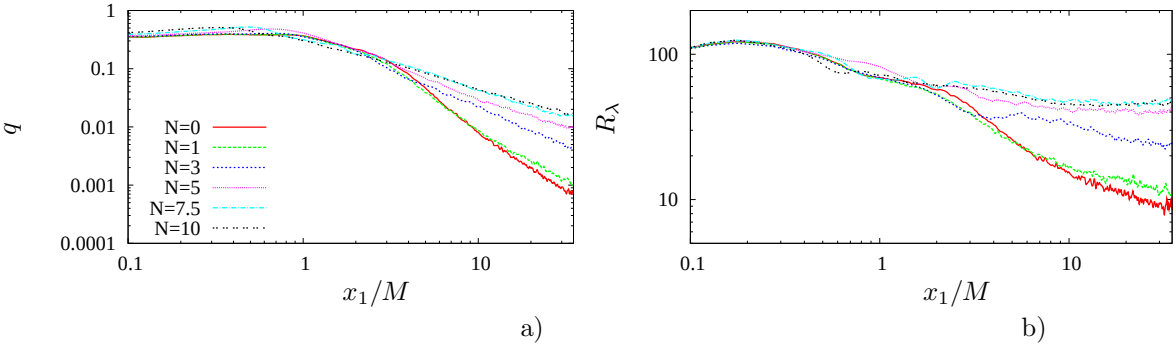

Figure 1: Profiles of a) q and b) R_λ versus x_1/M at different values of N.

Preliminary simulations show a large reduction of m with N (Fig.1a). The streamwise oscillations of q, not so evident in this figure because of the log scale, in a normal scale show a decrease of the amplitude and an increase of the wave length with the increase of N . This is an evidence that the vortical structures become longer when N raises. This effect has been recently observed in rotating tank experiments by Moisy *et al.*[2] where the turbulence is generated at $t = 0$ and then decays in time. Here the conditions are different being the small scales generated at the inlet, and survive together with those downstream which are modified by the rotation. The additional effect of rotation is to reduce the energy transfer from large to small scales and therefore the rate of energy dissipation. This is demonstrated by the streamwise evolution of R_λ in Fig.1 where, at high N, R_λ is constant ($m \approx 1$).

To understand in more detail the streamwise evolution across the anisotropic and isotropic regions it is worth looking at the u_1 equation in rotational form, where the kinetic energy q appears together with the components of the Lamb vector ($\lambda = \mathbf{v} \times \omega$), related to the energy transfer from large to small scales

$$\frac{\partial q}{\partial x_1} - \langle u_2\omega_3 \rangle + \langle u_3\omega_2 \rangle = -\frac{\partial \langle p \rangle}{\partial x_1} = \frac{\partial \langle u_1^2 \rangle}{\partial x_1} \tag{1}$$

In this equation the direct effect of N does not enter, which instead acts on the other two velocity components modifying λ_1. To understand the effects of N on the streamwise evolution of the velocity rms $\langle u_l^2 \rangle$, which for $N = 10$ are compared in Fig.2a with those for $N = 0$. For $N = 0$ $\langle u_1^2 \rangle$ grows for the positive contribution

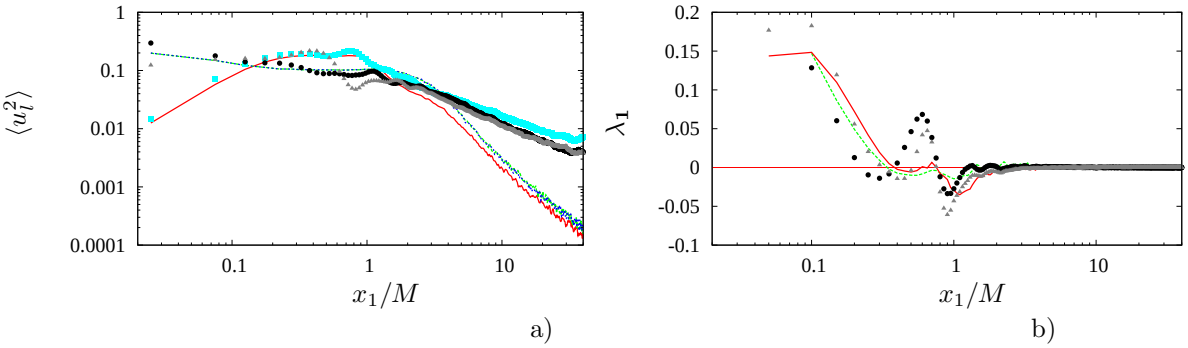

Figure 2: Profiles of a) the velocity rms (——— , ■, $l = 1$ - - - - , ● , $l = 2$ ····· , ▲, $l = 3$ and b) the component λ_1 (- - - - , ■) and $\frac{\partial \langle p \rangle}{\partial x_1}$ (——— , ▲) versus x_1/M; lines $N = 0$, solid symbols $N = 10$. ———

of the λ_1 component (Fig.2b), and the other two equal stresses decrease in x_1. At the end of the anisotropic region ($x_1/M \approx 3$) all the stresses decrease, although $\langle u_1^2 \rangle$ is slightly smaller than the other two. The transport equations for $\langle u_l^2 \rangle$ ($l \neq 1$) stresses show a positive contribution of N for one and negative for the other, this is visible in Fig.2a, where, for $N = 10$ in the anisotropic region, $\langle u_2^2 \rangle$ and $\langle u_3^2 \rangle$ are different. Through this imbalance a greater $\langle u_1^2 \rangle$ than that for $N = 0$ is obtained. The cause is visible in Fig.2b where positive values of λ_1 occur in correspondence of the $\langle u_1^2 \rangle$ bump.

By increasing the solid body rotation the helicity density $h = \mathbf{v} \cdot \omega$ increases, which from the identity $|\mathbf{v} \times \omega|^2 + |\mathbf{v} \cdot \omega|^2 = |\mathbf{v}|^2 |\omega|^2$ reduces the transfer from large to small scales, and the energy remains at the large scales. The helicity distribution is zero in the non-rotating case and grows with the rotation rate, with a positive contribution up to $x_1/M \approx 1$ and negative downstream. The analysis of the Lamb vector and the helicity density will be presented in more detail at the conference. The transfer of energy to the large scales, characteristic of rotating flows, can be observed by the spectra together with streamwise vorticity visualizations at the same location. In particular at $x_1/M = 2$ and at $X_1/M = 10$ the transverse spectrum $E_{33}(k_2)$, for all values of N, and, for $N = 0$ and $N = 10$, contour plots of $\omega_1(x_2, x_3)$ are considered. The spectra in Fig.3a together with the ω_1 contours in Fig.3b show that the influence of the inlet disturbance at $x_1/M = 2$ is large for $N = 0$ and that it reduces by increasing N. In Fig.3c, at high N, the inlet disturbances are less visible, while larger structures appear. The spectra show better the transfer of energy to large scales. At $x_1/M = 10$ the figures 3d-f clearly demonstrate the formation of energetic large scales at $N = 10$, which are those giving $m = 1$.

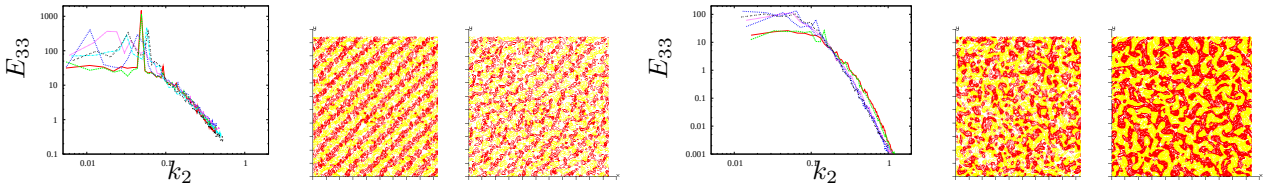

Figure 3: Transverse spectra, a) $x_1/M = 2$, d) $x_1/M = 10$ different N lines as Fig.1; contours plot of ω_1 b) for $N = 0$ c) $N = 10$ at $x_1/M = 2$ with $\Delta\omega_1 = 1$ e) for $N = 0$ f) $N = 10$ at $x_1/M = 10$ with $\Delta\omega_1 = 0.1$

References

[1] L., Jacquin, O., Leuchter, C., Cambon, & J., Mathieu Homogeneous turbulence in the presence of rotation. *J. Fluid Mech.* **220**, 1–52 (1990)

[2] F., Moisy , C., Morize , M., Rabaud & J., Sommeria Decay laws, anisotropy and cycloneanticyclone asymmetry in decaying rotating turbulence *J. Fluid Mech.* **666**, 5–35 (2011)

EUROMECH Colloquium 525, 21–23 June 2011, Écully, France
Instabilities and transition in three-dimensional flows with rotation

TURBULENT FLOW IN ROTATING RIBBED CHANNEL WITH CORIOLIS FORCES AND CENTRIPETAL BUOYANCY

René VAN DEN BRAEMBUSSCHE, Filippo COLETTI, Irene CRESCI & Tony ARTS
Turbomachinery and Propulsion Department, von Karman Institute for Fluid Dynamics Chausse de Waterloo 72, 1640 Rhode-Saint-Gense, Belgium

1 Background

In turbomachinery, one of the applications in which rotational effects are most relevant is the coolant flows in the internal cavities of rotating turbine blades. The flow in internal cooling channels in stator blades is already complex due to the intricate shape of the passages and the presence of turbulence promoters such as ribs. In rotor blades Coriolis forces affect the stability of the shear layers and induce secondary flows. Moreover, because of the thermal boundary layers along the hot channel surfaces, the centrifugal acceleration induces radial buoyancy in the vicinity of the walls. The latter turns the typical forced convection regime in a mixed convection regime. In most past experimental studies concerned with rotating channel flows, point-wise velocimetry techniques are used (e.g. [1]), which cannot identify coherent instantaneous flow structures and velocity gradients. Few studies in literature present full field data in rotating channels using PIV, but typically the imaging system is attached to the fixed frame [2]. The relative velocity inside the channel is obtained by subtracting the peripheral velocity from the measured absolute velocity, resulting in low temporal and spatial resolution and in large uncertainties, especially at high rotation rates. Due to the lack of detailed experimental data, often numerical models need to be validated against more accurate simulations for validation, namely LES and DNS. The latter are anyway extremely expensive, if not unaffordable, due to the complexity of the cooling geometries.

2 Present experimental approach

The present contribution addresses the effect of Coriolis and buoyancy forces in a rotating channel with one ribbed wall, reproducing a turbine blade cooling channel. Two-dimensional PIV measurements are performed in a rotating facility where both the test section and the measurement chain rotate on a turntable up to 130 rpm [3]. The Reynolds number value based on the bulk velocity (2.8 m/s) and the hydraulic diameter (79 mm) is $1,5 \cdot 10^4$. A rotation number value equal to 0.35 is achieved both in clockwise and counter-clockwise sense. The ribbed wall, machined out of copper, is heated to a uniform temperature of about 100^oC by means of electrical resistances powered by an on-board PDI controller. This allows obtaining a buoyancy number equal to 0.3. As the flow is outward the buoyancy is centripetal. In-plane velocity fields are measured along the channel symmetry plane by means of a 25 W continuous laser diode and a high-speed CMOS camera. Both ensemble-averaged and time-resolved measurements are performed. In the latter case the realizations are acquired at 3.3 kHz, allowing to resolve the resolution of the fine temporal flow scales. To the authors' best knowledge, these are the first time-resolved PIV measurements in a channel flow under rotational buoyancy.

2.1 Results

Figure 1 displays the mean streamlines for the non-rotating and rotating cases. With respect to the non-rotating case (fig.1a), the anti-cyclonic rotation (fig.1b) leads to the augmentation of free shear entrainment, which produces a stronger streamline curvature, and hence an earlier reattachment. The opposite holds for cyclonic rotation (fig.1c). Adding the effect of buoyancy forces in the cyclonic rotating case (1d) produces an even larger recirculation spanning the whole inter-rib area, which enhances mixing and transport. Figure 2 depicts the spatio-temporal travelling of the spanwise vortices shed by the rib in different rotating conditions. The vortical structures are identified by regions exceeding a positive threshold of swirling strength. Vortices which have a significant extension in the space-time domain satisfy the requirement of temporal coherence, which cannot generally be imposed analyzing instantaneous realizations. With anti-cyclonic rotation (fig.2a) higher convective velocities and fewer counter-clockwise rotating vortices are found with respect to cyclonic rotation (fig.2b). Furthermore the spanwise rollers are blurred by the destabilizing effect of anti-cyclonic rotation. In cyclonic rotation with centripetal buoyancy (fig.2c) the vortical structures are even neater, and counter-clockwise rotating vortices are fewer. It is argued that this is due to the buoyant flow streaming backward (negative X-direction), which interacts with the free shear flow past the rib: both streams create a pattern which is little affected by curvature, reminiscent of a mixing layer. The present data illustrate the great potential of the chosen

approach for exploring unsteady turbulent flows in rotating frames, both for complex configurations and for fundamental studies.

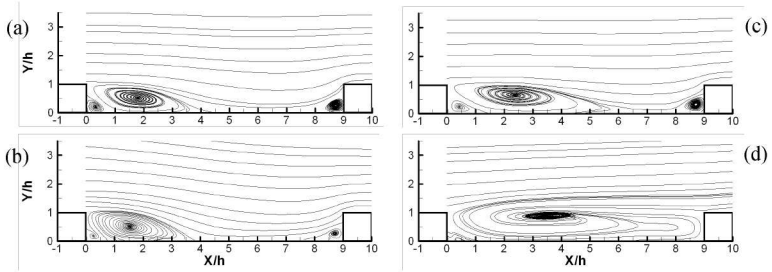

Figure 1: Mean streamlines. Flow from left to right.

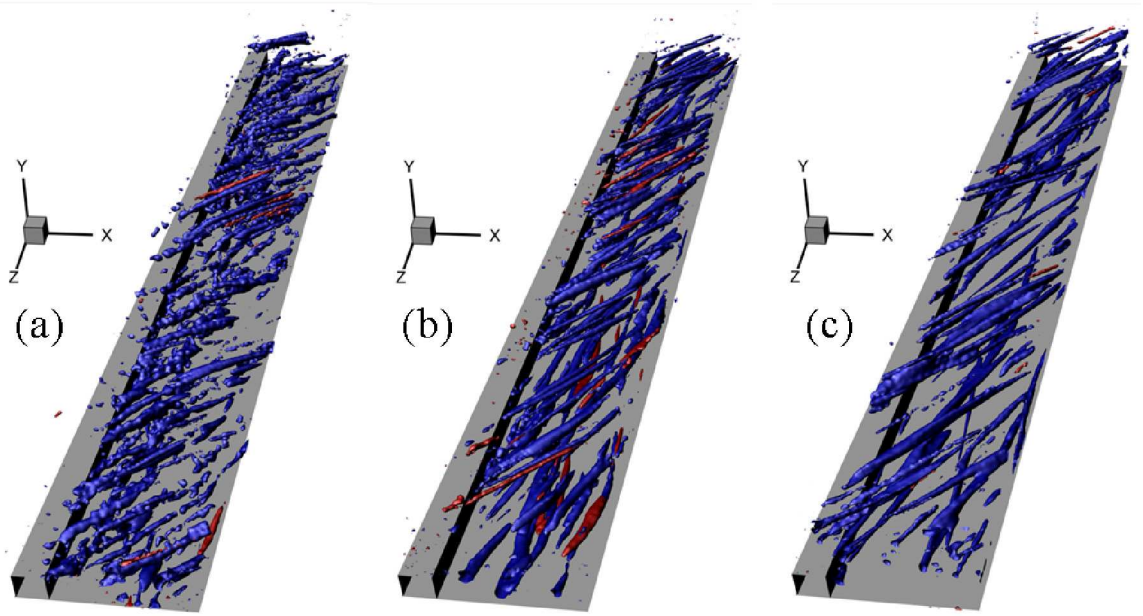

Figure 2: Iso-contours of signed swirling strength in the space-time domain. Flow in the positive X-direction. Time advances in negative Z-direction. Blue (red) indicates vortices which rotate clockwise (counter-clockwise) in the X-Y plane.

References

[1] K. Nakabayashi, O. Kitoh, Turbulence characteristics of two-dimensional channel flow with system rotation. *J. Fluid. Mech.* **528**, 355–377 (2005).

[2] M. Elfert, M. Voges, J. Klinner, Detailed Flow Investigation Using PIV in a Rotating Square-Sectioned Two-Pass Cooling System with Ribbed Walls. *ASME Paper* **GT2008**, 51183 (2008).

[3] A. Di Sante, R. Theunissen, R.A. Van den Braembussche, A new facility for time resolved PIV measurements in rotating channels. *Exp. Fluids* **44**, 179–188 (2008).

EUROMECH Colloquium 525, 21–23 June 2011, Écully, France
Instabilities and transition in three-dimensional flows with rotation

TURBULENCE AND INSTABILITIES IN ROTATING CHANNEL FLOW SIMULATIONS

G. BRETHOUWER, P. SCHLATTER & A.V. JOHANSSON
Linné FLOW Centre, KTH Mechanics, SE-100 44 Stockholm, Sweden

1 Introduction

In this study, we investigate periodic-like instabilities occurring in turbulent channel flow subject to rapid spanwise rotation. It is now well established that turbulence is enhanced on the so-called unstable side and damped on the stable side of a channel at low to moderate spanwise rotation rates [2], but at high rotation rates it is also strongly damped at the unstable side as shown by recent DNS at friction Reynolds number $Re_\tau = 180$ [1]. A linear stability analysis showed that beyond a critical rotation number $Ro_b = 2\Omega h/U_b$ all modes with $k_z \neq 0$ decay for a given $Re_b = U_b h/\nu$ [3]. Here U_b is the bulk mean velocity, h the channel half-width, ν the viscosity, Ω the rotation rate and k_z the spanwise wavenumber. This stability analysis was convincingly supported by DNS; when Ro_b was larger than the critical value a disturbed channel flow became fully laminar after some time. However, the so-called Tollmien-Schlichting (TS) modes with $k_z = 0$ are not directly affected by spanwise rotation. Commonly, the growth of TS waves is inhibited by turbulence in wall-bounded flows, but DNS by Wallin *et al.* [3] indicated that when turbulence is sufficiently weakened by rotation TS waves can grow and cause instabilities.

Numerical studies of rotating channel flow were so far restricted to low Re_b. Our aim is to study rotating channel flow at higher Re_b since it is likely that turbulence damping and flow relaminarization are sensitive to Re_b. In particular, we want to examine whether and when instabilities can occur and get a better understanding of their formation and evolution.

2 Direct numerical simulations

We have used a spectral code to perform DNS of fully developed spanwise rotating channel flow with Re_b fixed at 20000 for $Ro_b \leqslant 1.2$ and at 30000 for $1.5 \leqslant Ro_b \leqslant 2.4$. The domain size is $8\pi h \times 3\pi h$ in the streamwise and spanwise direction in all cases and the spatial resolution in terms of wall units is similar as in other well-resolved DNS. When statistically stationary, Re_τ based on the mean of the shear stresses at both walls is 1000 at $Ro_b = 0$ but declines when Ro_b is increasing. At the highest rotation rate $Ro_b = 2.4$ and $Re_b = 30000$, Re_τ is close to 300, which is the Re_τ of a fully laminar flow at this Re_b, indicating that turbulent stresses are very weak. The mean velocity profile in this run is accordingly close to the laminar Poiseuille profile.

When the rotation is not too high the turbulent kinetic energy, wall shear stresses and other flow statistics have similar temporal variations as for other wall-bounded flows according to time series, however, when $Ro_b \geqslant 0.9$ the temporal variations are suddenly much larger. Figure 1(a) shows as an example the time series of the averaged wall-shear stresses τ_w at the stable and unstable channel side and the volume integrated streamwise velocity fluctuation u_{rms} at $Ro_b = 1.2$ and $Re_\tau = 420$. Both τ_w at the stable side and u_{rms} show sudden, synchronous and sharp rises followed by a decay in a periodic-like manner. Figure 1(b) shows for the same simulation the mean profiles of the velocity fluctuations in all the three directions during the sudden bursts (dashed lines) and during the relatively calm periods in between those bursts (solid lines). We see that the turbulence in the unstable (left) part of the channel is hardly affected by the bursts whereas in the stable part the turbulence intensity is low in the period between the burst but that during the burst all three fluctuating velocity components are strongly enhanced. Similar periodic-like features are also observed in the other simulations with $Ro_b \geqslant 0.9$ although the time period between the bursts and their intensity depend on Ro_b.

An explanation of the periodic-like bursts is that at high Ro_b turbulence is weak at the stable channel side (figure 1.b) and therefore cannot inhibit the formation of two-dimensional Tollmien-Schlichting (TS) waves. Figure 2 gives evidence for the presence of such TS waves with wave length $2\pi h$ in one run. These TS waves can be observed on the stable side long before a burst occurs and grow slowly at first. However, after some time their growth rapidly accelerates and they become unstable producing Λ-shaped vortices. Figure 3(a) shows a visualization of such a Λ-shaped vortex in its early stage and figure 3(b) one in a later stage when it starts to break down and then produce intense turbulence as shown by figure 1(b). The turbulence destroys the TS waves and then it slowly decays so that after some time TS waves can grow again and the cycle repeats itself.

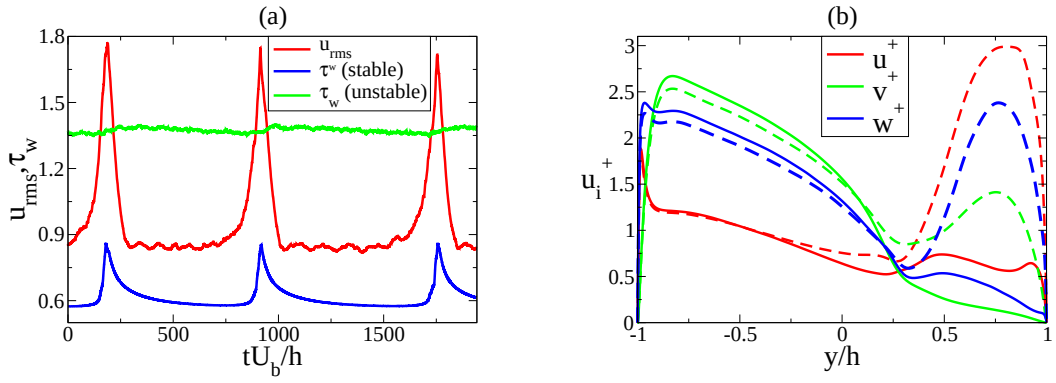

Figure 1: (a) Time series of the volume integrated u_{rms} and the mean wall shear stress τ_w at the stable and unstable channel side. (b) Rms values of the velocity fluctuations during a burst (dashed lines) and in the calm period in between the bursts (solid lines). In both cases $Ro_b = 1.2$ and $Re_\tau = 420$.

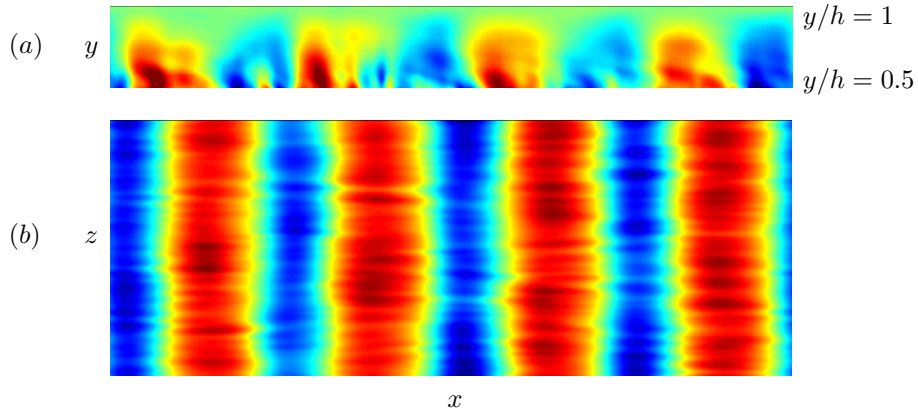

Figure 2: Snapshots of (a) the wall-normal velocity in a streamwise-wall normal plane near the stable channel side and (b) the streamwise velocity in a wall-parallel plane near the stable wall at $Ro_b = 1.2$.

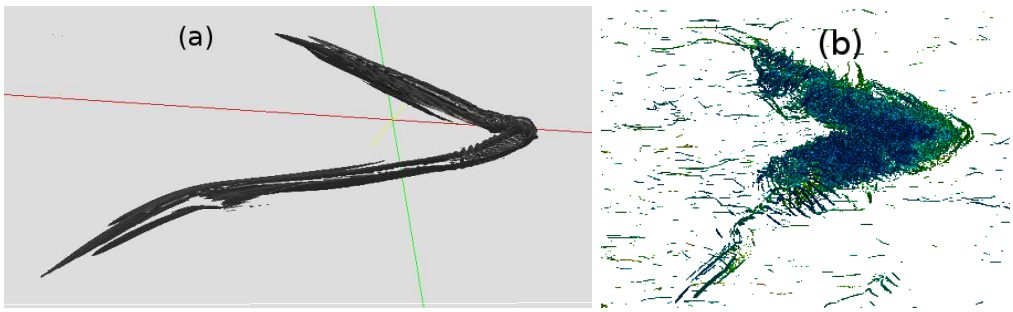

Figure 3: Visualizations of a Λ-shaped vortex near the stable wall (a) at $Ro_b = 1.2$ and (b) at $Ro_b = 1.5$.

References

[1] O. Grundestam, S. Wallin & A. V. Johansson, Direct numerical simulations of rotating turbulent channel flow. *J. Fluid Mech.* **598**, 177–199 (2008).

[2] J. P. Johnston, R. M. Halleen & D. K. Lezius, Effects of spanwise rotation on the structure of two-dimensional fully developed turbulent channel flow. *J. Fluid Mech.* **56**, 533–557 (1972).

[3] S. Wallin, O. Grundestam & A. V. Johansson, Linear stability analysis of rotating channel flow. *Submitted.*

LAMINAR-TURBULENT PATTERNS IN ROTATING PLANE COUETTE FLOW

Yohann Duguet[1], Geert Brethouwer[2] & Philipp Schlatter[2]
[1]*LIMSI-CNRS, UPR 3251, Université Paris-Sud, 91403 Orsay, France.*
[2]*Linné Flow Centre, KTH Mechanics, Osquars Backe18, Stockholm, SE-10044 Sweden.*

1 Numerical simulations

The present investigation focuses on alternately laminar and turbulent oblique patterns observed during the subcritical transition to turbulence in wall-bounded flows. It is shown in the example of plane Couette flow that cyclonic spanwise rotation can delay the formation of such patterns to arbitrary large values of the Reynolds number.

1.1 Transition to turbulence in non-rotating plane Couette flow

Plane Couette flow (pCf), the flow between two parallel walls moving in opposite directions, is the simplest canonical example of the effect of a wall-induced shear on a viscous fluid. The only nondimensional parameter ruling the flow is the Reynolds number, here defined as $Re = \frac{Uh}{\nu}$, where $\pm U$ is the velocity of the two walls, h is the half-gap between them, and ν is the kinematic viscosity of the fluid. We are interested in the way sustained turbulence appears in this system near the onset of transition, knowing that the laminar base flow is linearly stable for all Re. We present here direct numerical simulations in large periodic domains, using a pseudo-spectral code [4]. Two thresholds value for the Reynolds number characterise this subcritical transition: Re_g, below which all perturbations are found to eventually decay, and Re_t, above which turbulent motion, once triggered, contaminates the whole domain. In the interval $[Re_g, Re_t]$, the turbulent flow features robust coexisting laminar and turbulent domains separated by oblique fronts [2, 3, 4].

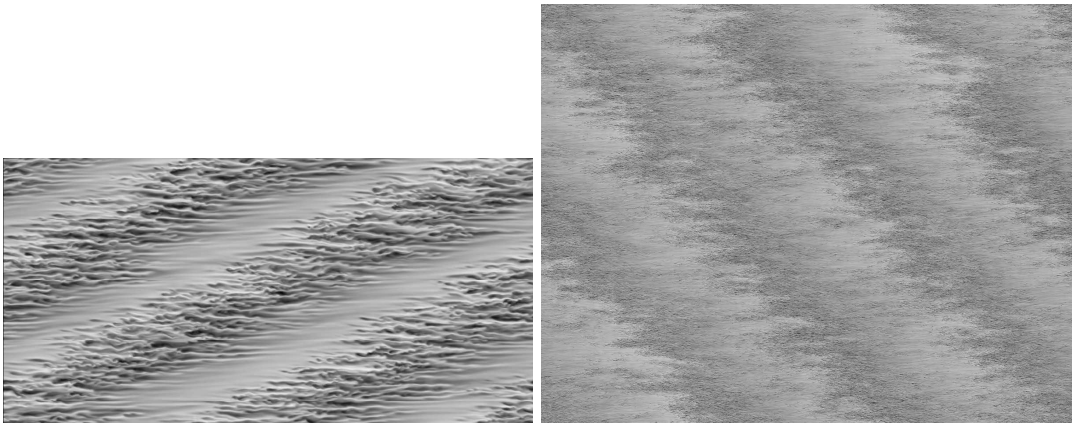

Figure 1: Streamwise velocity in the mid-plane between the plates. The mean flow direction is horizontal. Left: non-rotating pCf for Re=350. Right: rotating pCf for Re=6000 and Ro=-0.104. Domain sizes: $250h \times 125h$ (top) and $250h \times 200h$ (bottom).

1.2 Effects of a spanwise cyclonic rotation

Cyclonic rotation applied to pCf in the spanwise direction (i.e. where the rotation vector has the same direction as the mean flow vorticity) does not modify the laminar base flow. Furthermore it is known to stabilise the laminar state, thus potentially delaying transition to turbulence in pCf [1]. If F is a parameter measuring the amplitude of this cyclonic rotation (here the opposite of a Rossby number), experimental evidence suggests that the two previously defined thresholds Re_g and Re_t still exist yet directly increase with F. In particular, the flow just above Re_g is still characterised by the stable coexistence of alternatively laminar and turbulent domains. We show here numerical evidence of the laminar/turbulent patterns forming at arbitrary large values of Re in the presence of rotation (see Figure 1). Note that very similar conclusions can be drawn under other stabilizing external forces than rotation, such as a spanwise magnetic field or a stable density stratification.

2 Scale separation

Spectral analysis of the mean flow suggests the existence of two length scales for the patterned flow: a large-scale wavelength Λ_z (resp. Λ_x) corresponding to the oblique patterns and a small-scale wavelength λ_z (resp. λ_x) related to the presence of near-wall streaks, as in fully developed wall turbulence. It is shown that λ_z scales classically with wall units following the relation $\lambda_z \approx 100h^+$, while Λ_z scales directly in outer units of h. It follows that parameter space-tracking of the patterned regime at higher and higher rotation rates widens the associated scale separation. An analysis of the mean flow also reveals its complex three-dimensional structure. A tempting conclusion is that the small-scale (turbulent) fluctuations do not directly contribute to the mechanism for the formation of the patterns, apart throught their active role in sustaining the large-scale circulation.

Computer time provided by SNIC (Swedish National Infrastructure for Computing) is gratefully acknowledged.

References

[1] Tsukahara, T., Tillmark, N. & Alfredsson, P. H. 2010 Flow regimes in a plane Couette flow with system rotation. *J. Fluid Mech.*, **648**, 5–33.

[2] Prigent, A., Grégoire, G., Chaté, H., Dauchot, O. & van Saarloos, W. 2002 Large-scale finite-wavelength modulation within turbulent shear flows. *Phys. Rev. Lett.* **89**, 014501.

[3] Barkley, D. & Tuckerman, L. S. 2005 Computational study of turbulent laminar patterns in Couette flow. *Phys. Rev. Lett.* **94**, 014502.

[4] Duguet, Y., Schlatter, P. & Henningson, D. S. 2009 Formation of turbulent patterns near the onset of transition in plane Couette flow. *J. Fluid Mech.* **650**, 119–129.

STREAMWISE ROTATING POISEUILLE FLOW: MODAL AND NON-MODAL STABILITY ANALYSES

George KHUJADZE[1], Jean-Pierre HICKEY[2] & Martin OBERLACK[1,3,4]
[1] *Chair of Fluid Dynamics, TU Darmstadt, Petersenstr. 30, 64287 Darmstadt, Germany*
[2] *Department of Mechanical Engineering, Royal Military College, K7K 7B4 Kingston, Canada*
[3] *Center of Smart Interfaces, TU Darmstadt, Petersenstr. 32, 64287 Darmstadt, Germany*
[4] *GS Computational Engineering, TU Darmstadt, Dolivostr. 15, 64293 Darmstadt, Germany*

Summary A better understanding of transition to turbulence in a Poiseuille flow rotating about the streamwise axis is sought by investigating the stability of the flow. Using the classical linear modal analysis, we define the instability envelop and find that the rotation increases the exponential growth of the most unstable mode and, for high levels of rotation, we observe a re-stabilization of the flow. The influence of rotation on transient energy growth is also investigated as the set of linear equations is non-normal. We show that the energetic growth can be of the order of $O\left(10^3\right)$ in the sub-critical region but for high Ro the non-normality of the equation set is reduced, resulting in a decrease of the maximal energetic growth. The maximal growth is achieved by the purely spanwise disturbances until a certain point where the maximal energy growth is caused by oblique ones.

1 Governing equations and geometry of the flow

The application of system rotation to canonical wall-bounded flows is of great academic and engineering interest. From an academic perspective, these flows provide unique insight into the influence of body forces on the flow. From an engineering point of view, the presence of rotating flow is ubiquitous in most turbo-machinery applications making the study of these flows of great practical relevance. To the knowledge of the authors, [1] were the first to study the streamwise rotating Poisseuille flow using Lie group analysis and direct numerical simulations (DNS). Althought the flow setup share some similarities with the classical spanwise rotating channel flow, the streamwise rotation, in the present case, does not break the centerline symmetry. More recently, an experimental investigation was conducted at the RWTH-Aachen ([2]) and a DNS study was performed to verify the results by [3]. A study conduced by [4] shed light on the non-modal stability characteristics of this flow. However, their study overlooked the importance of non-modal transient growth in the flow.

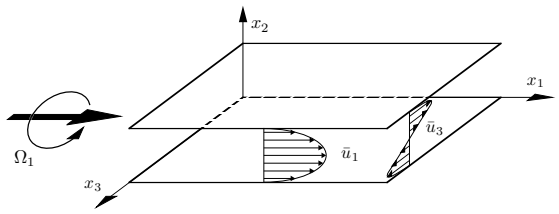

Figure 1: Streamwise rotating Poiseuille flow.

In the present work, we investigate the modal and non-modal stability characteristics of a streamwise rotating Poiseuille flow (figure 1). The non-dimensionalised Navier–Stokes and the continuity equations for the incompressible rotating channel flow are:

$$\frac{\partial \boldsymbol{u}}{\partial t} + (\boldsymbol{u}\cdot\boldsymbol{\nabla})\,\boldsymbol{u} = -\boldsymbol{\nabla}P + \frac{1}{Re}\nabla^2\boldsymbol{u} - Ro\times\boldsymbol{u}$$

$$\boldsymbol{\nabla}\cdot\boldsymbol{u} = 0$$

Reynolds and Rossby numbers are defined in the following form: $Re = U_{\max}h/\nu$, $Ro = 2\Omega_1 h/U_{\max}$. ν is the kinematic viscosity, $U_{\max}$ is the maximal base flow velocity and h is the half-height of the channel. We consider only a streamwise rotation (see figure 1), hence $\boldsymbol{\Omega} = (\Omega_1, 0, 0)$.

2 Exponential and transient growths

The numerical calculations were performed in MATLAB using a spectral collocation method based on Chebyshev polynomials modified from the code developed by S. Reddy ([5]). The original code was extended to include the additional system rotation.

By setting $Re = 100$ and evaluating the effective perturbations for different rates of rotation in the figures 2 we observe the appearance of spectral instabilities from a Rossby number of $Ro = 0.246$ at $\alpha \approx 0.55$ and $\beta \approx 2.0$. By increasing the Rossby number to $Ro = 0.5$ (right plot in the figure 2), one can see a great range of perturbations (represented by the shaded area) that are able to destabilise the flow.

In modal analysis, a conclusion on the stability must be made without regards to the evolution of the problem at the near initial state. We present the results of non-modal analysis of the flow and determine the

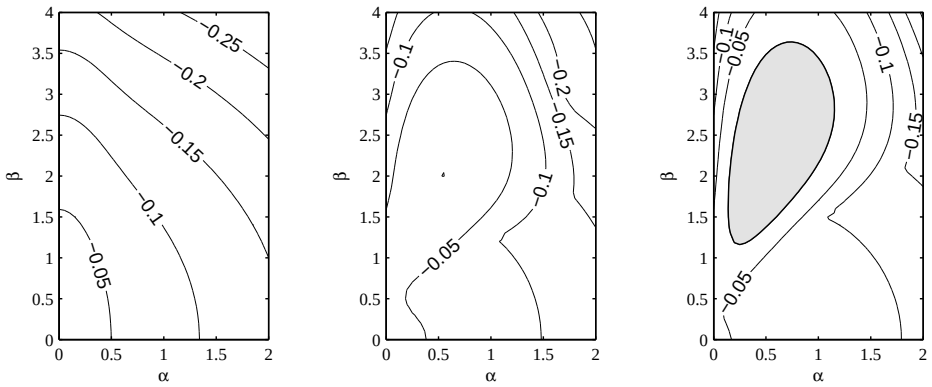

Figure 2: $Re = 100$. Results corresponding to Rossby numbers $Ro = 0,\ 0.246,\ 0.5$ are presented on left, middle and right plots correspondingly. The contour lines represent the value of the maximal imaginary eigenvalue for every perturbation couple. The first spectral instability for $Re = 100$ is seen at a rotation of $Ro = 0.246$.

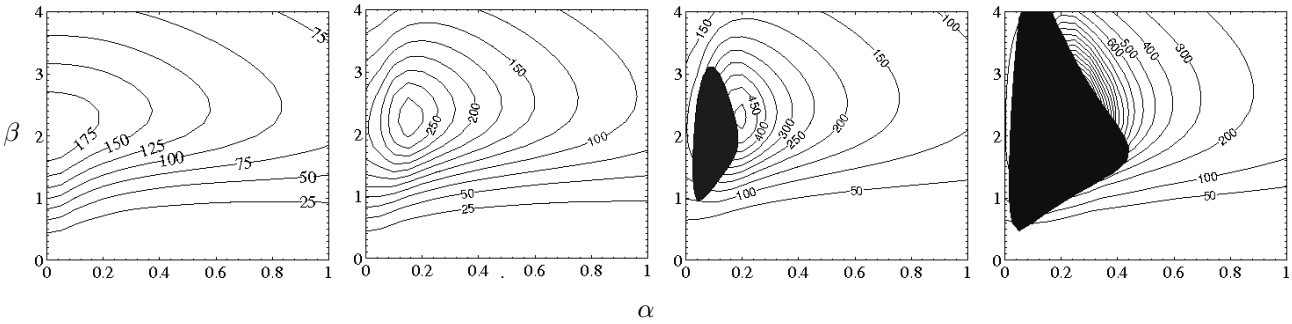

Figure 3: The energetic transient growth is shown for a large spectrum of perturbations at $Re = 1000$ with $Ro = 0.001$, 0.015, 0.025 and 0.05. The shaded area represents spectral instability calculated with the help of modal analysis. Contour lines represent the ratio of the maximum turbulent kinetic energy growth defined as $sup\frac{|u^2(\cdot,t)|}{|u^2(\cdot,0)|}$.

possible energetic growth the the perturbations. Non-modal analysis reveals that streamwise rotation allows for a significant level of transient energy growth to occur (up to $O(10^3)$) in exponentially stable flow. At high Ro, the transient growth is significantly reduced as the linearised governing equation set reaches an (nearly) anti-symmetric form for which the non-normality of the operator set is greatly reduced. For a given Ro, the initial conditions leading to the maximal energy growth change from a 2D (streamwise independant) to a $3D$ perturbation at a given Reynolds number. As the rotational terms are streamwise dependant, the shift represents the minimal Reynolds number at which the transient growth is caused primarily by the rotational body force.

References

[1] Oberlack, M., Cabot, W. & Rogers, M. M. 1998 Group analysis, DNS and modeling of a turbulent channel flow with streamwise rotation. *Proceedings of the Summer Program of the CTR, Stanford* **1**, 221–242.

[2] Recktenwald, I., Weller, T., Schroder, W. & Oberlack, M. 2007 Comparison of DNS and PIV data of turbulent channel flow rotating about the streamwise axis. *Phys. Fluids* **19**, 085114.

[3] Oberlack, M., Cabot, W., Pettersson, R. & Weller, T. 2006 Group analysis, direct numerical simulation and modeling of a turbulent channel flow with streamwise rotation. *J. Fluid Mech.* **562**, 383–403.

[4] Masuda, S., Fukuda, S. & Nagata, M. 2008 Instabilities of plane Poiseuille flow with a stream-wise system rotation. *J. Fluid Mech.* **603**, 189–206.

[5] Schmid, P. J. & Henningson, D. S. 2001 *Stability and transition in shear flows*, *Applied Mathematical Sciences*, vol. 142. Springer.

TRANSITION FROM QUASI-2D TO 3D IN A ROTATING ELECTROMAGNETICALLY FORCED DIPOLAR FLOW STRUCTURE

Matias Duran-Matute[1,2], Gabriella Di Nitto[3], Ruben Trieling[1] & GertJan van Heijst [1]
[1] *Fluid Dynamics Laboratory & J.M. Burgers Centre, Eindhoven University of Technology, Eindhoven, The Netherlands*
[2] *Currently at: LEGI-CNRS, Grenoble, France*
[3] *DICEA, Sapienza, Rome, Italy.*

1 Introduction

Background rotation is assumed to enforce the two-dimensionality of flows. If the rotation is fast enough, the flow far away from the boundaries becomes independent of one coordinate. Furthermore, the characteristics of the boundary layers that form next to the boundaries perpendicular to the rotation axis (known as Ekman boundary layers) allow to model the evolution of decaying rotating flows using the two-dimensional vorticity equation

$$\frac{D\omega}{Dt} = \lambda_{Ek}\omega, \tag{1}$$

where D/Dt is the material derivative, ω is the vorticity component parallel to the rotation axis of the system, and λ_{Ek} is a constant known as the Ekman damping coefficient. If a flow obeys eq. (1), the flow can be said to be quasi-two-dimensional [1]. Equation (1) is *a priori* only valid if the Coriolis acceleration is much stronger than the advective acceleration (i.e. the Rossby number Ro is small) and if the flow evolves freely.

In the current work, we determine experimentally the limit of applicability of the linear Ekman theory, on which eq. (1) is based, to flows driven by a non-conservative body force. In other words, we determine the transition in the parameter space between a quasi-two-dimensional and a three-dimensional flow. In particular, we study a dipolar flow structure driven by time-independent electromagnetic forcing in a shallow fluid layer subjected to background rotation, and we characterize the response of the flow as a function of the parameters of the problem. The limit for the two-dimensionality of the flow is reflected as a change in the scaling of the response of the flow to the magnitude of the electromagnetic forcing, and against the common belief, it does not depend exclusively on the Rossby number.

2 Methods

The experiments were carried out in a water tank with a base of 34×30 cm^2 placed on top of a rotating table, which rotates at a frequency Ω. The tank is filled with a salt solution with a concentration of 178 g l^{-1} with a kinematic viscosity $\nu = 1.50 \cdot 10^{-6}$ m^{2}s^{-1} and a density $\rho = 1190$ kg m^{-3} to a depth H and covered with a transparent perspex lid to avoid free-surface deformations. To force the flow, two titanium electrodes are placed along two opposite sides of the tank, and three 30×10 cm^2 rectangular magnets are placed 1.1 cm underneath the tank bottom. The magnitude of the magnetic field of each these magnets is 0.018 T measured just above their centre. The magnet at the centre has its North Pole facing up, while the two side magnets have their North Pole facing down. A constant electric current I is applied through the fluid using a power supply with a precision of 10^{-2} A.

Particle Image Velocimetry (PIV) is used to measure the horizontal velocity field of the flow in a plane at mid-depth. The fluid is seeded with 106–150 μm polymethylmethacrylate (PMMA) particles, which are illuminated at mid-depth with a laser sheet produced by a double pulsed Nd:YAG laser.

Numerical simulations of the flow were performed using a finite-element code (COMSOL). These simulations serve two purposes: (1) to obtain the three-dimensional velocity field of the flow and (2) to reach regions of the parameter space that are inaccessible experimentally.

2.1 Non-dimensional parameters

Dimensional analysis yields three independent dimensionless control parameters:

$$Ch \equiv \frac{IBH}{\rho\nu^2}, \quad Ek \equiv \frac{\nu}{\Omega H^2}, \quad \delta \equiv \frac{H}{L}, \tag{2}$$

where the Chandrasekhar number Ch characterizes the EM forcing and represents the ratio of the Lorentz force to the viscous force; the Ekman number Ek characterizes the system's rotation rate and represents the ratio

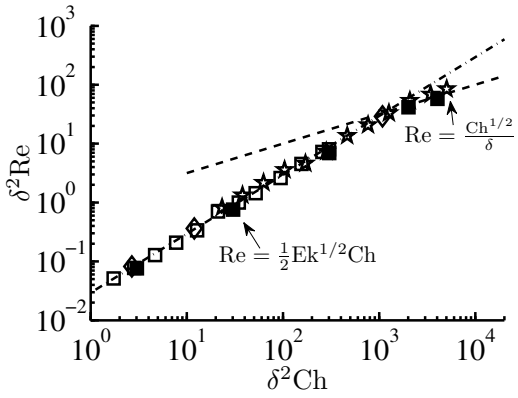

Figure 1: Response of the flow to electromagnetic forcing. Results from experiments (empty symbols) and simulations (filled symbols) for $Ek = 3.5 \cdot 10^{-3}$ and $\delta = 0.0353$ (squares), $\delta = 0.0588$ (diamonds), $\delta = 0.0941$ (stars). The dashed lines represent theoretical approximations obtained from dimensional analysis.

of viscous forces to the Coriolis force; and the aspect ratio of the container δ characterizes the geometry of the flow domain. B is the magnitude of the magnetic field at mid-depth above the center of a magnet.

In addition, as the response parameter of the problem, we define the Reynolds number

$$Re \equiv \frac{UL_x}{\nu}, \tag{3}$$

which represents the ratio of inertia forces to viscous forces, with U the spatial average of the horizontal velocity at mid-depth. In other words, $Re = Re(Ch, Ek, \delta)$. The Rossby number can be written in terms of the other dimensionless parameters as $Ro = \delta^2 EkRe/2$.

3 Results

Figure 1 presents the response of the flow as function of the forcing for experiments and simulations with $Ek = 3.5 \cdot 10^{-3}$ and different values of δ. Note that the axes have been multiplied by δ^2, resulting in the collapse of the curves for different δ-values. As can be seen, there are two scaling regimes for all Ek-values. For small values of $Ch\delta^2$ there is a linear regime where $Re \propto Ch$, while for large values of $Ch\delta^2$, there is a non-linear regime where $Re \propto Ch^{1/2}$. The transition reflects the growing importance of the advective acceleration, and is similar to the transition found in the case of shallow flows without background rotation [2].

From dimensional analysis, it can be estimated that the transition between the two different regimes occurs when

$$\frac{\delta^2 Ch\, Ek}{4} = \frac{Ro}{Ek^{1/2}} \approx 1, \tag{4}$$

showing that it does not depend exclusively on the Rossby number.

For strong background rotation (small Ek-values), viscous dissipation is dominated by Ekman damping in the linear regime. However, numerical simulations show that the Ekman boundary layers are deformed in the non-linear regime. Hence, linear Ekman damping is no longer a good approximation in this regime, and the flow cannot be considered as quasi-two-dimensional. This can be true even for small Ro-values. The deformation of the Ekman boundary layers is then not due to non-linearities in the bulk of the fluid. Instead, the balance between viscous forces and the Coriolis force, which essential for the existence of Ekman boundary layers, is broken due the electromagnetic forcing within the boundary layer.

References

[1] F.V. Dolzhanskii, V.A. Krymov, and Y.D. Manin, An advanced experimental investigation of quasi-two-dimensional shear flows. *J. Fluid Mech.* **241**, 705–722 (1992).

[2] M. Duran-Matute, R.R. Trieling, and G.J.F. van Heijst, Scaling and asymmetry in an electromagnetically forced dipolar flow structure, *Phys. Rev. E* **83**, 016306 (2011).

4 Posters

EUROMECH Colloquium 525, 21–23 June 2011, Écully, France
Instabilities and transition in three-dimensional flows with rotation

BY-PASS TRANSITION DESCRIPTION USING AN ORTHOGONAL DECOMPOSITION OF THE VELOCITY FIELD

Marc BUFFAT, Lionel LE PENVEN, Anne CADIOU & Julien MONTAGNIER
Laboratoire de Mécanique des Fluides et d'Acoustique, Université de Lyon, Université Claude-Bernard Lyon1/ CNRS/ Ecole Centrale de Lyon/ Insa de Lyon

In the last two decades, theory and computer simulations have led to significant advances in the understanding of boundary layer bypass transition induced by free-stream disturbances [5]. It has been shown that transition can be initiated by the growth of velocity perturbations taking the form of streaks elongated in the streamwise direction and modulated in the spanwise direction. As the streaks grow downstream, they become susceptible to high-frequency secondary instability and breakdown to turbulence finally occurs. The physical process explaining the emergence of streaks is known as the lift-up effect and is the result of interactions between streamwise vorticity and the boundary layer shear. Streaks can be generated by perturbations inside the boundary layer or by free-stream turbulence. The secondary instability can be initiated by free-stream turbulence, by selecting a high-frequency perturbation mode [8] or by streak interactions [2]. Numerical analysis of bypass transition can be found in [6], [7]. The main objective here is to study by numerical simulations (and to describe) boundary layer bypass transition between two parallel walls using an orthogonal decomposition of the velocity into two solenoidal fields.

The numerical simulations are performed using a spectral Galerkin projection method based on an orthogonal decomposition of the velocity into two solenoidal vector fields [3]. Since, by construction, the two orthogonal vector fields of the decomposition are associated with the Orr-Sommerfeld and the Squire modes of the linear stability theory respectively, the method makes it possible to evaluate kinetic energy transfers due to the coupling between these two modes and their interactions with the base flow. The code, developed in our team, is parallelized by an hybrid OpenMP/MPI approach and runs efficiently on ten thousand CPU cores. The studied problem is a plane channel flow with thin boundary layers and the computational domain is supposed to be far enough from the inlet section such that the potential effect of the leading edges can be neglected.

Different approaches can be used to select the disturbance that generates the streaks. Using the variational approach of [4], the optimal perturbation which sustains maximum temporal growth in the linear regime can be determined. This optimal perturbation consists of a spanwise wave with a streamwise wavenumber $\beta \approx 2/\delta$ inside the boundary layer and is zero outside the boundary layer. Such an optimal perturbation can be used to model disturbances inside the boundary layer. Free-stream turbulence can be described as a superposition of modes of the continuous spectrum of the Orr-Sommerfeld-Squire equations. To characterise the modes that generate streaks, Zaki et al [8] studied the forced Squire response to an Orr-Sommerfeld eigenfunction. They defined a coupling coefficient between an Orr-Sommerfeld eigenfunction and the Squire modes to characterize their interaction and the ability of the Orr-Sommerfeld mode to generate streaks.

To model the generation of streaks by free-stream turbulence, we follow a similar methodology adopted by [8], and study the transient response of the linearised equations to an Orr-Sommerfeld mode, chosen as initial condition. Using the same orthogonal decomposition of the velocity field as in the DNS code, the linear system of two equations is obtained using a weak formulation, and is equivalent to the classical Orr-Sommerfeld-Squire equations. Instead of using the two classical scalar fields: the normal velocity v and the normal vorticity η, this formulation allows us to analyse the solution in terms of two orthogonal velocity fields: the Orr-Sommerfeld (OS) $\boldsymbol{u}_{os}(v)$ and the Squire (SQ) $\boldsymbol{u}_{sq}(\eta)$ velocities, associated with two orthogonal velocity spaces W_{os} and W_{sq}. In our numerical approach, the eigenvectors are splitted into two distinct sets, depending on their orthogonality with the subspace W_{os}: the set $\{\boldsymbol{u}^-\} \subset W_{sq}$, associated with the Squire modes of the homogeneous Squire equation, and the complementary set $\{\boldsymbol{u}^+\}$. The projection $\boldsymbol{u}^+_{os}$ of $\boldsymbol{u}^+$ in W_{os} is associated with an Orr-Sommerfeld eigenmode and its projection $\boldsymbol{u}^+_{sq}$ in W_{sq} with the coupled Squire eigenmode. The ratio $r_\perp = ||\boldsymbol{u}^+_{sq}||/||\boldsymbol{u}^+_{os}||$ of these two projections characterize the non-orthogonality of an eigenvector $\boldsymbol{u}^+$ with the set $\{\boldsymbol{u}^-\}$, a large value of $r_\perp$ indicating an important nonorthogonality (non normality). By analysing the transient response with an initial condition equal to $\boldsymbol{u}^+_{os}$, we found that the most amplified $\boldsymbol{u}^+_{os}$ are associated to eigenvectors $\boldsymbol{u}^+_r$ with a normal to the wall wavelength (outside the boundary layer) of the order of 2δ. These eigenvectors $\boldsymbol{u}^+_r$ have large value of $r_\perp$, indicating an important non-orthoganlity with $\{\boldsymbol{u}^-\}$. An optimal problem can be solved for this transient problem, and the optimal initial condition is similar to the optimal perturbation calculated with the optimal growth theory. This optimal perturbation consists mainly of an OS velocity (streamwise vortices inside the boundary layer) at the initial time, transformed after the transient time into a streamwise SQ velocity. However, as this optimal perturbation is zero ouside the boundary layer, it cannot be chosen as a model of free-stream turbulence. By analysing the expansion of this optimal perturbation in the eigenvectors basis, the optimal modes are found to be a combination of eigenmodes around the eigenvectors $\boldsymbol{u}^+_r$ having the maximum

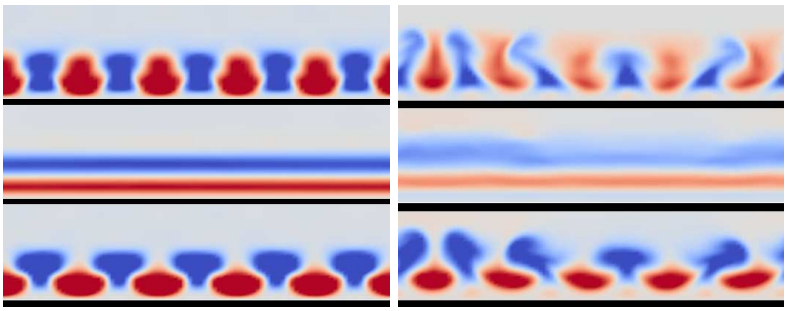

(a) $x = 4h$ (b) $x = 6.9h$

Figure 1: Instantaneous contours of streamwise velocity perturbation displayed using the orthogonal decomposition in two cross sections: (a) in the streaks region and (b) near the turbulent burst. From top to bottom: SQ velocity, OS velocity, total perturbation.

value of $r_\perp$. A remarkable finding is that the shape of the transient response is nearly identical for an initial condition equal to the optimal initial condition (or the optimal mode) and for an initial condition equal to the W_{os} projection of modes $\boldsymbol{u}_r^+$, and that only the amplitude of the transient response depends on the particular initial condition. For all these initial conditions, the transient response corresponds to SQ velocity or streaks characterised by a large peak of the streamwise velocity component inside the boundary layer. Based on this analysis, we use henceforth the ratio $r_\perp$ to select the inlet perturbation in our simulations.

In the simulations, the inlet boundary layers are thin compared to the distance $2h$ between the two parallel walls ($\delta/h = 0.05$). The inlet Reynolds number, based on the displacement thickness, is equal to 344 (corresponding to $Re_x = 40000$). The first perturbation is chosen as an oblique wave u_{os}^+ with $\beta_\delta = 2$ and $\alpha_\delta = 0.04$ having the largest value of $r_\perp$.To initiate the transition of the streaks, a second perturbation with a larger streamwise wavenumber $\alpha_\delta \approx 1$ and a smaller spanwise wavenumber $\beta_\delta \approx 0.3$ is introduced at the inlet as in [8]. This second perturbation is a vector $\boldsymbol{u}^+$ having a small value of $r_\perp$ Without external perturbations, the flow remains laminar and the classical Blasius skin friction coefficient is recovered. Using the two previous perturbations, by-pass transition is induced in the boundary layers. As the boundary layer thickness is small compared to the channel height, similar results are obtained to those presented by [8] and [7] for a boundary layer over a flat plate. Using the orthogonal decomposition of the velocity, specific information about the structure of streaks of finite length can be obtained (see Figure 1). Specifically, the streaks are found as the sum of two orthogonal contributions, one part is the SQ velocity field, which is a streamwise oriented contribution representing 60% of the total kinetic energy, the other part is the OS velocity field which is a spanwise invariant term with 40% of the kinetic energy. In the early steps of the transition, the secondary instability affects mainly the SQ streamwise velocity, whereas the OS streamwise velocity remains almost unaffected. In the transition region, strong oscillations of the streaks are observed in the spanwise direction. In that region, the plot of the streamwise perturbation (lower plot in Figure 1b) clearly shows spanwise oscillations of the low speed streaks on top of the boundary layer. Figure 1b shows that the instability mainly affects the SQ streamwise velocity, whereas the OS streamwise velocity remains almost unaffected. At the early stage, before breakdown, this instability occurs through perturbations of the SQ streamwise velocity and looks very similar to the transverse instabilities studied by [1].

References

[1] P. Andersson, L. Brandt, A. Bottaro, and D. S. Henningson. *J. Fluid Mech.*, 428:29–60., 2001.

[2] L. Brandt and H. C. de Lange. *Physics of Fluids*, 20:024107, 2008.

[3] M. Buffat, L. Le Penven, and A. Cadiou. *Computers & Fluids*, 42:62–72, March 2011.

[4] K. M. Butler and B. F. Farrell. *Phys. Fluids A*, 4:1637–1650, 1992.

[5] P. Durbin and X. Wu. *Annual Review of Fluid Mechanics*, 39:107–128, 2007.

[6] R. G. Jacobs and P. A. Durbin. *J. Fluid Mech*, 428:185–212, 2001.

[7] P. Schlatter, L. Brandt, H. C. de Lange, and Dan S. Henningson. *Physics of Fluids*, 20:101205, 2008.

[8] T. A. Zaki and P. A. Durbin. *Journal of Fluid Mechanics*, 85-111, 2005.

GLOBAL STABILITY ANALYSIS OF FLOW THROUGH AN ANEURYSM

Shyam Sunder Gopalakrishnan, Benoît PIER & Arie BIESHEUVEL
Laboratoire des mécanique des fluides et d'acoustique (CNRS - Université de Lyon).
École centrale de Lyon, 36 avenue Guy-de-Collongue, 69134 Écully, France.

The global linear stability analysis of flow through a model fusiform aneurysm is carried out numerically. A gaussian profile was used to model the wall channels to account for the bulge, that gradually straightens out to a uniform circular pipe in the upstream and downstream direction. The model configuration considered in the study is characterised by the bulge length and the maximum diameter of the bulge. These parameters for our model (*Model A*) were $3.0D$ and $2.0D$ consistent with the one used in [1] and *Model 3* in [2], where D is the inlet pipe diameter. A steady parabolic velocity profile was imposed at the inlet along with a swirl prescribed using a sinuous function ($w_0 \sin(\pi r/R)$ where w_0 is a constant parameter used to quantify the inlet swirl and R is the inlet pipe radius) for the azimuthal flow component. The global stability analyses were carried out on base flows that were axisymmetric on which non-axisymmetric perturbations were allowed to grow. For *Model A* in the absence of inlet swirl ($w_0 = 0$), the flow was found to be weakly unstable to global eigenmodes of azimuthal modenumbers 4 and 5 at a Reynolds number (based on the maximum centerline velocity and pipe diameter) $Re \approx 9700$. The least stable eigenmodes are concentrated at the downstream end of the bulge and were characterised by their slow oscillatory nature. The swirl prescribed at the inlet was varied by changing w_0 and was found to have a stabilizing effect on the stability properties with the flow becoming unstable at a higher Reynolds number. The results obtained are found to be consistent with those presented in [1].

Motivation

Aneurysms are localized permanent arterial dilations caused due to disease or other complex processes that result in the weakening of the arterial walls [3]. Among these, fusiform aneurysms, that are commonly found in the abdominal aorta and are characterised by a bulge about the vessel centerline are the focus of the present study. In the recent years, there has been an increase in the studies carried out on blood flows from a fluid mechanics perspective. In particular, the studies on flows in constricted pipes designed to model stenosis have shed light on flow behaviour and stability in such geometries [4]. However, the research on flow through aneurysmal channels has been limited [2, 5]. These studies comprised of experiments [2] and numerical simulations [5] in axisymmetric aneurysm models investigate the role of wall shear stresses in the rate of enlargement of aneurysms.

The present study aims to explore the stability of the flow in aneurysms for steady inlet flows and to quantify their behaviour by studying the nature of instabilities inherent in these geometries. The analyses were carried out in the same spirit as in the recent article by Sheard & Blackburn [1].

Methodology

We use the incompressible Navier–Stokes equations written in cylindrical coordinates to simulate the flows considered in this study. Fully developed Poiseuille flow with maximum centerline velocity U was input upstream at the inlet. To compute the base flow, we adopt the procedure used by Marquet *et al.* [6] wherein a time-dependent simulation of the two-dimensional Navier–Stokes equations is first used to obtain an approximate solution of the steady solution at low Reynolds number where it is stable to two-dimensional perturbations. A Newton iteration is then applied to solve the stationary Navier–Stokes equations, starting the procedure with the approximate steady solution as an initial guess. The Newton algorithm requires the inversion of a non-symmetrical sparse matrix which is carried out by a direct method, the UMFPACK library being used to perform a sparse LU factorisation.

For the linear stability analysis, the base flows were assumed axisymmetric due to the general agreement in literature that blood flow in abdominal aortic aneurysms is dominated by axisymmetric flow structures [3]. The three-dimensional perturbation field was discretized in the azimuthal direction using Fourier modes, which are individually decoupled. This permits the stability analyses of individual azimuthal modenumbers (m) to be computed separately on the same axisymmetric domain as used for the base flow computations. The resulting eigenvalue problem was solved using a 'shift-and-invert' strategy as in [6].

The two-dimensional stationary Navier–Stokes equations and the general eigenvalue problem are solved numerically by a finite element method. The spatial discretization is a mixed finite-element formulation using P2-P1 Taylor–Hood elements: six-node quadratic triangular elements with quadratic interpolation for velocities (P2) and three-node linear triangular elements for pressure (P1). The meshes as well as the discrete matrices resulting from the variational formulation of the problems and projected onto those meshes are generated with the software FreeFem++ (http://www.freefem.org).

Preliminary Results

The computations shown in figure 1 were carried out on *Model A* for $w_0 = 0$. Figure 1a shows the leading global modes characterized by their axial, radial and azimuthal velocity components (top to bottom) for azimuthal modenumber $m = 4$ at $Re = 9700$. The spatial distribution of the global modes shows that they are localized at the downstream end of the bulge. Figure 1b shows a typical eigenvalue spectrum obtained from the linear stability analysis at $Re = 9700$ for various values of m. The temporal growth rate of the eigenmodes σ is plotted in the y-axis and their frequency ω in the x-axis. The least stable eigenmodes are observed for $m = 4, 5$ with a non-zero frequency.

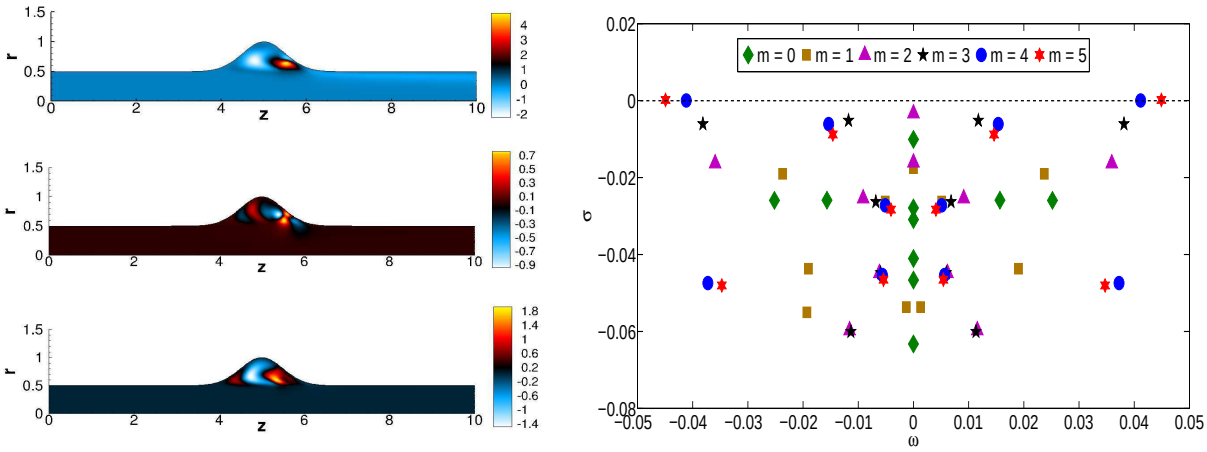

(a) (b)

Figure 1: (a) Global modes visualized by their axial, radial and azimuthal (top to bottom) velocity components. Parameter settings: *Model A*, $m = 4, Re = 9700, w_0 = 0$. (b) Typical eigenvalue spectrum in the (ω, σ) plane for different azimuthal modenumbers m. Parameter settings: *Model A*, $Re = 9700, w_0 = 0$.

We intend to present the results obtained from our stability analyses along with the effect of varying inlet swirl on *Model A* during the conference.

References

[1] G. J. Sheard and H. M. Blackburn, Steady inflow through a model aneurysm: global and transient stability. *17th Australasian Fluid Mechanics Conference, Auckland, New Zealand*, 5–9 December (2010).

[2] A.-V. Salsac, S. R. Sparks, J.-M. Chomaz and J. C. Lasheras, Evolution of the wall shear stresses during the progressive enlargement of symmetric abdominal aortic aneurysms. *J. Fluid Mech.* **560**, 19–51 (2006).

[3] J. C. Lasheras, The biomechanics of arterial aneurysms. *Annu. Rev. Fluid Mech.* **39**, 293–319 (2007).

[4] M. D. Griffith, M. C. Thompson, T. Leweke, K. Hourigan and W. P. Anderson, Wake behaviour and instability of flow through a partially blocked channel. *J. Fluid Mech.* **582**, 319–340 (2007).

[5] G. J. Sheard, Flow dynamics and wall shear stress variation in a fusiform aneurysm. *J. Eng. Math.* **64**, 379–390 (2009).

[6] O. Marquet, M. Lombardi, J.-M. Chomaz, D. Sipp and L. Jacquin, Direct and adjoint global modes of a recirculation bubble: lift-up and convective non-normalities. *J. Fluid Mech.* **622**, 1–21 (2009).

CONFINEMENT OF TURBULENT FLOWS WITH ROTATION EFFECTS WITH A PENALIZATION METHOD

Clément Jause-Labert, Fabien S. Godeferd
clement.jause-labert@ec-lyon.fr
Laboratoire de Mécanique des Fluides et d'Acoustique
École Centrale de Lyon, Université de Lyon, France.

We want to analyse the structuration and dynamics of homogeneous turbulence in a cylindrical container with open periodic ends, placed in a rotating frame. To that extent, we performed pseudo-spectral Direct Numerical Simulations at different Rossby and Reynolds numbers using a penalization technique to take into account the radial confinement.

A first part of the presentation is dedicated to the validation of this numerical method by considering the impact of a vortex ring on a flat "penalized" wall and compare the results obtained with the existing experimental data. A second part will then describe the dynamics of the cylindrical flow as well as its anisotropic structure and its main Lagrangian statistics.

1 Context and motivation

Homogeneous turbulence is obviously an idealized picture of actual or experimental flows, as boundaries are always present in nature. Moreover, actual flows in nature or in industry are also subjected, to a certain extent, to body forces such as the Coriolis force when considering rotation effects in geophysical flows, buoyancy in the case of stratified flows or the Lorentz force in the case of an electrically conducting fluid submitted to a magnetic field.

In the present work, we propose to explain some basic features of turbulent flows in a cylindrical enclosure, a geometry which bears some similarities with current experimental settings for studying high Reynolds number turbulence (von Karman flows). This geometry is also chosen because it retains homogeneity in two directions (the azimuthal and the vertical ones). We also propose to add to this confined flow the effect of the Coriolis force that appears when considering background rotation. We will take advantage of the axis of symmetry of the confinement and align the axis of rotation with it. This configuration will allow to evaluate the effect of confinement onto rotating turbulence, and contrast its properties with the well-described dynamics of homogeneous rotating flows [2].

2 Presented work

We use a tri-periodic pseudo-spectral code with an immersed boundary method, namely the volume penalization method. This class of methods has been introduced in 1972 by Peskin (see [5]) and allows the computation of bounded flows on Cartesian grids (meaning that no refinement close to the boundary is needed). The method consists in adding an external force field in the Navier-Stokes equations, where a mask function splits the computational mesh between fluid and solid/porous regions. A penalization parameter allows to describe an impermeable domain in the asymptotic zero limit. A mathematical demonstration of the convergence of the penalized equations to the Navier-Stokes ones with no-slip boundary conditions has been achieved by Angot *et al.* [1]. However, when computing the set of penalized equations with an explicit scheme for evaluating the penalized term, a stability issue appears which hardly constrains the time-step. An original way to avoid this restriction has been developed and is formulated in [3]. In the latter work, we also highlight the fact that the penalization term is compressible and explicitly acts on the pressure term.

First, we propose to test the numerical method by considering the impact of a vortex ring on a wall introduced thanks to the penalization method. Walker *et al.* [6] showed that, in a defined range of Reynolds number, a secondary ring is created and the interaction of those two vortex rings leads to a third one. The comparison of our simulations with this experimental work (see figure 1) is very interesting and reveals that the penalization method is able to reproduce the features described in [6].

We then perform Direct Numerical Simulations (DNS) of confined freely decaying turbulence with and without the addition of the Coriolis force to observe and compare the decay of such flows. A qualitative viewpoint is given by figure 2 at the beginning of the computation. Some trajectories of tracer particles are used to obtain a Lagrangian viewpoint of the global effect of confinement.

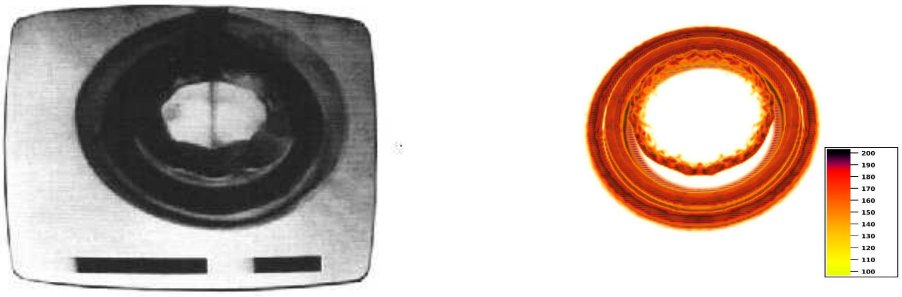

Figure 1: Impact of a vortex ring on a flat wall – Re=1250. Creation of secondary and tertiary vortex rings. Left : Experimental observation by Walker *et al.*. Right : Present penalized simulation with $\eta = 10^{-6}$, visualization of the enstrophy field.

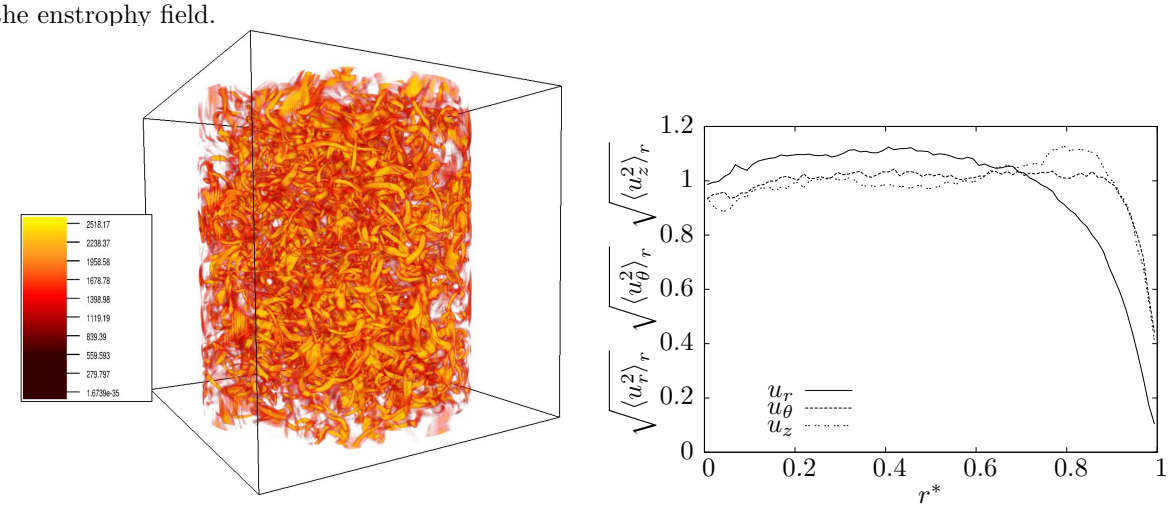

Figure 2: Left: Eulerian qualitative aspect of confined turbulence (no rotation). Visualization of the enstrophy $W = \frac{1}{2}\omega_i\omega_i$. Right: Radial evolution of the *rms* velocities obtained for the non-rotating case.

The principal goal of this work is to present the variation of different statistics in the flow depending on the distance to the wall. Such statistics are the orientation of the velocity vectors, the *pdf* of the different components of the velocity, the radial evolution of the normalized *rms* velocities, the directional length scales, etc. Figure 2 shows the radial distribution of the three *rms* velocities in the cylindrical coordinates.

Our presentation during Euromech Colloquium 525 will include Eulerian statistics from an extended database with high resolution DNS, as well as Lagrangian dispersion statistics.

References

[1] Angot, P., Bruneau, C.-H., Fabrie, P. 1999 A penalization method to take into account obstacles in incompressible viscous flows, *Numer. Math.* **81** 497–520

[2] Cambon, C., Mansour, N.N. & Godeferd, F.S. 1997 Energy transfer in rotating turbulence *J. Fluid Mech.* **337**, 303–332

[3] Jause-Labert, C., Godeferd, F.S. & Favier, B. 2011 Numerical validation of the volume penalization method in three-dimensionnal pseudo-spectral simulations. *In preparation.*

[4] Kolomenskiy, D. & Schneider, K. 2009 A Fourier spectral method for the Navier-Stokes equations with volume penalization for moving solid obstacles. *J. of Comp. Phys.* **228** (16), 5687–5709

[5] Peskin, C.S. 1972 Flow patterns around heart valves: A numerical method., *J. of Comp. Phys.* **10** (2), 252–271

[6] Walker, J.D.A., Smith, C.R., Cerra, A.W. & Doligalski, T.L. 1987 The impact of a vortex ring on a wall *J. Fluid Mech.* **181**, 99–140

EUROMECH Colloquium 525, 21–23 June 2011, Écully, France
Instabilities and transition in three-dimensional flows with rotation

HYDRODYNAMIC INSTABILITIES IN THE ECCENTRIC TAYLOR–COUETTE–POISEUILLE FLOW

Colin Leclercq, Benoît Pier & Julian Scott
Laboratoire de mécanique des fluides et d'acoustique (CNRS–Université de Lyon)
École centrale de Lyon, 36 avenue Guy de Collongue, 69134 Écully Cedex, France

1 Objectives

Since Taylor's first theoretical results obtained almost a century ago [5], researchers have dedicated a relentless effort in modelling the extremely rich dynamical behaviour displayed by a fluid trapped between two concentric cylinders in differential rotation. Taylor–Couette centrifugal instability discovery has lead to the development of hydrodynamic instability theory and the study of transition to turbulence, thanks to a reduced geometric complexity that made analytical studies tractable back in the early 20^{th} century. Since then, increasing complexity has been considered through additional ingredients modifying the canonical configuration: effect of eccentricity, axial flow, non-Newtonian behaviour, etc. Asymptotic analyses and experiments have progressively been complemented by an increasing computational power that allowed a larger parameter space to be explored quantitatively [1, 3, 2].

Only recently, numerical computations reached the degree of efficiency allowing to tackle hydrodynamic stability issues impacting a more realistic industrial configuration, namely here: the three-dimensional flow of mud that is drained upwards in an eccentric annular domain, between a rotating flexible drillstring and the rock face of an oil well, during drilling operations. In that configuration, the inner cylinder is rotating so as to drive the drill bit at the bottom of the well. Mud is pumped down through the drillstring then flows back to the surface through the annular domain. This mud flow is intended to carry the rock cuttings out, avoid their sedimentation when drilling is stopped, limit friction, and finally maintain the right pressure level in the annular domain to prevent gases trapped in the rock to leak inwards the well and cause damage.

In the resulting eccentric Taylor–Couette–Poiseuille flow, how does eccentricity and axial flow impact the centrifugal instability thresholds? In such an open flow, how big of a flow rate is needed to convect the most unstable perturbations downstream and prevent them to overwhelm the laminar basic state? Finally, what new states can be expected after onset of instability? Another topic of interest is the impact of the fluid on drillstring vibrations: under the influence of the hydrodynamic forces, what will be the trajectory of the drillstring (periodic, quasi-periodic, chaotic, ...)?

2 Methodology & results

A DNS solver, specifically designed for eccentric annular domains, is currently being developed to solve the three-dimensional time-dependent incompressible Navier–Stokes equations in primitive variables (assuming a Newtonian behaviour). Considering non-dimensional variables, two control parameters appear in the equations: a Reynolds number Re based on the inner cylinder velocity and a measure of the gap width, and a non-dimensional pressure gradient G_z.

$$\partial_t \mathbf{u} + (\mathbf{u}\cdot\nabla)\,\mathbf{u} + \nabla\pi + G_z = \frac{1}{\mathrm{Re}}\Delta\mathbf{u}$$

$$\nabla\cdot\mathbf{u} = 0$$

Bipolar coordinates are relevant to the geometry and yield a separable variable Laplacian operator. Using an appropriate conformal transformation (modified bipolar coordinates, Wood [6]) together with a dilatation on the "pseudo-radial" coordinate, the eccentric annular region is mapped onto the rectangular domain $D = \{(\xi,\phi) \in [-1,1]\times[0,2\pi[\}$, where all fields are periodic in the "pseudo-azimuthal" coordinate ϕ. The transformations use two dimensionless geometric parameters, an aspect ratio η based on the two cylinder radii, and an eccentricity parameter e ranging from axisymmetry to the limit of touching cylinders.

Pseudo-spectral approximations are used for enhanced accuracy, with Fourier modes in the periodic "pseudo-azimuthal" direction ϕ, and Chebyshev collocation on Gauss–Lobatto points over the "pseudo-radial" direction ξ. Different multi-step time schemes are tested, all treating the convective term explicitly and the diffusion term semi-implicitly. A projection method is used to decouple pressure and velocity, similar to the modified Goda's algorithm introduced by Raspo et al. [4]. This algorithm is used to calculate the axially invariant base flow for

each setting of control parameters $(\mathrm{Re}, G_z, \eta, e)$. Subsequently, the linear and non-linear stability of these base flows will be investigated, using a Fourier decomposition along the axial z-coordinate.

We will first present a series of results validating our code for axially invariant flow, and benchmarking its efficiency against existing solvers. Then an exploration of the parameter space will be carried out in order to identify the flow patterns pertaining to this system. For configurations relevant to the oil industry, hydrodynamic forces acting on the inner cylinder will be calculated in order to evaluate the stability of the drillstring depending on its radial position.

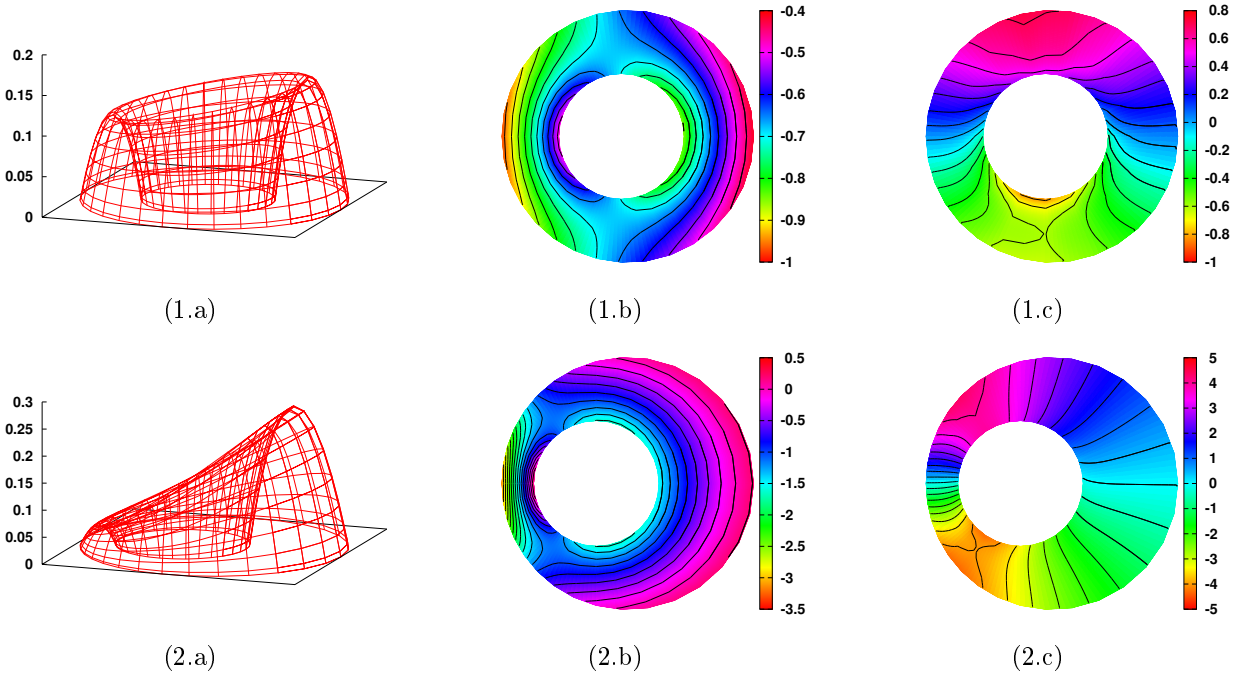

Figure 1: Base flows ((a) axial velocity, (b) axial vorticity, (c) pressure) for (1) weak and (2) moderate eccentricity.

References

[1] D. L. Cotrell and A. J. Pearlstein. The connection between centrifugal instability and Tollmien–Schlichting-like instability for spiral Poiseuille flow. *J. Fluid Mech.*, 509:331–351, 2004.

[2] M. P. Escudier, P. J. Oliveira, and F. T. Pinho. Fully developed laminar flow of purely viscous non-Newtonian liquids through annuli, including the effects of eccentricity and inner-cylinder rotation. *Int. J. Heat Fluid Flow*, 23:52–73, 2002.

[3] D. Martinand, E. Serre, and R. M. Lueptow. Absolute and convective instability of cylindrical Couette flow with axial and radial flows. *Phys. Fluids*, 21(104102), 2009.

[4] I. Raspo, S. Hugues, E. Serre, A. Randriamampianina, and P. Bontoux. A spectral projection method for the simulation of complex three-dimensional rotating flows. *Computers & Fluids*, 31(4–7):745–767, 2002.

[5] G.-I. Taylor. Stability of a viscous liquid contained between two rotating cylinders. *Phil. Trans. Roy. Soc. Lond. A*, 223:289–343, 1923.

[6] W. W. Wood. The asymptotic expansions at large Reynolds numbers for steady motion between non-coaxial rotating cylinders. *J. Fluid Mech.*, 3:159–175, 1957.

TRANSITION OF MHD FLOWS IN CONFINED GEOMETRIES WITH HELICAL BOUNDARY CONDITIONS

Jorge A. MORALES[1] & Wouter BOS[1]
[1]*Laboratoire de Mécanique des Fluides et d'Acoustique*
CNRS, École Centrale de Lyon, Université de Lyon, France

1 Introduction

The present work reports on a study of flows of conducting fluids in confined geometries, driven by magnetic boundary conditions. The visco-resistive magnetohydrodynamic equations are solved using a pseudo-spectral parallel DNS solver combined with a volume penalization method. The volume penalization technique, which is an immersed boundary method, allows in the present case to use other than periodic boundary conditions in a pseudo-spectral approach. In particular, this type of methods is characterized by a high flexibility in changing the geometry of the considered flow. The use of the volume penalization method was only recently validated in MHD flows [1], and in the present communication we will present results in three-dimensions. As a validation, section 2 contains results of three-dimensional Taylor-Couette flow. Section 3 reports on the flow induced in a conducting liquid by the presence of an imposed helical magnetic field.

2 Validation: simulations of three-dimensional Taylor-Couette flow

Three-dimensional simulations of Taylor-Couette flow are performed at different resolutions for different Reynolds numbers. For the geometry studied the critical Reynolds number, above which Taylor-vortices appear, is known to be around 68 [2]. We observe this bifurcation at $Re = 87$ for our simulation at a resolution of 128^3 grid-points. In Figure **1** we show the vorticity field which clearly illustrates the presence of counter-rotating vortices and their associated boundary layers. The results improve with resolution. For example, a critical Reynolds number is found to be around 72 for a 256^3 grid-point simulation. The bifurcation diagram is shown in Figure **2**. Clearly, the method approaches rapidly the analytical value and any precision can be obtained if sufficient computational resources are available.

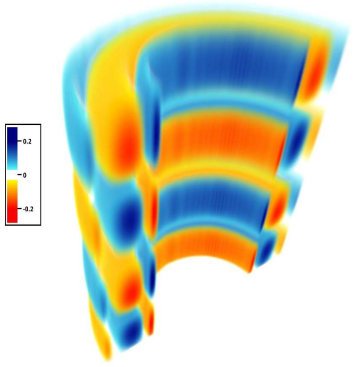

Figure 1: Taylor counter-rotating vortices, azimuthal vorticity colormap

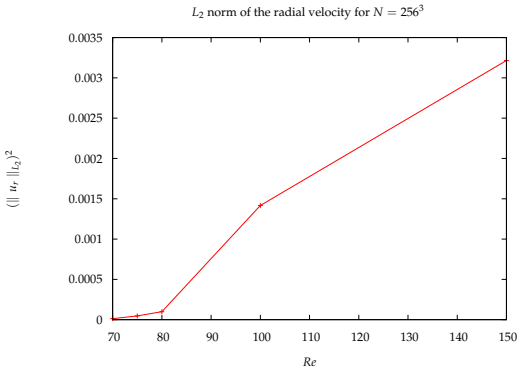

Figure 2: Bifurcation diagram for Taylor-Couette flow

3 MHD dynamics in cylindrical geometry

The main goal of our investigation is the understanding of the velocity fields which are induced in plasmas or conducting fluids by the magnetic field boundary conditions. The present approach is thereby an extension of existing studies by Montgomery and coworkers [3]. Using the penalization method we impose no-slip boundary conditions on the velocity field, and the magnetic field at the wall is imposed to be helical. The pinch ratio Θ, defined as the ratio between the imposed poloidal magnetic field and the imposed axial field ($\Theta = B_\theta/B_z$) is varied and its influence on the flow is monitored. At very low values of the pinch ratio, the velocity field tends to its static limit. At intermediate pinch ratios, a laminar helical velocity field is observed in Figure **4**. The

flow is essentially axial and it is composed of two pairs of helical structures, moving in the positive and negative axial direction. We also present the kinetic energy evolution which shows that at long times the kinetic energy tends to a finite and constant value (Figure **3**).

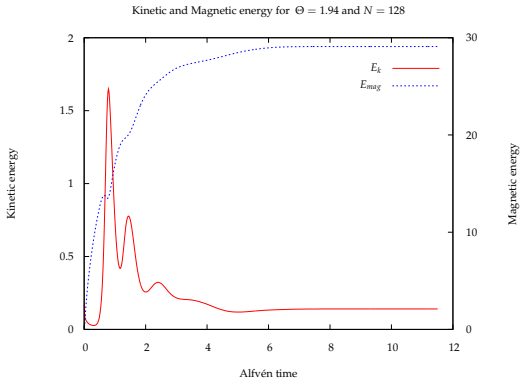

Figure 3: Energies for $\Theta = 1.94$

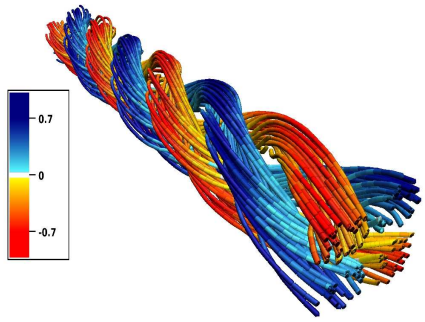

Figure 4: Velocity streamlines and colormap of u_z for $\Theta = 1.94$ and $N = 128^3$

Increasing the pinch-ratio, the laminar flow bifurcates and a multi-mode turbulent flow is observed. A calculation was performed for a pinch ratio $\Theta = 19.4$ ($Re_{rms} = Rm_{rms} \approx 114$). The turbulent behavior is illustrated by showing in Figure **5** the energy evolution which shows a nonstationary, fluctuating behavior. Figure **6** displays less organized streamlines than the laminar flow. Helical modes are still present but many other modes are excited as well.

Further work will consider the influence of breaking the symmetry of the geometry on the flow patterns which are generated, both in cylindrical and toroidal geometry.

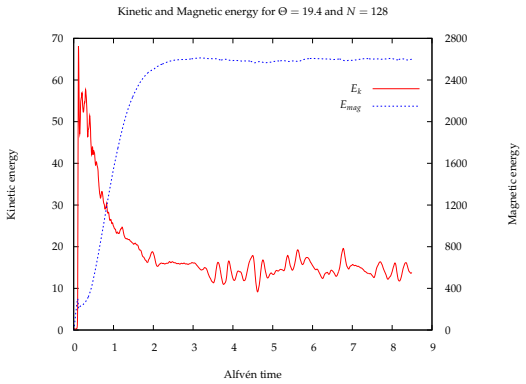

Figure 5: Energies for $\Theta = 19.4$

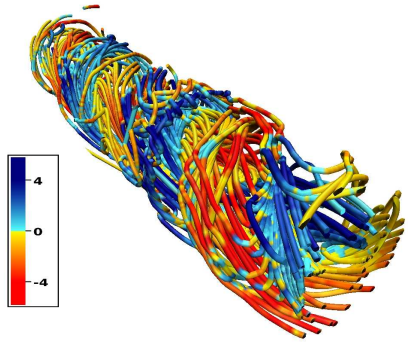

Figure 6: Velocity streamlines and colormap of u_z for $\Theta = 19.4$ and $N = 128^3$

Acknowledgments: The authors acknowledge interaction and discussion with Alexandre Delache, Fabien Godeferd, Clément Jause-Labert, David Montgomery and Kai Schneider.

References

[1] S. Neffaa, W.J.T Bos and K. Schneider, The decay of magnetohydrodynamic turbulence in a confined domain. *Physics of Plasmas*. **15**, 092304, (2008).

[2] J.L. Guermond, R. Laguerre, J. Léorat, and C. Nore, Nonlinear magnetohydrodynamics in axisymmetric heterogeneous domains using a Fourier/finite element technique and an interior penalty method. *Journal of Computational Physics*. **228**, 2739–2757, (2009).

[3] X. Shan, D.C. Montgomery and H. Chen, Nonlinear magnetohydrodynamics by Galerkin-method computation *Physical Review A*. **10**, 6800–6818, (1991).

A STUDY OF HOMOGENEOUS TURBULENCE WITHIN BAROCLINIC CONTEXT

A. Pieri[1], C. Cambon[1] & F.S. Godeferd[1]
[1] *Laboratoire de Mécanique des Fluides et d'Acoustique, Université de Lyon, France*

We present direct numerical simulations and linear models for homogeneous turbulence submitted to the combined distorsions of constant vertical mean shear, vertical solid body rotation and vertical stable stratification, representative of situations in geophysical flows. Depending on the parameters, optimally reduced to the Richardson number and a baroclinic parameter, the baroclinic instability is triggered and modifies the dynamics and structure of the flow. We characterize turbulence in these different states, which present specific anisotropic features, using physical-space quantities (energies, correlation lengths, velocity structure functions) and spectral statistics (directional poloidal/toroidal/potential energy spectra).

1 Introduction to the baroclinic context in turbulent flows

The baroclinic context is characterized by a superposition of three coupled phenomena, required for the existence of baroclinic instability: (1) the Coriolis force, caused by earth rotation in geophysical flows; (2) stable stratification due to density gradients in the atmosphere, which lead to buoyancy forces in the vertical direction; (3) high vertical velocity gradients, as at the altitude of the tropopause in atmospheric flows, in the form of jet streams, which, in first approximation, are modelled by homogeneous shear. Due to admissibility conditions [1, 8], a spanwise density gradient is necessarily created and added to the previous vertical one. Under these conditions, tilting of isopycnal surfaces is induced [14], and, although the mean density gradients are stable in the sense that they lead to positive restoring forces, the misalignment of isopycnal surfaces with the horizontal plane can lead to unstable dynamics [14, 15], hence the baroclinic instability.

The first works on baroclinic instability where done by Charney (1947) [16] using quasi-geostrophic equations in the β-plane approximation. He derived a necessary condition for instability to occur formulated simply by an inequality implying the Rossby radius of deformation. Further contribution by Eady (1949) [17] using the f-plane approximation was later added. Eady considered a simpler model — a Couette-like configuration — of the atmosphere and obtained an instability condition resting on a critical wavenumber [14]. Following Eady, we also place the study within the f-plane approximation. We replace the two-boundary plates approximation by an infinite Couette flow to model shear effects [10].

2 DNS results of baroclinic turbulence

Investigations of homogeneous turbulent flows submitted to the separate effects of homogeneous shear, stable vertical stratification or rotation were done in the past decade [2, 3, 4, 5, 6]. Here, we focus on the following new approach: Direct Numerical Simulation (DNS) of homogeneous turbulence including the complete coupled three previous distorsions — the so-called 'baroclinic' context. Unlike the previously mentioned contexts, the baroclinic instability is a reservoir of energy which does not impose to add an artificial forcing to the simulations, or to have to deal with decaying flows. The aim of our study is first to provide a detailed characterization of the Eulerian properties of developped baroclinic turbulence. The parametric space is very large, since it not only includes the properties of turbulence itself, Reynolds number, cut-off wavenumbers, but also the choice of the intensities of rotation, stratification and shear. A reduction of the parametric space is obtained by considering the Richardson number defined as $Ri = N^2/S^2$ and the baroclinic parameter $\varepsilon = Sf/N^2$ which is also the mean slant angle of the isodensity surfaces. Here, $S = \partial_y U_x$ is the mean velocity gradient, $N = \left(-g\partial_y \overline{\rho}/\rho_0\right)^{1/2}$ is the Brunt-Väisälä frequency and $f = 2\Omega$ is the rotation rate. We shall investigate ranges of these parameters between $[0:2]$ for Ri and $[0:1]$ for ε. The Navier-stokes equations in the Boussinesq approximation are solved using pseudo-spectral Direct Numerical Simulation. Periodicity is assumed in the three directions. Under the action of shear, the mesh is deformed and a periodic remeshing is needed using the algorithm by Rogallo [10] (the anisotropic adaptation of the Orszag-Patterson algorithm) in spectral space (p, q, r). De-alisasing is done following Delorme [12] method. The code used in this study is a MPI-based parallel code : the turbulence box is cut into slabs following the algorithm by Coleman et al. [11]. Fast Fourier transforms are done using the library FFTW by Frigo and Johnson [13]. Time-advancing is done according to the third order Runge-Kutta (RK3) method. Lastly, the rotational form of the non-linear term has been implemented. We start by considering two-point spectra of Eulerian velocity and buoyancy fields, as well as the evolution of additional scalars which are introduced in the flow, with different Schmidt numbers. The time evolution of quantities such as the deviatoric

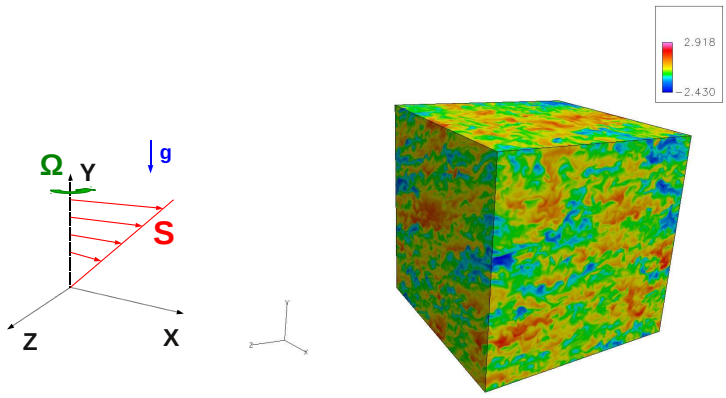

Figure 1: Sketch of the mean flow (left). Buoyancy distribution (right). DNS with 512x768x512 degrees of freedom with Richardson number $Ri = 0.5$ and baroclinicity parameter $\varepsilon = 0.2$. $Re_\lambda(0) = 44.1$ and $\frac{Sk}{\epsilon_\nu} = 2.55$. With ϵ_ν the kinetic energy dissipation. $\tau = tS = 7$.

part of the Reynolds stress tensor, the componentality and dimensionality tensors [7, 9], potential and kinetic energy directional spectra are analized to bring out and understand the complex anisotropic structure of the flow. A link with extended structure functions is also proposed, in order to assess the possible application, or disagreement, of scalings available for isotropic turbulence in the context of Kolmogorov theory. We will also study two-point correlations for characterizing the turbulent structures, and their properties. Large scale structures will be quantified with directional correlation length obtained from the velocity correlation tensor, whereas two-point vorticity correlations put to the fore smaller turbulent structures. The Lagrangian properties are also studied, and related to Eulerian data, especially considering the dual characterization of anisotropy. To refine our study, we thus obtain results concerning mixing properties of the flow by looking at both the stratifying agent concentration (see for instance the distribution of buoyancy on figure 1) and passive scalars advection. We also put the emphasis on the analysis of possibly unstable dynamics of turbulence within the baroclinic context, in a second part. Inertial transfers will be investigated, considering energy exchanges between the kinematic and the potential modes, but also the interscale and directional energy drain. This structuring of the flow, of nonlinear, irreversible nature since it is due to quadratic terms in the equations, is also compared to the predictions of linear theory (often called Rapid Distorsion Theory, RDT), which provides lots of valuable information on the spectral energy distribution reorganization by the mere body forces (Coriolis and buoyancy) and shear. Since RDT is also computationally much lighter than DNS, it also permits a preliminary opening of the parametric space, allowing to choose the most relevant parameters for the high resolution simulations.

References

[1] A. D. D. Craik, W. O Criminale, *Proc. R. Soc. London A*, **406**, 13-26 (1986).

[2] F. S. Godeferd, C. Cambon, *Phys. Fluids*, **6**, pp. 2084-2100 (1994).

[3] F. G. Jacobitz, S. Sarkar, C. W. Van Atta, *J. Fluid Mech.*, **342**, pp. 231-261 (1997).

[4] A. Salhi, C. Cambon, *J. Fluid Mech.*, **347**, pp. 171-195 (1997).

[5] C. Cambon, F. S. Godeferd, F. Nicolleau, J. C. Vassilicos, *J. Fluid Mech.*, **499**, pp 231-255 (2004).

[6] L. Liechtenstein, F. S. Godeferd, C. Cambon, *J. Turbulence*, **6**, pp 1-18 (2005).

[7] C. Cambon, L. Jacquin, J. L. Lubrano, *Phys. Fluids A*, **4**, pp. 812-824 (1992).

[8] A. Salhi,C. Cambon, *J. Appl. Mech.-Trans*, **73**, pp. 449-460 (2006).

[9] S. C. Kassinos, W. C. Reynolds, M. M. Rogers, *J. Fluid Mech.*, **428**, pp. 213-248 (2001).

[10] R. S. Rogallo, *Nasa Technical Memorandum*, **81315** (1981).

[11] G. N. Coleman, J. Kim, P. R. Spalart, *J. Fluid Mech.*, **416**, pp. 107 (2000).

[12] P. Delorme, *PhD Thesis*, ONERA, 1985.

[13] M. Frigo, S. G. Johnson, *FFTW for version 3.1*, Massachussets Inst. of Tech., 2006.

[14] J. Pedlowsky, *Geophysical Fluid Dynamics*, Springer-Verlag (1987).

[15] P. G. Drazin, W. H. Reid, *Hydrodynamic stability*, Cambridge University Press (1981).

[16] J. G. Charney, *K. Phys. Oceanogr.*, **4**, 135 (1947).

[17] E. T. Eady, *Tellus*, **1**, pp. 33-52 (1949).

EXPERIMENTAL CHARACTERISATION OF TURBULENT FLOW RÉGIME IN THE THREE-DIMENSIONAL ROTATING-DISK BOUNDARY LAYER

M. Ehtisham SIDDIQUI, Mukund VASUDEVAN, Benoît PIER, Julian SCOTT, Alexandre AZOUZI, Roger MICHELET, Christian NICOT
Laboratoire de mécanique des fluides et d'acoustique (CNRS — Université de Lyon)
École centrale de Lyon, 36 avenue Guy-de-Collongue, 69134 Écully, France.

Fully developed turbulent flows are known to display some universal features when bounded by a solid wall. The flow due to a large disk rotating in otherwise still fluid undergoes transition from laminar to turbulent dynamics at a nondimensional radius $R \simeq 500$. The turbulent régime prevailing beyond this critical radius is unsual in several respects [4, 3, 2, 1]: it is sandwiched between a solid moving surface and the outer fluid at rest, and it develops in the radial direction while the main flow and shear components are in the azimuthal direction.

The aim of the experimental work presented here is to characterise some features of this particular turbulent boundary layer.

1 Experimental setup

The experimental setup consists of a 50 cm diameter glass disk that is rotated at constant angular speeds, up to 1500 rpm. Disk rotation and viscosity produce a three-dimensional boundary layer of constant thickness $\delta = \sqrt{\nu/\Omega_d}$ (a typical value is $\delta = 400$ μm), where ν is the kinematic viscosity and Ω_d the disk rotation rate. Non-dimensional (based on δ) radial and azimuthal coordinates R and Z are introduced; non-dimensional azimuthal velocities V are used, based on the local linear disk velocity $R\delta\Omega_d$.

Flow measurements are carried out by constant-temperature hot-wire anemometry. The hot wire is positioned by a computer-controlled high-precision two-axes traversing mechanism and provides azimuthal velocity time series. These time-series are processed to obtain the flow characteristics, in particular the mean-flow velocity profiles and the spectral analysis.

2 Mean-flow velocity profiles

Azimuthal mean velocity profiles are obtained by averaging the hot-wire measurements for 100 disk revolutions at each location. From these measurements it is observed that the mean-flow profiles very closely follow the analytic profile for $R \leq 480$ and that weak mean-flow corrections prevail over the range $490 \leq R \leq 540$. For $R \geq 550$, strong mean-flow distortions develop that progressively extend to beyond $Z = 15$ by $R = 600$. Such boundary-layer thickening is characteristic of the development of a turbulent boundary layer. In figure 1, mean-flow velocities for $550 \leq R \leq 650$ are plotted against Z using a logarithmic scale. It is found that the velocity profiles are nearly linear in $\log Z$ for $R \geq 600$, which is the characteristic low of the wall of fully turbulent boundary layers. Velocity profiles for $R \leq 590$ are not linear in $\log Z$, suggesting that the flow is not yet fully turbulent and still in the transitional régime. Thus, we conclude from the mean-velocity measurements that the flow begins transition around $R \simeq 540$ and is fully turbulent by $R \simeq 610$.

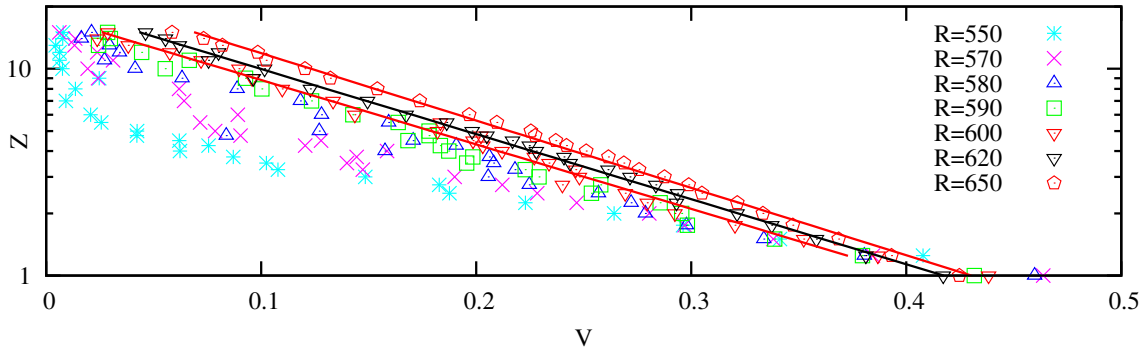

Figure 1: Mean-flow velocity profiles of the transitional and fully turbulent flow regimes plotted against Z on a logarithmic scale. Solid lines are linear fits to the data in the range $1 \leq Z \leq 16$ for $R = 600$, 620 and 650 (slopes are respectively $dV/d\ln(Z) = -0.139$, -0.138 and -0.133). The root-mean-square error of each fit is around 0.005.

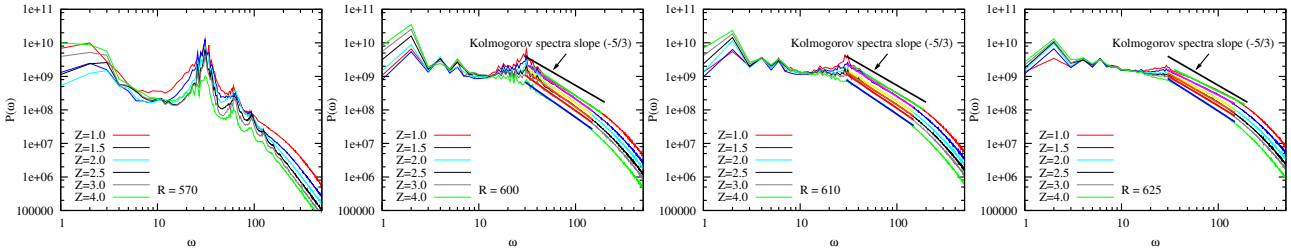

	$Z = 1.0$	1.5	2.0	2.5	3.0	4.0	Average
$R = 600$	−1.94	−2.03	−2.03	−2.09	−2.03	−2.21	−2.06
610	−1.76	−1.85	−1.81	−1.89	−1.96	−1.96	−1.87
620	−1.51	−1.59	−1.63	−1.73	−1.79	−1.88	−1.68
625	−1.42	−1.45	−1.55	−1.68	−1.72	−1.85	−1.61

Figure 2: Log-log plots of spectra in turbulent régime. For $R \geq 600$, linear fits are computed for data in the range $30 \leq \omega \leq 200$ and shown together with a reference line of slope $-5/3$. The slope values shown in the table have a root-mean-square error of around 0.05.

3 Spectral analysis

Fourier spectra are calculated to show the frequency content of the azimuthal velocity time series at different non-dimensional radii and disk normal positions. In figure 2, spectra corresponding to the transitional and fully turbulent régimes are plotted using a log-log scale to bring out a possible power-law behaviour. For $R = 570$, the modal peak and its harmonics is still apparent, whereas at $R = 600$ and above, the peak is absent and there is a linear range extending over a good fraction of a decade in frequency upwards from where the peak would occur. The figure shows linear fits to the data in the range $30 \leq \omega \leq 200$ for $R \geq 600$. Such linear behaviour corresponds to spectral power laws with exponents equal to the slopes of the lines, listed in the table. For reference purposes, the figure also shows a straight line with the Kolmogorov slope $-5/3$. It is seen that these power-law exponents are not far from the Kolmogorov value, particularly at the largest values of R where the turbulence is most developed. Also apparent from the table, the power-law exponent depends on both R and Z, tending to decrease in absolute value as R increases and to increase with Z.

4 Discussion

A possible explanation of these variations, more qualitative than quantitative, refers to the physics of the turbulent energy cascade from large to small scales which forms the basis of Kolmogorov's theory. Large scales, here corresponding to frequencies at and below $\omega \simeq 30$, break down to smaller and smaller scales, which leads to the $-5/3$ law by dimensional analysis when assuming a constant rate of energy supply from the large scales.

Imagine following a packet of turbulence as it is convected by the mean flow. If the energy supply rate from the large scales increases with time, the energy flux was lower in the past and, given that the cascade takes a certain time, we expect the spectral energy of the small scales to be less than it would have been had the energy supply been constant, hence a steeper slope on the log-log plot. This suggests larger absolute values of the exponent in the presence of an increasing supply rate, and smaller ones for decreasing supply rate. In the table of figure 2, the absolute value of the Z-averaged exponent is seen to be higher than 5/3 for the first three values of R. This is to be expected since the turbulent intensity, and hence the energy supply rate, increases with R in the transitional region. Both $R = 600$ and $R = 610$ have exponents above 5/3 for all Z, suggesting an increasing supply rate at all distances from the disk. This is reasonable because the turbulence is developing up to $R = 610$. For $R = 620$ and $R = 625$, the exponent is less than 5/3 towards the disk and greater than 5/3 at higher Z. This suggests a decreasing supply rate near the disk and an increasing one further out.

References

[1] A Holstad, H. I. Andersson and B. Pettersen, *Int. J. Numer. Meth. Fluids* **62**, 875–905 (2010).

[2] J. P. Johnston and K. A. Flack, *J. Fluids Eng.* **118**, 219–232 (1996).

[3] H. S. Littell and J. K. Eaton, *J. Fluid Mech.* **266**, 175–207 (1994).

[4] S. K. Robinson, *Annu. Rev. Fluid Mech.* **23**, 601–639 (1991).

5 Author index